1 OF 1
PB
292 820

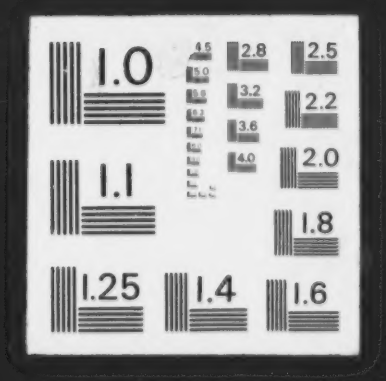

U.S. DEPARTMENT OF COMMERCE
National Technical Information Service

PB-292 820

Characterization of the EPA/IERL-RTP Pilot-Scale Precipitator

(U.S.) Industrial Environmental Research Lab, Research Triangle Park, NC

Feb 79

United States
Environmental Protection
Agency

Industrial Environmental Research
Laboratory
Research Triangle Park NC 27711

EPA-600/7-79-052
February 1979

PB 292820

EPA

Characterization of the EPA/IERL-RTP Pilot-Scale Precipitator

Interagency Energy/Environment R&D Program Report

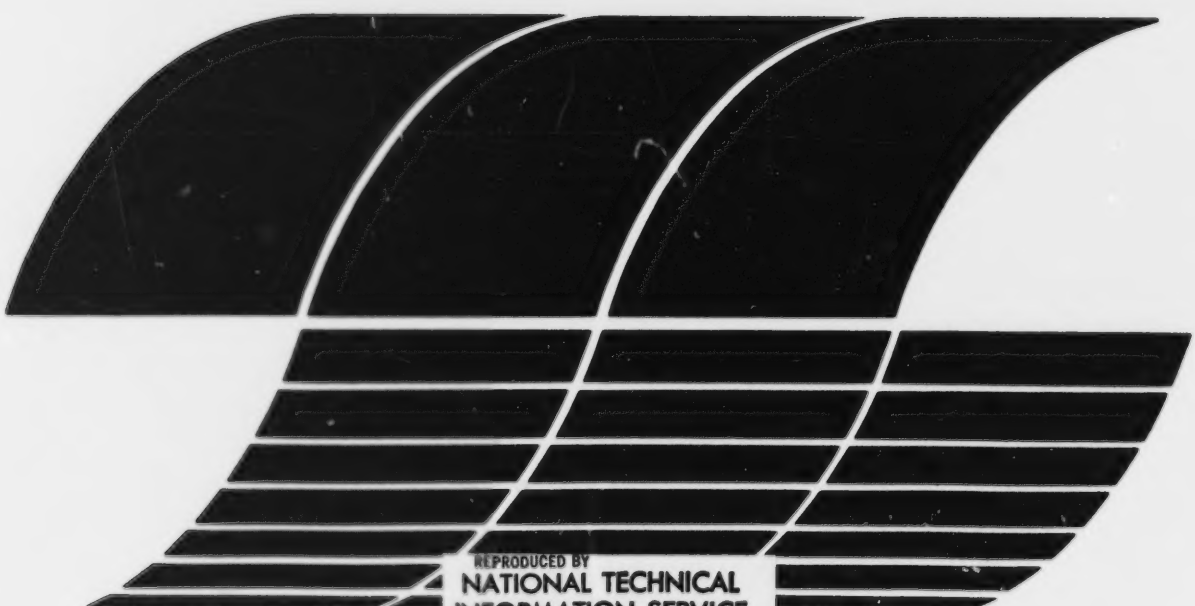

REPRODUCED BY
NATIONAL TECHNICAL
INFORMATION SERVICE
U. S. DEPARTMENT OF COMMERCE
SPRINGFIELD, VA. 22161

RESEARCH REPORTING SERIES

Research reports of the Office of Research and Development, U.S. Environmental Protection Agency, have been grouped into nine series. These nine broad categories were established to facilitate further development and application of environmental technology. Elimination of traditional grouping was consciously planned to foster technology transfer and a maximum interface in related fields. The nine series are:

1. Environmental Health Effects Research
2. Environmental Protection Technology
3. Ecological Research
4. Environmental Monitoring
5. Socioeconomic Environmental Studies
6. Scientific and Technical Assessment Reports (STAR)
7. Interagency Energy-Environment Research and Development
8. "Special" Reports
9. Miscellaneous Reports

This report has been assigned to the INTERAGENCY ENERGY-ENVIRONMENT RESEARCH AND DEVELOPMENT series. Reports in this series result from the effort funded under the 17-agency Federal Energy/Environment Research and Development Program. These studies relate to EPA's mission to protect the public health and welfare from adverse effects of pollutants associated with energy systems. The goal of the Program is to assure the rapid development of domestic energy supplies in an environmentally-compatible manner by providing the necessary environmental data and control technology. Investigations include analyses of the transport of energy-related pollutants and their health and ecological effects; assessments of, and development of, control technologies for energy systems; and integrated assessments of a wide range of energy-related environmental issues.

EPA REVIEW NOTICE

This report has been reviewed by the participating Federal Agencies, and approved for publication. Approval does not signify that the contents necessarily reflect the views and policies of the Government, nor does mention of trade names or commercial products constitute endorsement or recommendation for use.

This document is available to the public through the National Technical Information Service, Springfield, Virginia 22161.

TECHNICAL REPORT DATA (Please read Instructions on the reverse before completing)		
1. REPORT NO. EPA-600/7-79-052	2.	3. RECIPIENT'S ACCESSION NO. PB292820
4. TITLE AND SUBTITLE Characterization of the EPA/IERL-RTP Pilot-Scale Precipitator		5. REPORT DATE February 1979 6. PERFORMING ORGANIZATION CODE
7. AUTHOR(S) P. A. Lawless (RTI), B. E. Daniel, and G. H. Ramsey		8. PERFORMING ORGANIZATION REPORT NO.
9. PERFORMING ORGANIZATION NAME AND ADDRESS See Block 12.		10. PROGRAM ELEMENT NO. EHE624A 11. CONTRACT/GRANT NO. N.A.
12. SPONSORING AGENCY NAME AND ADDRESS EPA, Office of Research and Development Industrial Environmental Research Laboratory Research Triangle Park, NC 27711		13. TYPE OF REPORT AND PERIOD COVERED Inhouse; 9/77 - 5/78 14. SPONSORING AGENCY CODE EPA/600/13
15. SUPPLEMENTARY NOTES IERL-RTP project officer is L. E. Sparks, MD-61, 919/541-2925.		

16. ABSTRACT The report describes the EPA/IERL-RTP pilot scale electrostatic precipitator, a research device used for testing and verifying new precipitator concepts and models of precipitator operation. It describes the basic capabilities of the precipitator, and contains measurements of precipitator operating characteristics which were obtained in the first months of investigation. The precipitator performed to its design specifications in initial tests, and its utility as a research tool was quickly established. Several proposed experiments which will be performed on the precipitator are described.

17. KEY WORDS AND DOCUMENT ANALYSIS			
a. DESCRIPTORS		b. IDENTIFIERS/OPEN ENDED TERMS	c. COSATI Field/Group
Pollution	Fly Ash	Pollution Control	13B 21B
Research	Measurement	Stationary Sources	14B
Dust		Particulate	11G
Aerosols		Back Corona	07D
Electrostatic Precipitators			13I
Coronas			20C

18. DISTRIBUTION STATEMENT	19. SECURITY CLASS (This Report)	21. NO. OF PAGES
Unlimited	Unclassified	86
	20. SECURITY CLASS (This page) Unclassified	22. PRICE A05-A01

EPA Form 2220-1 (9-73)

EPA-600/7-79-052

February 1979

Characterization of the EPA/IERL-RTP Pilot-Scale Precipitator

by

P.A. Lawless (RTI), B.E. Daniel, and G.H. Ramsey

Environmental Protection Agency
Office of Research and Development
Industrial Environmental Research Laboratory
Research Triangle Park, North Carolina 27711

Program Element No. EHE624A

EPA Project Officer: L.E. Sparks

Prepared for

U.S. ENVIRONMENTAL PROTECTION AGENCY
Office of Research and Development
Washington, DC 20460

ABSTRACT

The EPA/IERL-RTP pilot-scale electrostatic precipitator is a research device used for testing and verifying new precipitator concepts and models of precipitator operation. This report describes the basic capabilities of the precipitator, and contains measurements of precipitator operating characteristics which were obtained in the first months of investigation.

TABLE OF CONTENTS

		Page
ABSTRACT		ii
FIGURES		iv
TABLES		v
ACKNOWLEDGMENT		vi
Section		
1.0	INTRODUCTION	1
1.1	Design Features	1
1.2	Credits	4
2.0	OPERATION OF THE ESP ELECTRICAL SYSTEM	4
2.1	Transformer-Rectifier Sets	4
2.2	Corona Frame and Collecting Plates	4
2.3	Measurement System	5
2.4	Voltage-Current Characteristics	6
3.0	TEMPERATURE CONTROL AND MEASUREMENT	13
3.1	Control and Measurement Thermocouple Placement	13
3.2	Temperature Profile	15
3.3	Time to Equilibrate	15
3.4	Uneven Temperature Distribution	19
4.0	GAS FLOW DISTRIBUTION	19
4.1	Measurement Techniques	20
4.2	Flow Velocity Results	20
4.3	Sneakage Measurements	22
4.4	Variation of Velocity Through the ESP	23
5.0	AEROSOL GENERATION AND DISPERSION	27
5.1	Aerosol Generator	27
5.2	Fly Ash Size Distribution	28
5.3	Iron Oxide Size Distribution	30
6.0	PLANNED FUTURE EXPERIMENTS	30
6.1	ESP/Scrubber Combinations	34
6.2	Comparison of Eastern and Western Fly Ash	34
6.3	Variations of Wire and Plate Geometry	35
6.4	Residence Time Experiments	35
7.0	SUMMARY AND CONCLUSIONS	36
8.0	REFERENCES	36
	APPENDIX A. ESP FLOW CONTOUR PLOTS	37

FIGURES

No.		Page
1.1	Diagram of pilot-scale ESP	3
2.1	Sample of the printer output	7
2.2	Theoretical V-I curve and experimental data points at 20°C	9
2.3	Theoretical V-I curve and experimental data points at 118°C	10
2.4	Theoretical V-I curve and experimental data points at 216°C	11
2.5	Theoretical V-I curve and experimental data points at 350°C	12
2.6	Dirty plate data	14
3.1	Location of thermocouples on the ESP	16
3.2	Temperature profile along the ESP	17
3.3	Approach of ESP to operating temperature	18
4.1	A typical velocity contour plot	21
4.2	Variation of flow velocity with location. Plate spacing 12.7 cm	24
4.3	Variation of flow velocity with location. Plate spacing 25.4 cm	25
4.4	Variation of flow velocity with location. Plate spacing 38 cm	26
5.1	Inlet and outlet size distributions	31
5.2	Inlet size distribution with cyclone	32
5.3	Inlet size distribution for iron oxide dust	33
A1.A-E	Flow distribution in nominal 5-in. channel. Volume flow of 42 m^3/min.	38-42
A2.A-E	Flow distribution in nominal 5-in. channel. Volume flow of 23.5 m^3/min.	43-47
A3.A-E	Flow distribution in nominal 5-in. channel. Volume flow of 7.0 m^3/min.	48-52
A4.A-E	Flow distribution in nominal 10-in. channel. Volume flow of 77 m^3/min.	53-57
A5.A-E	Flow distribution in nominal 10-in. channel. Volume flow of 42.5 m^3/min.	58-62
A6.A-E	Flow distribution in nominal 10-in. channel. Volume flow of 28 m^3/min.	63-67
A7.A-D	Flow distribution in nominal 15-in. channel. Volume flow of 89 m^3/min.	68-71
A8.A-E	Flow distribution in nominal 15-in. channel. Volume flow of 49 m^3/min.	72-76

TABLES

No.		Page
4.1	Normalized Standard Deviation	27
5.1	Particulate Distribution	29

ACKNOWLEDGMENT

The contributions of P. A. Lawless of the Research Triangle Institute were funded by EPA under contract 68-02-2612, Task 36.

1.0 INTRODUCTION

The performance of an electrostatic precipitator (ESP) can be described in terms of the ESP's inputs (dust characteristics, gas flow and temperature, electrical operating points) and functional units (number of sections, plate areas, baffling, etc.). However, the complexity of the total ESP system, the cost of conducting experiments, and the difficulty of controlling variables in industrial operations preclude evaluating the effectiveness of each variable in full-scale ESP's operating on industrial processes. Thus, it was desirable to construct a dedicated pilot-scale ESP with enough flexibility for an experimental investigation of the effects of individual functional units on overall performance.

In addition to allowing direct experiments on its operation, the pilot-scale ESP is a valuable verification tool for evaluating a computer analysis model describing ESP behavior. A preliminary computer model of an ESP system has been developed and modified under EPA/IERL-RTP contracts[1,2,3]. The purpose of the modification was to upgrade the model to more closely predict the behavior of real ESP systems. The pilot-scale ESP is an easily controlled experimental unit providing data for evaluating the computer model under ideal and non-ideal conditions.

1.1 Design Features

To make the pilot-scale ESP as flexible as possible, its design incorporated the following features:

1. The ESP can be operated over a temperature range of ambient to 350°C, at gas velocities from 0.3 to 6 m/sec (1 to 20 fps).
2. Gas velocity distribution through the ESP is uniform: normalized standard deviation is less than 0.25.
3. Sampling ports at the inlet and outlet and between electrical sections permit measuring gas velocity distribution, mass loading, temperature distribution, particulate resistivity, and gas composition.
4. Total gas volume flow is measured at the ESP outlet.

5. Extensive baffling maintains sneakage through the ESP as low as practical.
6. Gases can be injected upstream of the precipitator.
7. The collection plates are 1.2 m high and plate-to-plate spacing can be varied from 12.7 to 38 cm (5 to 15 in.); wire-duct geometry is used.
8. The specific collector area (SCA) of the ESP is 28 $m^2/m^3/sec$ (140 ft^2/1000 acfm) at a plate spacing of 23 cm and a gas velocity of 1.5 m/sec.
9. There are four electrical sections in the direction of flow, and there is only one lane for gas flow.
10. The collector electrodes are isolated from ground so that the current to them can be measured directly.
11. The number of corona wires, wire-to-wire spacing, and type of wire electrode used can be changed easily.
12. The power supplies can operate to 100 kV with current up to 10 mA, half- or full-wave rectified, filtered or unfiltered.
13. Current and voltage waveforms can be displayed on an oscilloscope for monitoring.
14. Currents and voltages for all sections, the temperatures of the inlet and outlet of each section, and the pressure drop across the flow measuring orifice are measured, displayed digitally, and can be recorded on a line printer.

Figure 1.1 is a schematic view of the precipitator showing the relative location of major parts. It is approximately to scale. Detailed discussions of ESP major subsystems follow.

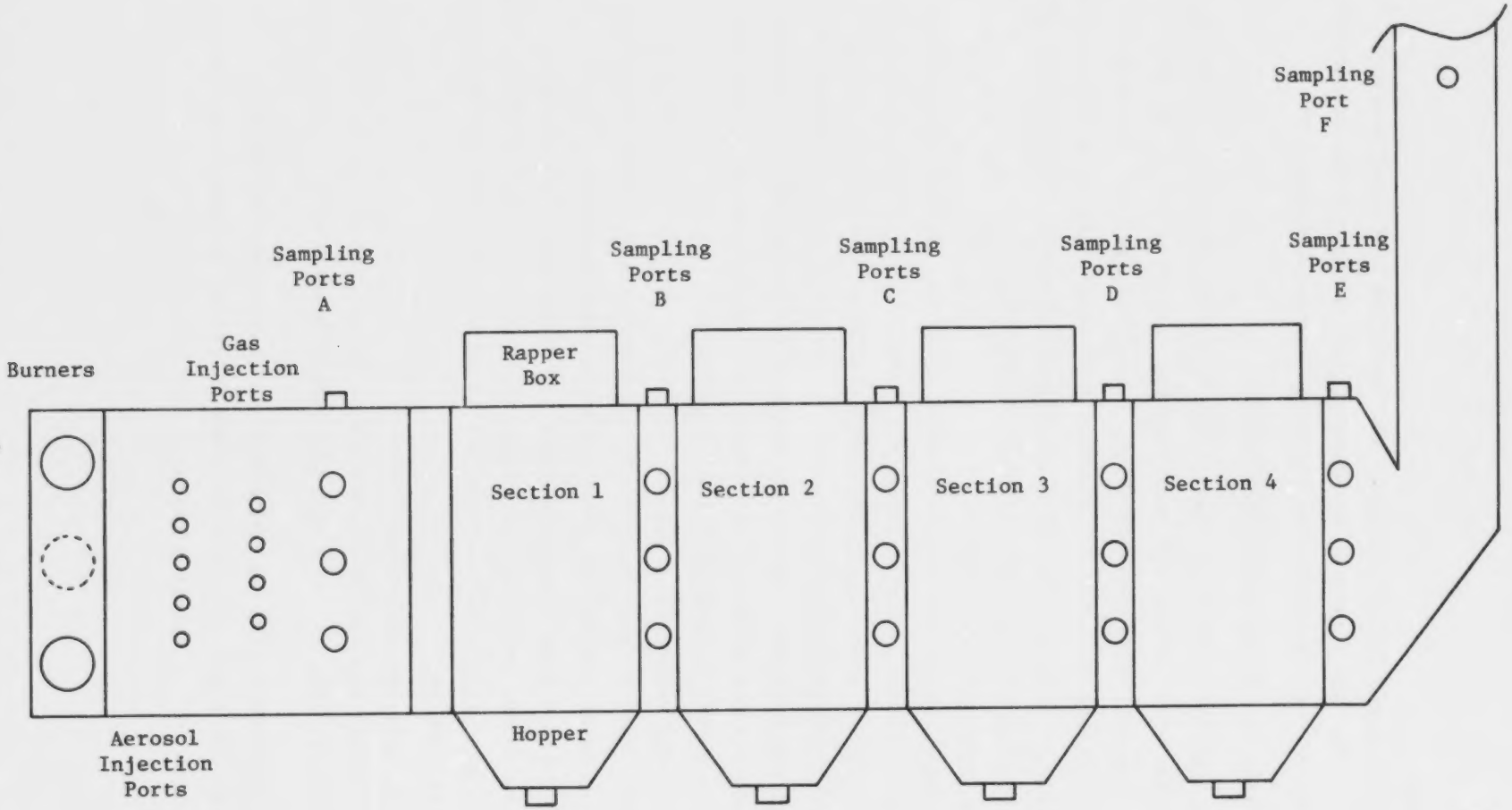

Figure 1.1. Diagram of pilot-scale ESP.

1.2 Credits

The pilot-scale ESP was designed and installed by Denver Research Institute.* The Institute also constructed and calibrated the measurement system. The ESP was fabricated by Stainless Equipment Company.**

2.0 OPERATION OF THE ESP ELECTRICAL SYSTEM

Since IERL-RTP's ESP consists of four identical sections, a description of one section will suffice for understanding the operation of the unit. For safety reasons, numerous interlocks, both electrical and mechanical, remove all voltages from the ESP sections when the integrity of the machine is breached; for instance, for sampling between sections. Description of the electrical system will not include these interlocks.

2.1 Transformer-Rectifier Sets

Each power supply is a Hipotronics*** T8100-10, capable of delivering 0-100 kV dc at 10 mA. Rectification is accomplished by solid-state diodes in either half- or full-wave bridge configurations. The output of the power supply can be filtered with a 0.01 μF capacitor, or the capacitor can be left disconnected. The power supply contains an internal voltage divider resistor for measuring the output voltage; the return connection of the power supply is available for measuring dc.

The primary voltage is changed from zero to 208 Vac by a variable transformer. Current limiting devices between the transformer output and power supply input protect the power supply during sparkover. These devices comprise a high inductance choke in series with high wattage resistors which are switchable in values of zero, 5, 10, and 20 ohms. When high operating voltages and currents are to be measured, the series resistance must be lowered.

2.2 Corona Frame and Collecting Plates

High voltage is supplied to the corona wires through the corona frame, a 5-cm diameter pipe, 1.25 m long, with closed rounded ends. It is suspended

*Denver Research Institute, University of Denver, Denver, CO 80210.

**Stainless Equipment Co., 2829 S. Santa Fe Drive, Englewood, CO 80110.

***Hipotronics, Inc., Drawer A, Brewster, NY 10509.

from above at each end by rods which pass up into the rapper box. The support rods hang in cylindrical metal tunnels, spaced well away from the rods, and terminate at the top in large corona balls (about 20 cm in diameter). The balls rest on insulating plates across the top of each tunnel.

The corona frame is shaped to support weighted wires in a variety of configurations. Over the 1.3-m length of the high-voltage frame, 48 wire receptacles are spaced 2.5 cm apart, allowing from 2 to 10 or 12 wires per section to be set up quickly and easily. The receptacles are cone-shaped depressions which match cones swaged to the ends of the corona wires; the wire cones hang in the receptacles and support the weight of the wire. In the early stages of using the ESP, the wires have been a standard 0.32 cm (1/8 inch) in diameter.

Each collecting plate has an effective area of 1.5 m^2, and each is hung from a support that travels on a rotating threaded rod. When the rod is turned, using an external crank, the supports travel toward or away from one another to vary the plate spacing. The motion is symmetrical with respect to the corona wires.

An air-operated rapper, above each plate, moves with it. The air lines, flexible enough to accommodate the plate motion, also electrically isolate the rapper from the system ground.

The collector plate is electrically isolated from its support frame by strips of a mica-based material. The entire plate area opposite the corona wires is electrically connected, separate from the frame and baffles at the sides and bottom of the frame. A lead from the collector plate in each electrical section returns to the power supply ground through a sensing resistor, permitting direct measurement of plate current from both collectors in each section. Separate leads from each plate are connected externally for this measurement; however, the current to each plate can be measured using each lead individually.

2.3 Measurement System

The measurement system of the pilot-scale ESP consists of transducers, signal conditioning preamplifiers, digitizing and display circuits, and a hard-copy printer. The outputs from the voltage transducers range from zero

to 1 V full-scale; from the current transducers, from zero to 0.5 V full-scale; from the temperature transducers, zero to 100 mV full-scale; and from the pressure transducer for the flow measurement, zero to 10 V full-scale.

Voltage and current signals can be viewed directly on a dual-channel oscilloscope, one section at a time, selected by switches. For measurement, all signals are filtered and amplified or attenuated between zero and 100 mV by a separate preamplifier for each signal channel. The filtering removes noise pulses and power-line-induced pickup from the conditioned signals, and helps protect the preamplifier inputs from surges during sparking.

Preamplifier outputs are sampled in succession at the rate of about twice a second by a multiplexer. The multiplexer output is fed to an analog-to-digital converter (ADC). The ADC produces a three-digit representation of the signal presented to it by the multiplexer and puts that representation on a data bus. The data on the bus is put into the proper display unit by an unlatching pulse fed to the unit in question. The unlatching pulses are directed by a digital multiplexer that operates in the same sequence as the signal multiplexer.

In normal operation, each display is updated approximately twice a second. The multiplexer can be locked onto any channel for more rapid updating, if necessary.

The same data bus feeds a parallel-to-serial converter whose output goes to a standard 80-character thermal line printer. The data are punctuated and formatted by characters stored in a read-only memory (ROM). A heading that can be printed manually is also stored in the ROM. Data printing can be initiated manually at any time, or can be performed automatically at 1- or 10-minute intervals, controlled by a digital clock. The clock operates continuously from the power line, providing initiation pulses and time of data collection for each line on the printer. A manual keyboard on the printer can be used to enter information about the data being printed.

Figure 2.1 is a sample of the digital output.

2.4 Voltage-Current Characteristics

The variation of corona current (I) with applied voltage (V) was measured with clean collection plates and wires at four temperatures covering the operating range of the ESP. As the operating temperature rises, the ESP

10-24-77

THIS IS A SAMPLE OF THE
PRINTER OUTPUT AT AMBIENT
CONDITIONS

V1KU	I1MA	V2KU	I2MA	V3KU	I3MA	V4KU	I4MA	T1F	T2F	T3F	T4F	T5F	TPF	DP	TIME
-59.9	0.40	-58.3	0.33	-60.7	0.39	-61.0	0.38	060	060	061	057	063	057	0.16	02:58
-59.7	0.39	-58.2	0.33	-60.7	0.39	-61.0	0.38	060	060	061	057	063	057	0.17	02:59
-59.8	0.39	-58.2	0.32	-60.7	0.38	-60.9	0.38	061	061	062	058	063	058	0.17	03:00
-59.7	0.40	-58.2	0.32	-60.7	0.38	-61.0	0.38	061	061	062	058	064	058	0.16	03:01
-59.7	0.40	-58.2	0.32	-60.7	0.38	-61.0	0.38	061	061	062	058	063	058	0.15	03:02
-60.0	0.40	-58.3	0.33	-60.8	0.39	-61.1	0.38	060	060	062	057	062	057	0.17	03:03
-59.9	0.40	-58.3	0.32	-60.8	0.38	-61.0	0.38	061	061	063	058	064	058	0.14	03:04
-59.9	0.40	-58.3	0.32	-60.8	0.38	-61.1	0.38	061	061	063	058	064	058	0.13	03:05
-59.8	0.40	-58.3	0.32	-60.7	0.38	-61.1	0.38	061	061	063	058	064	058	0.14	03:05
-59.4	0.40	-58.4	0.32	-60.9	0.38	-61.2	0.38	061	061	063	059	064	059	0.17	03:10
-59.9	0.40	-58.4	0.32	-60.8	0.38	-61.2	0.38	061	061	063	059	064	059	0.15	03:20
-59.8	0.40	-58.3	0.32	-60.8	0.38	-61.1	0.37	062	062	063	059	064	058	0.16	03:30
-60.0	0.40	-58.5	0.32	-61.0	0.39	-61.3	0.38	061	062	063	059	064	059	0.16	03:40
-59.9	0.40	-58.4	0.31	-60.9	0.37	-61.2	0.37	063	062	064	060	065	059	0.17	03:50

Figure 2.1. Sample of printer output showing manual information entry, stored heading, and automatic data collection features.

starting voltage decreases and the slope of the curve becomes steeper. The clean-plate V-I curves are compared with a theoretical curve predicted by a computer model similar to that in Reference 4. Figures 2.2 through 2.5 compare the results of the measurements and model predictions. The input parameters for the model are the same as the physical dimensions of the electrical section: wire diameter is 0.3175 cm; wire-to-plate spacing is 0.127 m; wire-to-wire spacing is 0.305 m, giving four wires per section; single-plate area is 1.5 m^2; and the roughness factor is 1.0.

The temperatures used in the model were typical of those measured between the sections. The ion mobility used obeyed the power-law relation:

$$\mu(T) = 1.684 \times 10^{-4} \left(\frac{T}{273}\right)^{1.63} \ m^2/V\text{-sec} \qquad (2\text{-}1)$$

where T is the absolute temperature in kelvins. This temperature dependence is considerably stronger than expected (where the exponent is equal to 1.0), but was experimentally derived from mobility measurements on laboratory air using a Beta/VII Plasma Chromatograph.* The value of mobility at any temperature affects primarily the slope of the V-I curve. Predicted and measured slopes are in good agreement.

The disagreement between theory and experiment, in terms of starting voltage and low current characteristics, is not explained simply. Part can be attributed to localized corona emitted from a small area; i.e., the Trichel pulses. A surface irregularity may allow the corona to be initiated at that point at a voltage much lower than the model predicts. For higher voltages, the glow discharge envelops the whole corona wire, as the model assumes. The small slope of the V-I curve, in the low current portion of the experimental data, is probably due in part to the waveform of the applied voltage. Full-wave-rectified unfiltered dc voltage has a peak value considerably higher than its average value. Thus for a part of the cycle, corona initiation can occur, even though the average voltage is less than the corona start voltage. This effect was not suspected when the V-I curves

*An ion-mobility spectrometer manufactured by the Franklin GNO Corp., P.O. Box 3206, West Plam Beach, FL 33402.

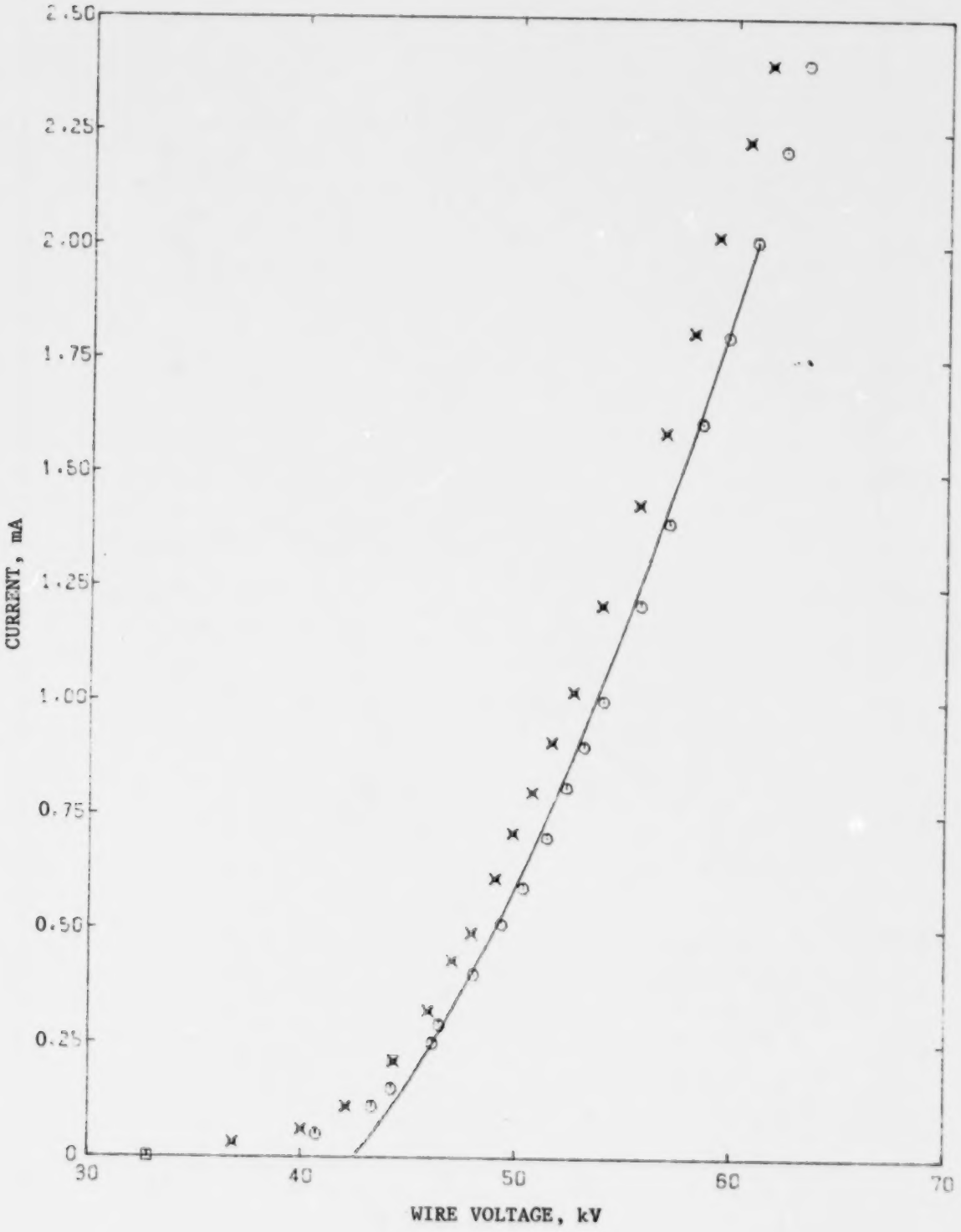

Figure 2.2. Theoretical V-I curve and experimen al data points at 20°C (68°F). o - Section 2; x - Section 4; □ - calculated starting voltage.

Reproduced from best available copy.

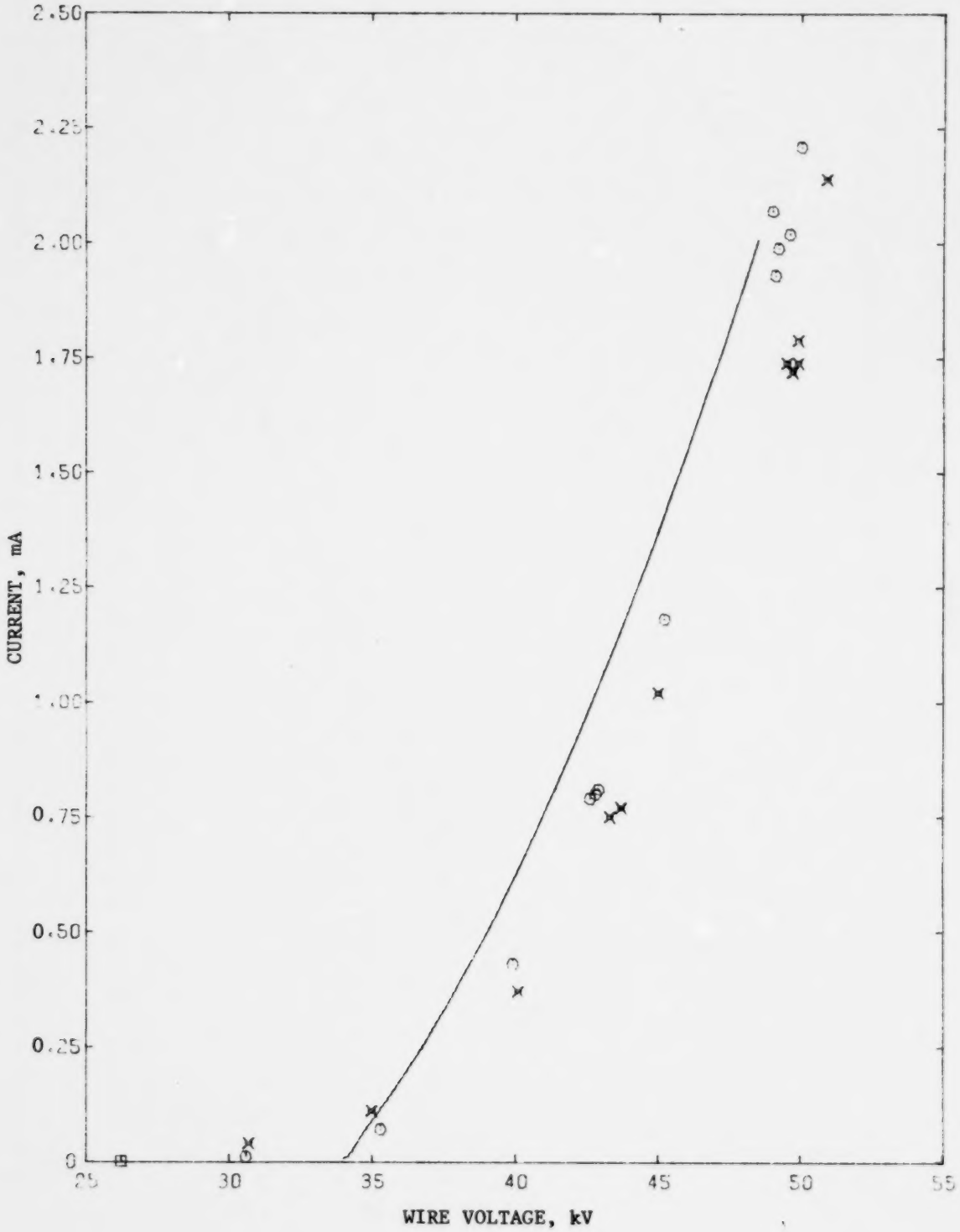

Figure 2.3. Theoretical V-I curve and experimental data points at 118°C (245°F). o - Section 2; x - Section 3; □ - calculated starting voltage.

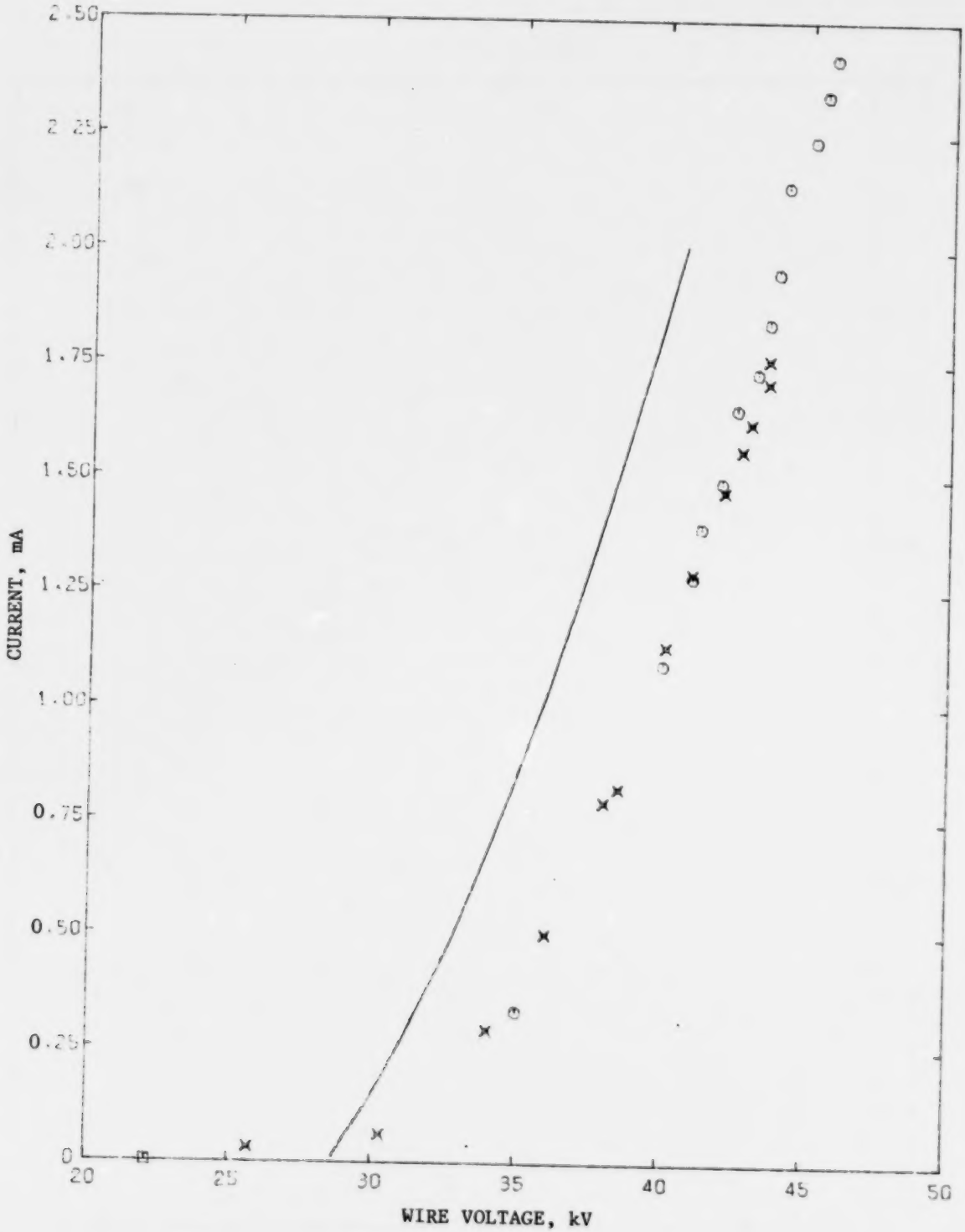

Figure 2.4. Theoretical V-I curve and experimental data points at 216°C (421°F). o - Section 2; x - Section 3; □ - calculated starting voltage.

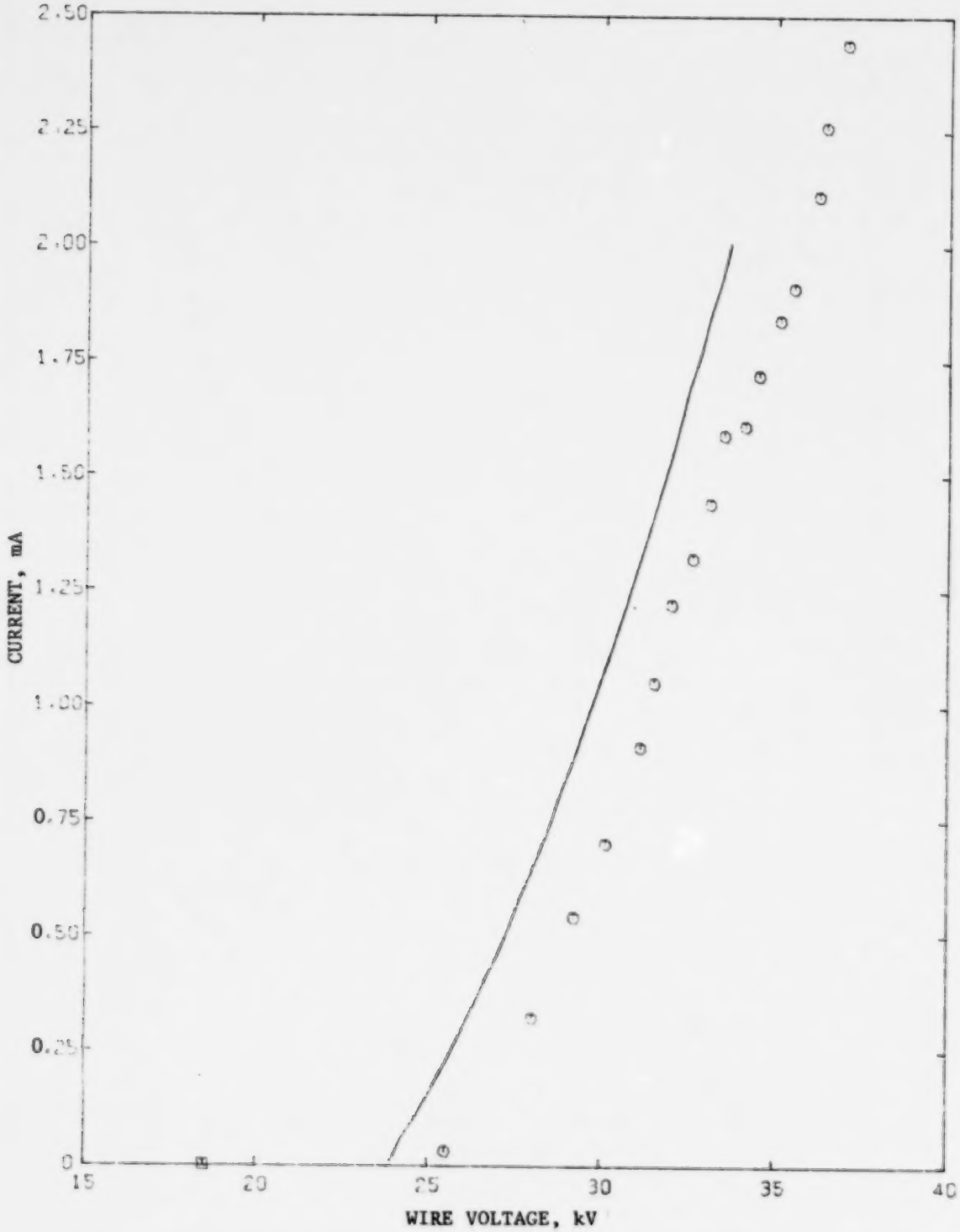

Figure 2.5. Theoretical V-I curve and experimental data points at 350°C (662°F). o - Section 2; □ - calculated starting voltage.

were measured, and so cannot be quantitatively tested. In the future, V-I curves should be measured with filtered dc.

The model under-predicts the starting voltage as the temperature rises; this is apparent as a voltage offset between the theory and experimental points, and is a deficiency in the model that bears further investigation.

Some V-I curves were also measured after the precipitator had been in operation with fly ash for an extended period. The collection plates were thoroughly rapped before the measurement. The theoretical model cannot yet account for the effects of dust on the plates and corona wires, so the experimental data are shown, in Figure 2.6, along with the predicted theoretical curve for clean-plate conditions. The experimental points exhibit both an offset to lower voltages, which can be explained as an increased roughness of the wires, and a hysteresis between increasing voltages and decreasing voltages. This hysteresis is associated with the presence of dust, and is probably an indication of back-corona. The arrow in Figure 2.6 indicates a point of sharply increasing current, characteristic of the onset of back-corona. Back-corona was expected with the current density and ash resistivity used for this test. Laboratory measurements indicate that the resistivity of the dust at the experimental conditions of gas moisture content and temperature was about 10^{12} ohm-cm.

3.0 TEMPERATURE CONTROL AND MEASUREMENT

The pilot-scale ESP has two separate temperature measuring systems. The first is in the control module, near the ESP inlet. The second is the operating measurement system which gives the temperature of the gas stream at numerous points along the length of the ESP. Both systems use thermocouple transducers to measure temperature. Figure 3.1 shows the locations of the thermocouples on the ESP.

3.1 Control and Measurement Thermocouple Placement

The two control thermocouples (1 and 2) are symmetrically above and below the midline of the precipitator. Thermocouple 1 is an over-temperature cutoff sensor which shuts down the burners at a predetermined temperature. Thermocouple 2 is the controller which is servoed to the burners. The controller has both proportional and rate-proportional action, and the

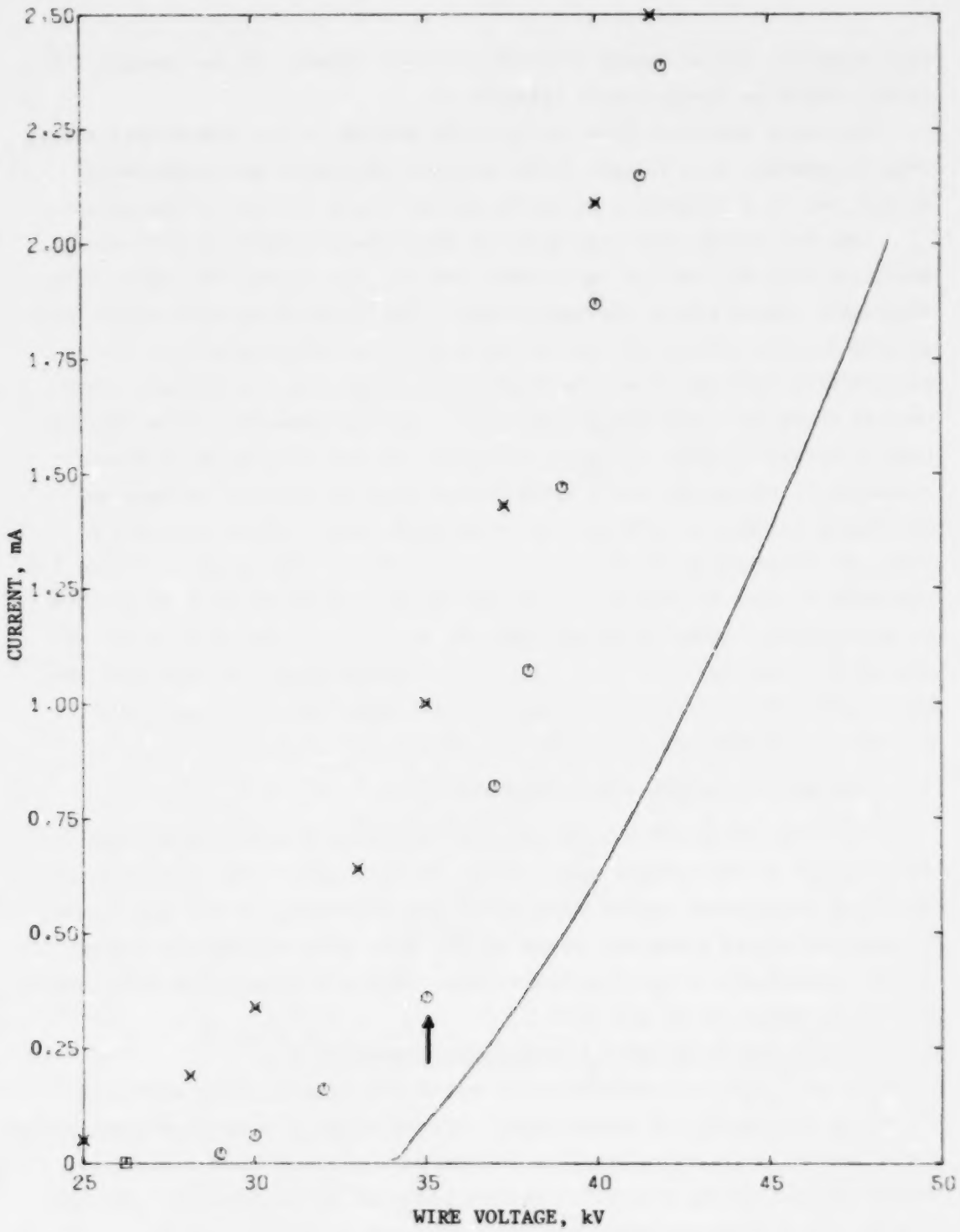

Figure 2.6. Dirty plate data. The curve is the clean plate theoretical characteristic. o - data points for increasing current; x - data points for decreasing current; □ - calculated starting voltage. Arrow indicates change of slope.

temperature at equilibrium, as measured by the controller, is stable within ± 5°C.

The measuring thermocouples for the ESP electrical sections are between sections of the ESP inlet and outlet. Thus, the average temperature of any section can be computed, as well as the temperature gradient along the length of the ESP. Thermocouple F (in Figure 3.1), at the flow measuring orifice, determines gas temperature, a factor in measuring gas flow.

3.2 Temperature Profile

With the burners at the inlet end, there is a thermal gradient along the length of the ESP, due to heat losses through the ESP walls. Electric heater strips, inside the ESP walls, correct for these losses. Each electrical section has separate heaters in the upper and lower halves of the walls, with power controls for each group in each section. These heaters have almost no measurable effect at 350°C, the maximum operating temperature. At much lower temperatures, the measured temperature can be raised by 5 to 10°C. (Note that measurements have not yet been made near the bottom of each section. Note also that the heaters can be expected to have more effect there.)

Figure 3.2 shows a plot of the temperature profile along the ESP at a nominal operating temperature of 350°C. The temperature drop is 43°C along the ESP length, or about 10°C per section. The total change, about 7 percent in absolute temperature, is rather small. The point at location F indicates that the temperature continues to drop in the outlet pipe, but is not related to the gradient through the precipitator proper.

3.3 Time to Equilibrate

Figure 3.3 shows the ESP approaching normal operating conditions. It is a plot of temperatures measured from a cold start to a nominal 350°C operating temperature. The burner control was advanced in stages to avoid excessive temperature overshoot in the first hour, which is reflected in some of the surges measured by thermocouple A. The temperatures are near equilibrium after the first hour, and change only a few percent after that. Thermocouple A shows the greatest variation since it is the most responsive to changes in burner output. For operation at lower temperatures, the

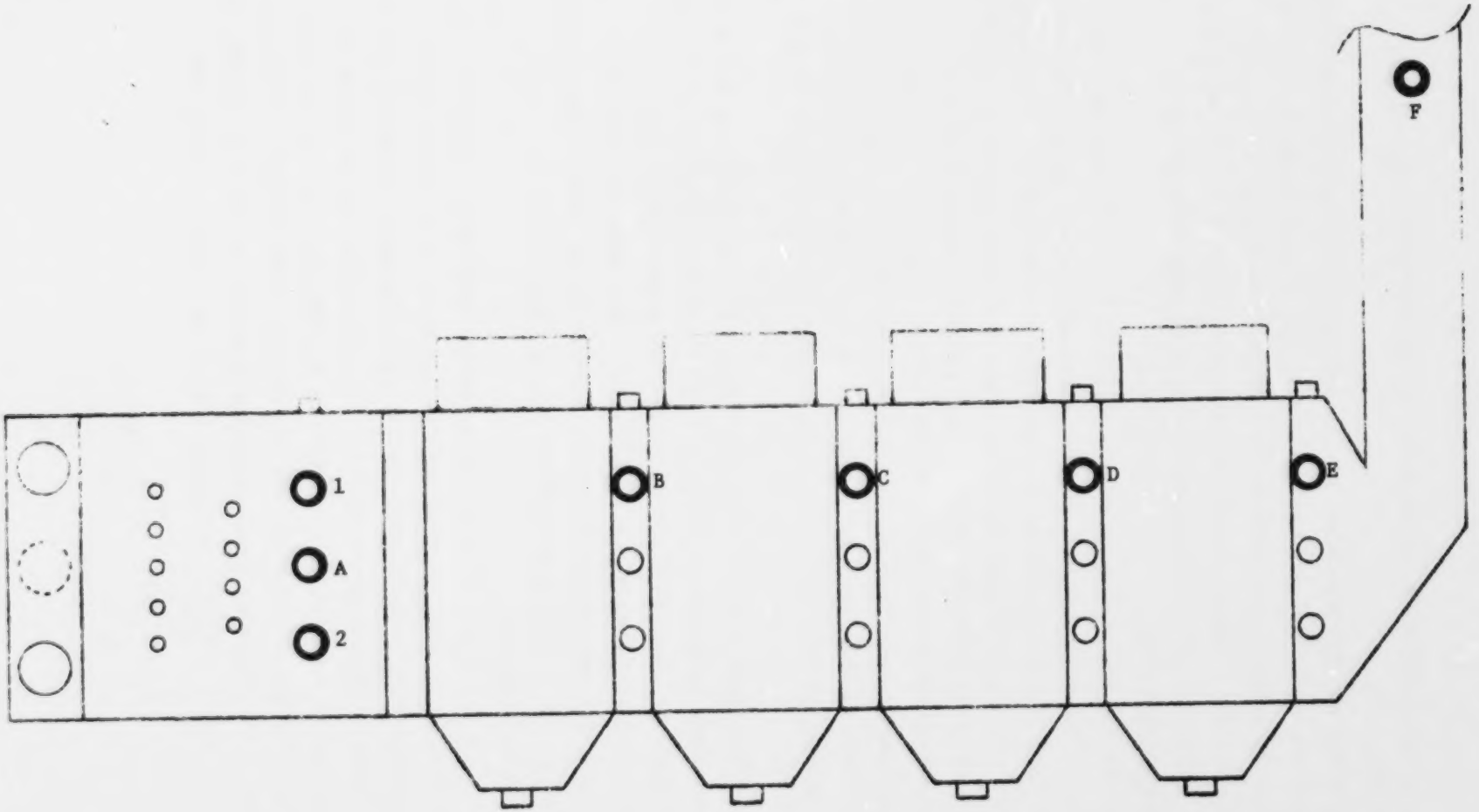

Figure 3.1. Location of thermocouples on the ESP.

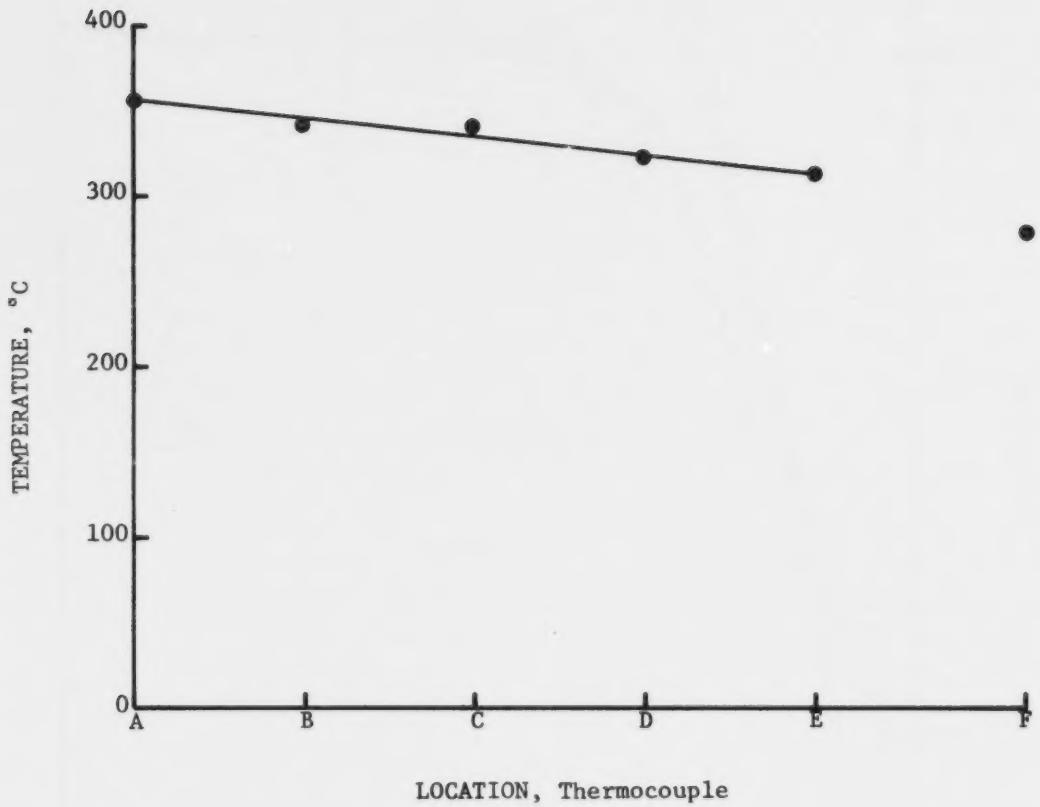

Figure 3.2. Temperature profile along the ESP.

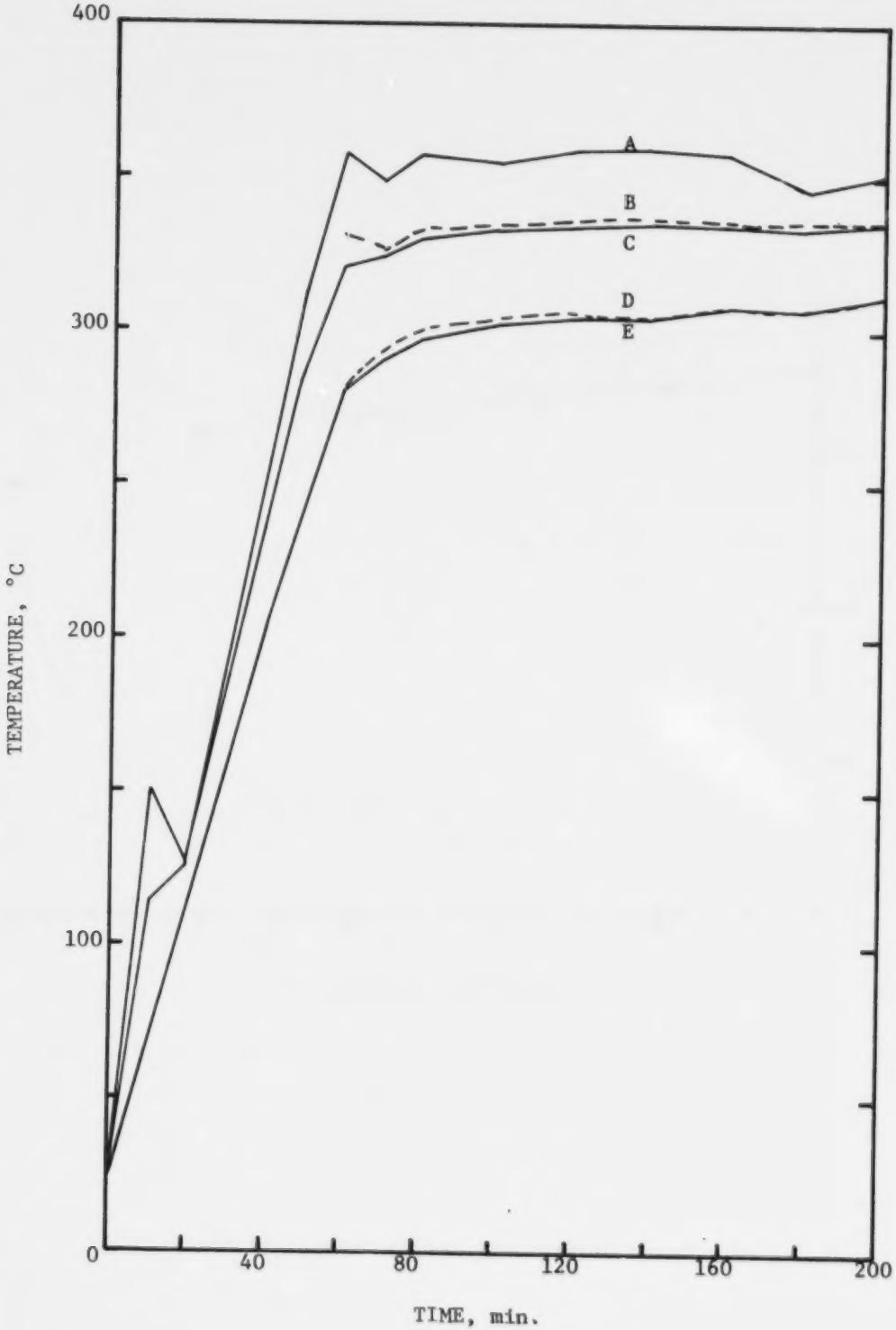

Figure 3.3. Approach of ESP to operating temperature.

approach to equilibrium can be accelerated by judicious allowance of temperature overshoot at the inlet.

In achieving the operating temperature, using all three burners (rated at 0.5×10^6 Btu/hr each) gives the most rapid rate of rise. Once the steady state condition is obtained, a single burner has sufficient operating margin to maintain the equilibrium temperature, at least for moderate airflow rates.

3.4 Uneven Temperature Distribution

In addition to the temperature gradient along the length of the ESP, there is also a vertical gradient at any point within the ESP. This has not been carefully measured over the length of the ESP, but the following observations have been made:

1. The controlling thermocouple (No. 2) is 0.3 m below the over-temperature thermocouple (No. 1).
2. During high burner output, thermocouple 1 indicates temperatures as much as 80°C higher than thermocouple 2.
3. When equilibrium is approached, the difference decreases to about 45°C.
4. Measurement thermocouple A also reads a higher temperature than thermocouple 1 under these conditions.

Operating the ESP with only the lowest burner can reduce the difference between thermocouples 1 and 2 to about 30°C. This also slightly reduces the gradient along the length of the ESP: thermocouples A and B read somewhat lower than with all burners on, and thermocouples C and D read slightly higher.

The magnitude of the vertical temperature gradient in each section remains to be measured, and compensated for by the use of the heaters within the walls.

4.0 GAS FLOW DISTRIBUTION

The gas flow distribution for an ESP includes both the variation of gas velocity across the ESP channel and sneakage, the percentage of flow that bypasses the active collection area. The gas velocity variation can be described in terms of linear flow velocity; however, sneakage is more properly described as more-difficult-to-measure volume flow.

4.1 Measurement Techniques

Gas velocity distribution was measured, for set flow rates and plate spacings, by traversing the channel from wall to wall at each sampling port, using a hot-wire anemometer. For wide plate spacings, traverse points were 2.54 cm apart; for the narrowest plate spacing, the traverse points were 1.27 cm apart.

Three sampling ports are between each pair of sections and at the inlet and outlet. They are spaced 0.305 m apart in line, and the center port is at the midline of the ESP. The wall separation at the position of the inlet ports is 33 cm. A movable set of plates provides a transition to the first section's collector plates. Similarly, at the outlet, a second set of transition plates connects the outlet collector plates to the exhaust duct. In this case, the sampling ports penetrate the transition plates, so that the actual spacing depends on the setting of the adjacent collector plates.

Although sneakage is a volume flow concept, the measurement of sneakage was performed with linear velocities. The hot-wire anemometer was inserted in sampling ports on top of the ESP, between each pair of sections and at the inlet and outlet, and also through the hopper drain at the bottom of each section. These measurements were taken near baffles in both the upper and lower parts of the ESP; the baffles would be expected to have considerable influence on the velocities obtained.

4.2 Flow Velocity Results

Flow velocity distribution is presented in two ways: as a contour plot of flow velocity throughout the volume of the channel; and as a plot of mean velocity as a function of location along the ESP. Figure 4.1 is a typical contour plot; although the velocities are in metric units, the traverse locations are in English units for convenience.

The contours correspond to mean velocity and to mean velocity $\pm n\sigma$, where σ is the standard deviation of the velocities measured. The flow is reasonably uniform over the major cross section of the ESP. A depression of gas velocity near the ESP center line corresponds to the position of the corona wires. Appendix A shows contour plots for various spacings and flow velocities.

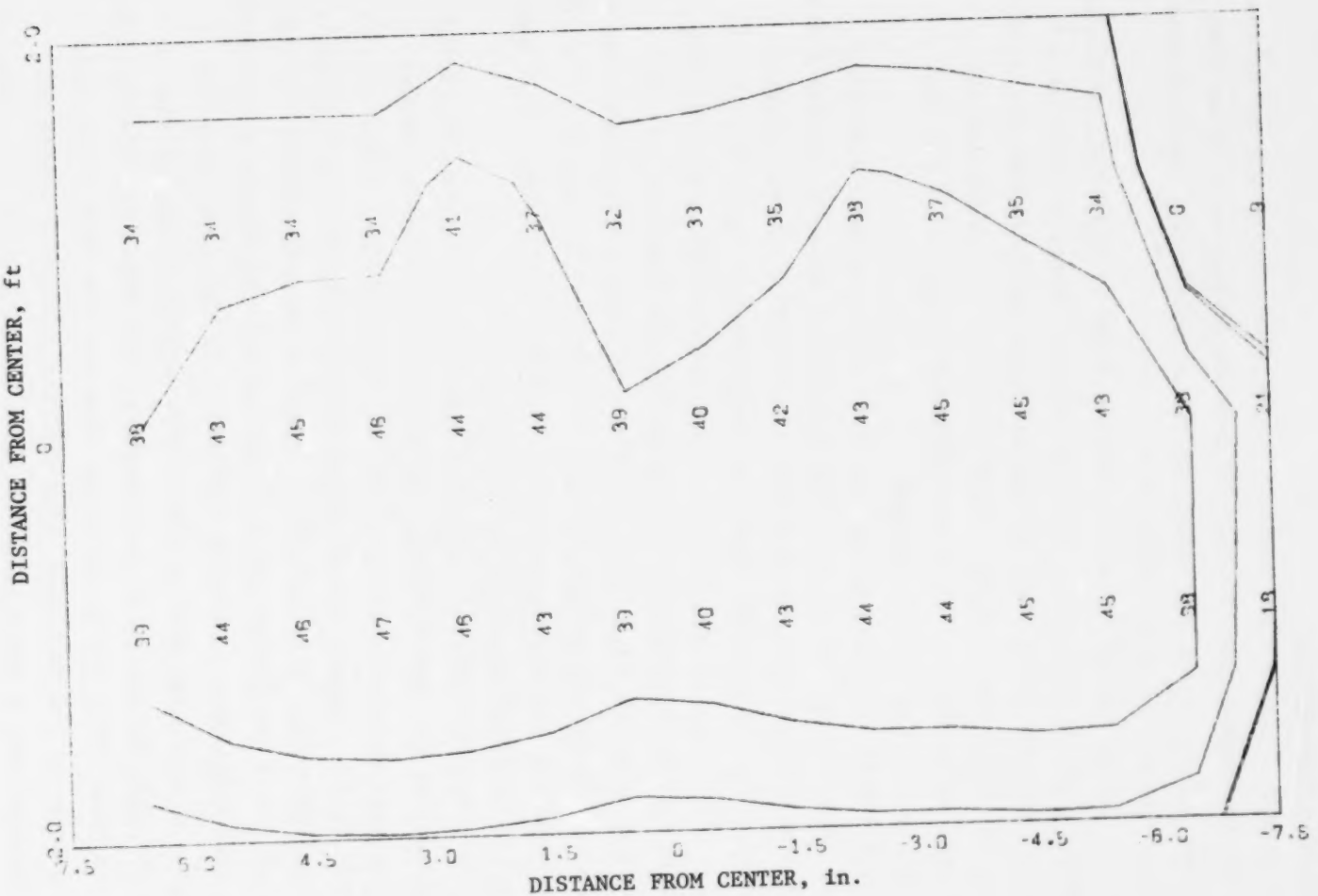

Figure 4.1. A typical velocity contour plot. Numbers in the plotting area are measured velocities in meters/min. The mean velocity is 38.4 meters/min (126 ft/min).

Reproduced from best available copy.

4.3 Sneakage Measurements

Since only a linear flow velocity was measured at the top and bottom of the ESP to characterize sneakage, it must be related to a volume flow rate by multiplying by an appropriate cross-sectional area, and presented as a percentage of the total volume flow.

At the top of the ESP, where the corona frame is suspended, no corona is generated, and so no particle charging occurs. However, there is a substantial electric field, and charged particles entering that region will be collected. The cross-sectional area of the top of the precipitator changes with plate spacing and is approximately 9 percent of the total cross section for flow at all spacings.

A single baffle extends across the flow channel between electrical sections, from the roof of the precipitator to just below the corona frame. Velocity measurements indicate that this single baffle is remarkably ineffective. Flow velocities, measured from within 2.5 cm of the roof to well below the baffle, ranged from 80 to 100 percent of the average flow velocity in the duct; however, the component of the flow in a vertical plane was not measured. This held true for all plate spacings used. On a volume flow basis then, sneakage through the top section amounts to 7-9 percent, at least for uncharged particles. For charged particles, since some collection is possible, sneakage would be less.

At the bottom of the precipitator, 15 cm deep vertical baffle plates form the floor of the flow channel. The movable plates can be removed easily to change the configuration. For these measurements, there were 17 baffles per section, spaced 7.5 cm apart, with spacing determined primarily by wire configuration. A second baffle below the movable baffles minimizes the flow of gas in the lowest parts of the hopper. The hoppers are inverted pyramids with cross-sectional areas independent of the collector plate separation. However, the area of the baffles exposed to the gas flow is directly dependent on collector plate spacing. The effective cross-sectional area is therefore difficult to calculate; however, its upper bound would be about 20 percent of the duct area. Measured gas velocities within the hopper, averaged over a vertical traverse, ranged from about 10 percent of

the mean gas flow velocity (at the widest plate spacing) to about 15 percent (at the closest plate spacing). This places an upper bound on sneakage through the hoppers at 3 percent, for both charged and uncharged particles.

4.4 Variation of Velocity Through the ESP

Although plate spacing is variable, the inlet and outlet duct sizes are fixed. Transition plates reduce the abruptness of the change in cross section. Figures 4.2 through 4.4 illustrate the effects of the change in size from inlet to outlet. Because the port locations shown do not strictly correspond to physical separations, the curves indicate trends rather than actual variation with distance. The axis is offset to indicate this. There is no plate spacing which minimizes the disturbance produced by both inlet and outlet simultaneously. Either the outlet produces a disturbance that extends upstream for wide plate spacings and high flows, or the inlet disturbance propagates downstream for narrow plate spacings at all flows.

A measure of the smoothness of flow throughout the ESP is the standard deviation of velocities about the mean value. A convenient number to use is the normalized standard deviation, equal to the standard deviation divided by the mean.

Within any single section, the normalized standard deviation is a measure of the uniformity of velocity across the duct flow area, and indicates how uniformly dust is carried through the ESP. Over the entire ESP, the normalized standard deviation measures, in addition to the cross-sectional variations, the longitudinal variation of velocity. In general, the smaller the normalized standard deviation, the better, because the collection of particles is not linear in transport velocity, but rather in residence time. Therefore, variations in velocity about a mean value do not average out in the collection of dust, and the overall efficiency with a varying velocity is lower than for the case when all the particles are transported at the mean velocity.

Table 4.1 gives examples of the normalized standard deviation for different plate spacings and flow rates for the entire ESP, and ranges for sectional normalized standard deviations. The narrowest plate spacing has the highest deviations for two reasons: the variation in velocity from

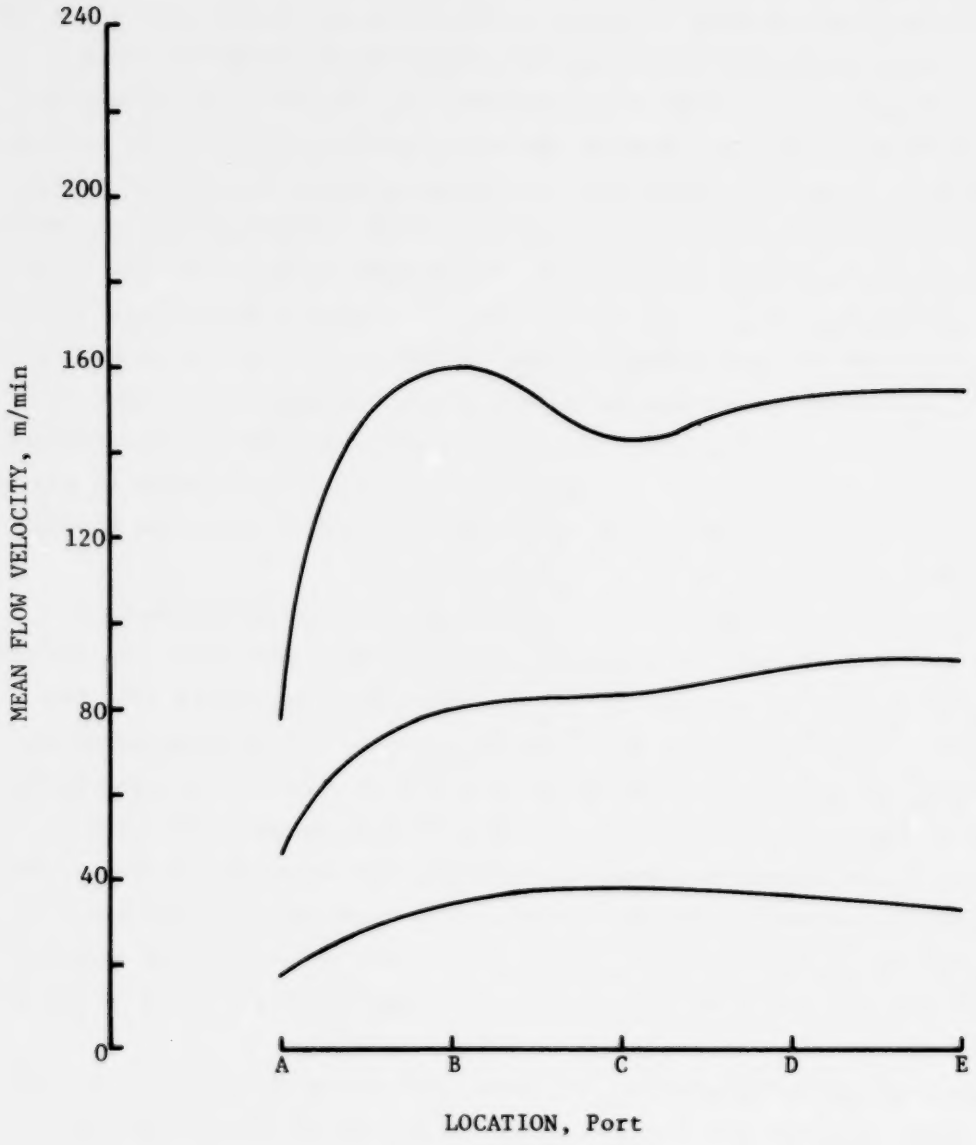

Figure 4.2. Variation of flow velocity with location. Plate spacing is 12.7 cm with three flow rates.

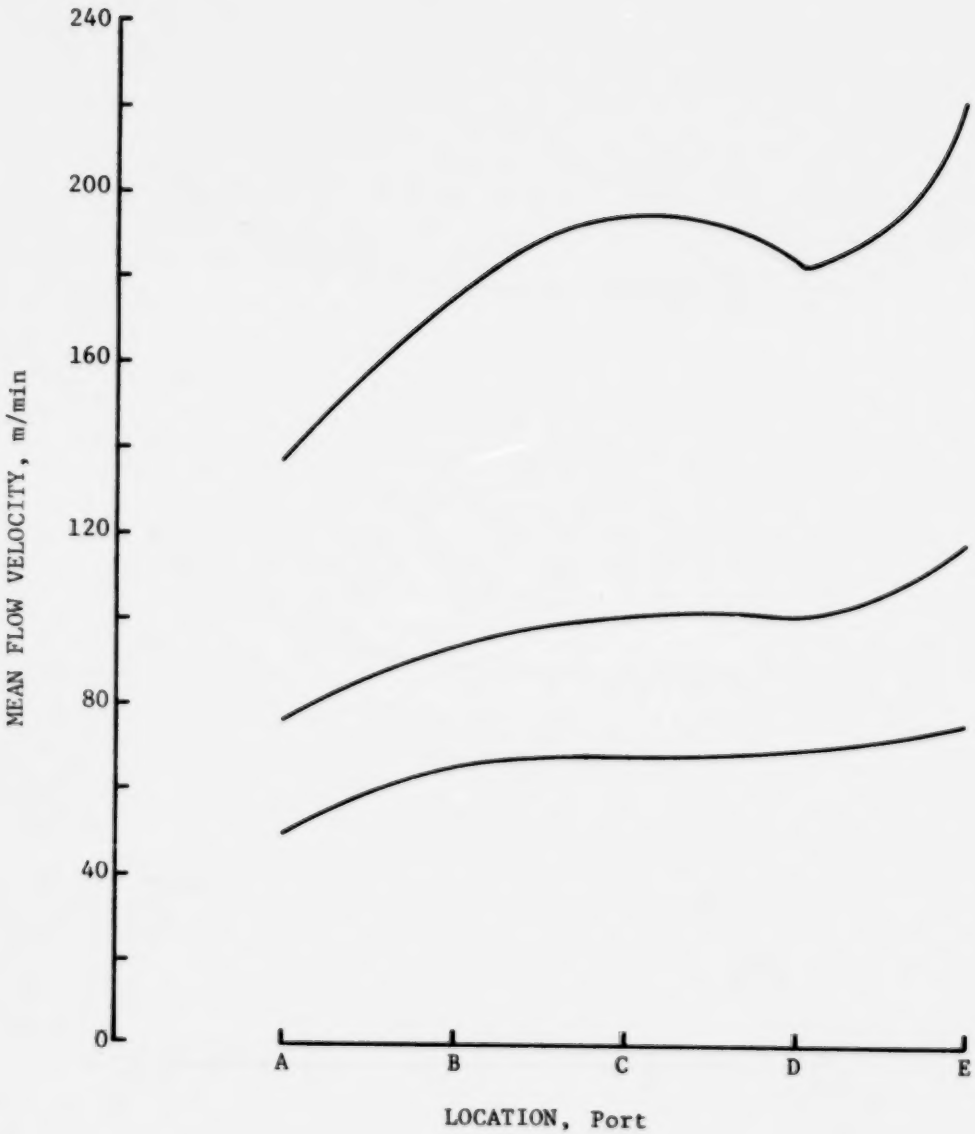

Figure 4.3. Variation of flow velocity with location. Plate spacing is 25.4 cm with three flow rates.

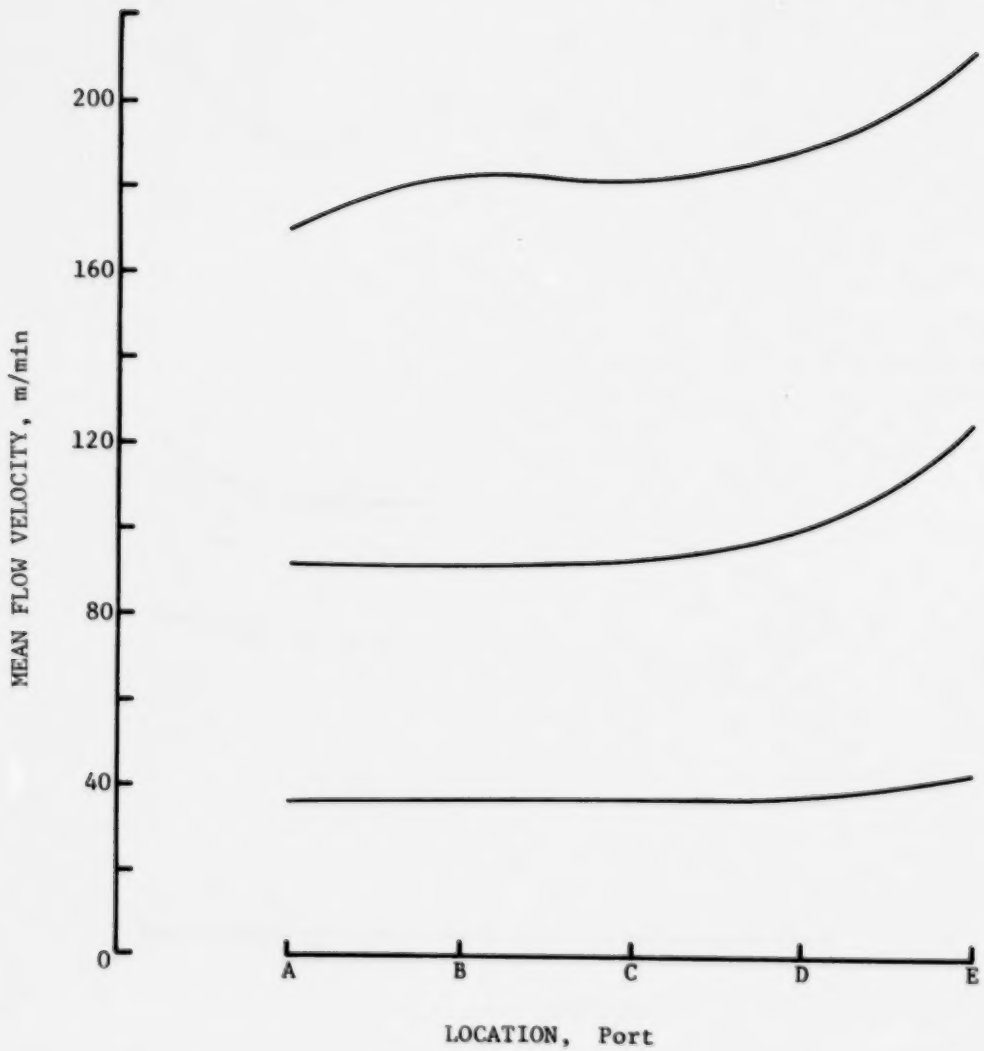

Figure 4.4. Variation of flow velocity with location. Plate spacing 38 cm with three flow rates.

inlet to outlet is the greatest for this case; and, because sectional velocity traverses were taken with half the step size used on the spacings, the measurements include more of the low-velocity boundary layer points near each wall. The latter effect lowers the mean value in each section and increases the normalized standard deviation of each section, except for the inlet section.

TABLE 4.1. NORMALIZED STANDARD DEVIATION

Plate Spacing	38 cm		25 cm		13 cm	
Volume Flow Rate	Velocity, m/sec	NSD	Velocity, m/sec	NSD	Velocity, m/sec	NSD
Low	38.4	0.46	65.6	0.37	31.4	0.56
Medium	100.7	0.45	98.5	0.43	78.4	0.66
High	188.0	0.49	182.0	0.58	138.0	0.58
Range of NSD in each section	0.15-0.25		0.10-0.20		0.05-0.38	

The overall standard deviation is needed when the ESP is to be described in terms of a single mean gas velocity. If more detailed calculations allow for sectional values of gas velocity, then sectional values for the normalized standard deviation are appropriate.

5.0 AEROSOL GENERATION AND DISPERSION

5.1 Aerosol Generator

Aerosol can be injected into the ESP at five ports, in a vertical line upstream of the controlling thermocouples. Aerosol is injected at these ports using low-cost, commercial, pneumatic sandblast guns, operating at an air pressure of 2×10^6 to 8×10^6 Pa (10 to 60 psig). At 3×10^6 Pa (15 psig), a volume flow of about 15.5 ℓ/s (10 scfm) is required.

Dust is delivered by an Acrison* screw-feeder to a single sandblast hopper. The flow of air through each gun creates a reduced pressure which

*Acrison, Inc., 20-T Empire Boulevard, Moonachie, NJ 07074.

draws the dust from the hopper and injects it into the ESP. Tubes in the ESP direct the dust from each gun into the face of the air flow to maximize its dispersal. If the supply air is kept dry, the guns should not clog.

Several gun configurations were tried, trying for the most uniform distribution of dust at the ESP inlet. Extensive measurements were made for two configurations: one with three guns and one with two guns. Uniformity of distribution was determined by sampling with an MRI* impactor downstream of the injection site. Table 5.1 shows the total mass of particles collected for each configuration.

The two-gun operation was deemed satisfactory for use with the ESP and had the advantage of requiring less supply air. The maldistribution of particulate using three guns was traced to a combination of effects: difficulty in dividing the dust from the screw-feeder equally between the guns and partial blockage of the guns due to moisture in the supply air, a condition aggravated by the extra air required by the third gun.

Additional refinements of the two-gun technique involved individual pressure regulators and a dust-feed divider to give more even distribution of dust to the two guns. Under these conditions, the vertical normalized standard deviation was reduced to 0.14 at Section A. Measurements of the horizontal distribution, at the middle port of Section A, produced normalized standard deviations of 0.12 for a 25-cm plate spacing and 0.04 for a 38-cm plate spacing, indicating that the dust is well dispersed across the duct area.

Additional experiments showed considerable particle fallout in the inlet region of the ESP. To correct this problem, which made frequent cleaning necessary, a small cyclone was inserted in the line between the feeder and the sandblast guns. This cyclone effectively removed all particles larger than 10 μm (aerodynamic diameter). There is little fallout in the ESP when the cyclone is used.

5.2 Fly Ash Size Distribution

The utility fly ash used in the particulate distribution runs was also used in tests of the operating ESP. The inlet and outlet size distributions

*Meteorology Research, Inc., Box 637, Altadena, CA 91001.

TABLE 5.1. PARTICULATE DISTRIBUTION

Gun Arrangement*	Sampling Port	Port Location	Amount Collected mg
●	Upper	Section B, after first electrical section	68.6
0			
●	Middle		130.3
0			
●	Lower		26.9
			mean = 75.3
			NSD = 0.69
0	Upper	Section A, before first electrical section	73.9
●			
0	Middle		58.1
●			
0	Lower		89.5
			mean = 73.8
			NSD = 0.21
	Upper	Section B (traverse sampling)	67.1
	Middle		95.7
	Lower		146.0
			mean = 102.9
			NSD = 0.39

*The gun locations are blackened.

were measured with an MRI impactor. Figure 5.1 shows the results of a series of runs at 120°C operating temperature. Each curve is the average of six individual runs at the same temperature and flow rate. Log-normal curve fits to this averaged inlet data give a mass median diameter (MMD) of 22 μm with a geometric standard deviation of 3.3 for each. At a temperature of 350°C, the inlet MMD was 24 μm with the same standard deviation. The difference in MMDs is not significant.

The ESP was operated with three electrical sections energized: a power supply problem in the fourth section resulted in the outlet distributions shown in Figure 5.1. The MMD has been decreased to about 7 μm and the geometric standard deviation reduced slightly to about 3. Mass samples taken at the inlet and outlet indicated a collection efficiency of 98-99 percent under these conditions.

Figure 5.2 shows the fly ash size distribution with the cyclone. It is approximately log-normal with an MMD of 7 μm and a geometric standard deviation of 2.4.

Impactor data taken on the inlet size distribution over a long period of time indicate that the aerosol generator is very stable, both during a particular day's work and in day-to-day operation. Light absorption measurements made with an MRI Plant Process Visimeter also indicate stability.

5.3 Iron Oxide Size Distribution

A short series of experiments was conducted to determine the ability of the aerosol generator to feed iron oxide dust. Figure 5.3 shows the iron oxide particle size distributions.

The iron oxide tended to plug the sandblast guns, probably due to moisture in the air lines or in the dust itself. If the hoppers and feed lines could be heated to minimize the moisture problem, the aerosol generator probably would be able to operate successfully for long periods.

6.0 PLANNED FUTURE EXPERIMENTS

With the pilot-scale ESP in operation, attention has been given to the course of experiments planned for early investigation. These include experiments aimed at resolving current problems encountered in operating ESPs and at understanding the processes involved in precipitation.

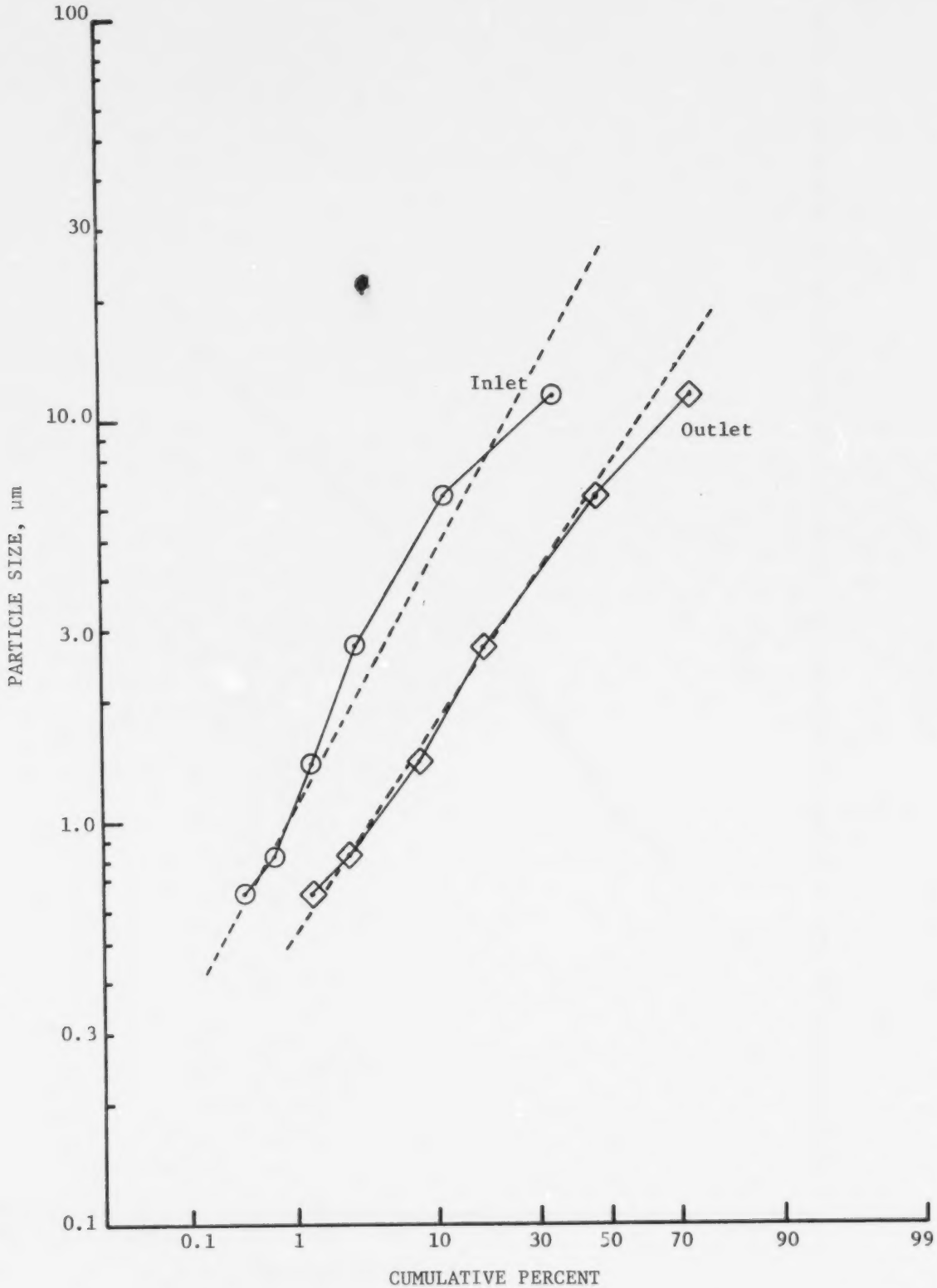

Figure 5.1. Inlet and outlet size distributions.

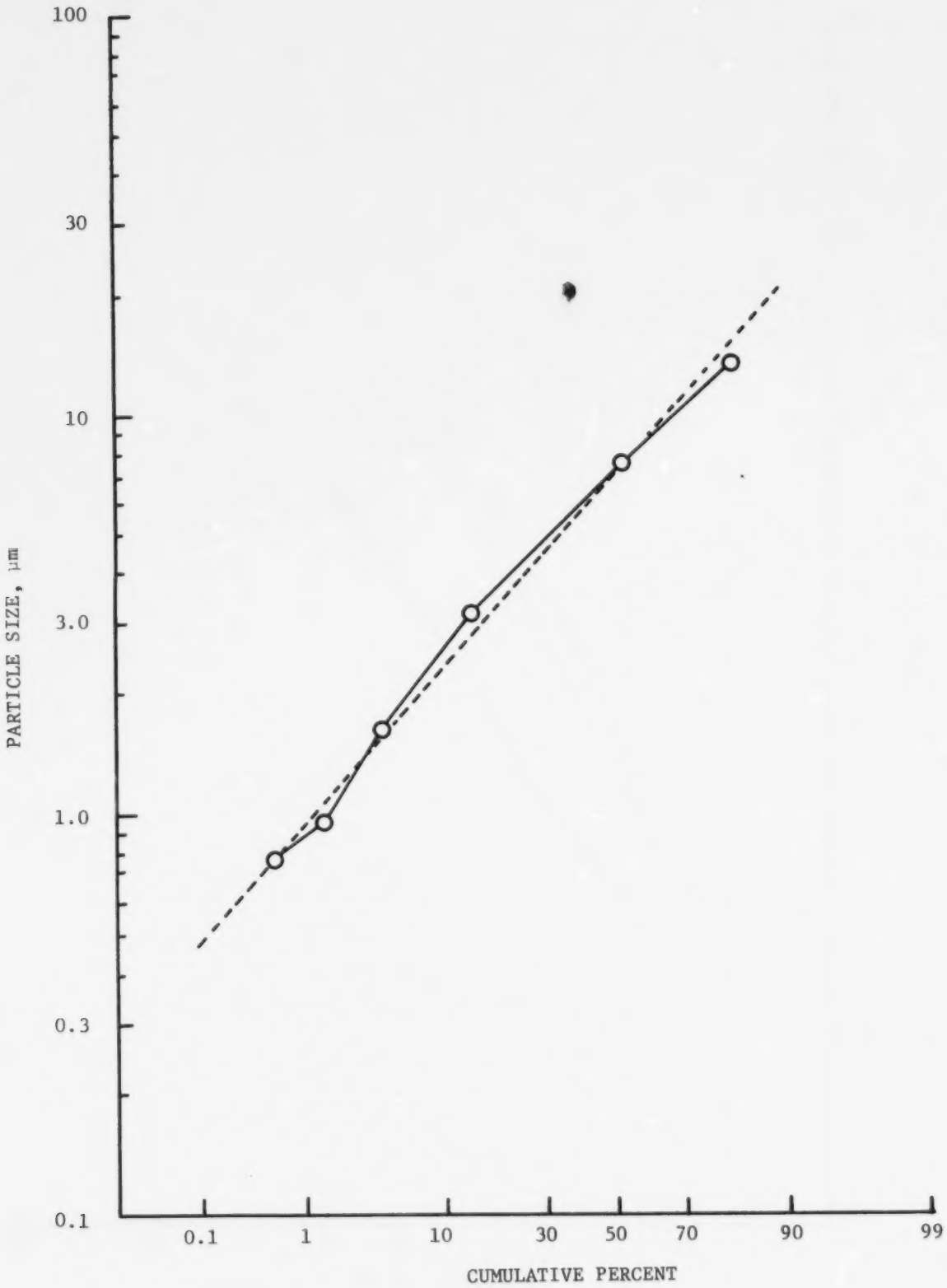

Figure 5.2. Inlet size distribution with cyclone.

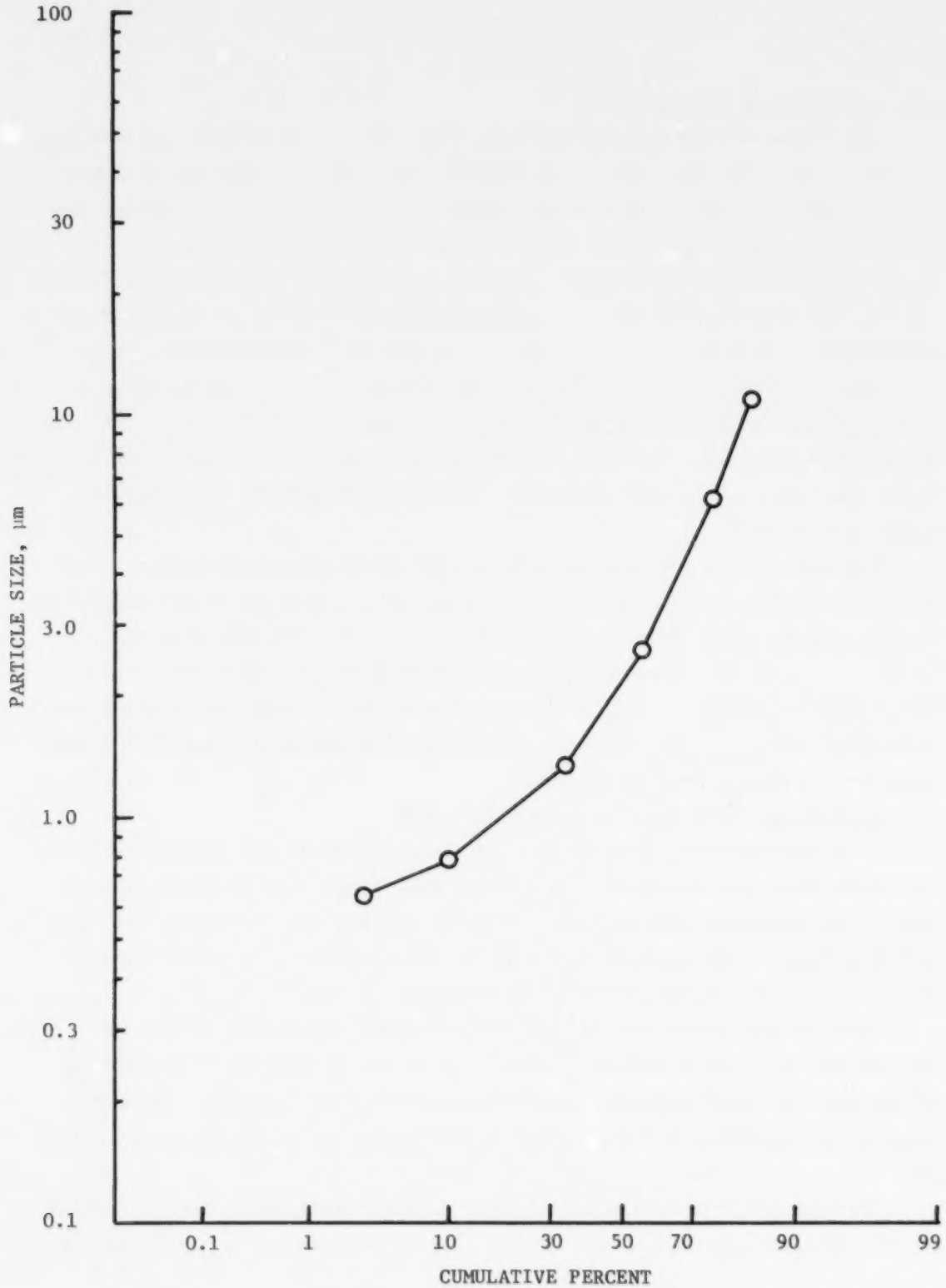

Figure 5.3. Inlet size distribution for iron oxide dust.

6.1 ESP/Scrubber Combinations

Venturi scrubbers are effective particulate control devices for moderate to large particles, but their effectiveness decreases rapidly for fine particles. Their actual effectiveness depends on the pressure drop across the venturi, with more fine particles collected at higher pressure drops. The energy expended in collection increases proportionately with pressure drop.

It has been claimed that, if the particulate entering the scrubber is electrically charged, the collection efficiency for fine particles can be enhanced without requiring a high venturi pressure drop. A moderately efficient ESP could thus be teamed with a low pressure drop scrubber to obtain the collection efficiency of a high pressure drop scrubber, but at a lower operating cost. Some commercial control devices have been designed using this concept.

The pilot-scale ESP will be used to test this collection scheme. ESP operating conditions can be varied to approximate a moderately efficient ESP to feed the scrubber, and it can also be turned off. The ESP's aerosol injection system will provide the proper loading for the scrubber as the ESP/scrubber combination. Particle penetration (as a function of size) and collection efficiencies of the two configurations will be compared to determine the merits of the combination.

6.2 Comparison of Eastern and Western Fly Ash

Some western high altitude ESPs fail to operate at the efficiencies for which they were designed, and compare unfavorably with similar eastern ESPs. The operating characteristics of the western units suggest that they are in a back-corona regime, even though coal resistivity is in the range where back-corona is not normally encountered.

Back-corona may be due to some as yet unexplained location-related phenomenon, such as an altitude effect, or it may be related to a property of the fly ash other than its resistivity. The first cause must be investigated in the field, but the second can be investigated in the pilot-scale ESP.

Eastern and western fly ashes of comparable resistivity will be tested in the ESP, with particular care given to the measurement of V-I curves to

detect back-corona. The collection efficiency of each type will also be measured. The overall objective of the experiments will be to determine if western fly ash characteristics degrade ESP performance significantly more than those of eastern fly ash.

6.3 Variations of Wire and Plate Geometry

Considerations of particle charging in an ESP show that the particles acquire most, if not all, of their charge in the first few feet (or even inches) of the ESP. Thereafter, only the precipitation operation occurs. Precipitation is a function of electric field only, and the objective of maximizing electric field can be met by raising the operating voltage of the later sections. Back-corona and sparking can occur, however, if the current in the section increases as the voltage increases.

It is possible to change the V-I characteristics of a given electrical section by varying wire-to-plate spacing, wire-to-wire spacing, and wire diameter. The precise effects of these variations are described in Reference 1. The goal of experiments on the pilot-scale ESP will be to determine the effectiveness of raising the operating voltage at a given current by varying the geometry of the wires and plates, both with regard to collection efficiency and control of back-corona and sparking.

6.4 Residence Time Experiments

Models of the precipitation process show a non-linear dependence of the collection efficiency of particles on the length of time spent in the ESP. The dependence is such that an ensemble of particles moving with instantaneous velocities widely distributed around a mean value is collected less efficiently than another ensemble of particles all moving at the same mean velocity.

Approximations of this behaviour have been made in the models, but the empirical evidence to test the models on this point is lacking. The pilot-scale ESP will be used to investigate experimentally the effects of residence time on ESP efficiency. Tracer studies and careful measurements of flow rate and direction will be made to determine the actual departures from ideal conditions and the effects of those conditions on collection efficiency. Methods of modelling this behaviour will be investigated in order to improve upon the approximations currently used.

7.0 SUMMARY AND CONCLUSIONS

The initial measurements and tests of the pilot-scale ESP indicate that it performs to or exceeds its specifications. The aerosol generator, though quite simple, performs well and is stable. Temperature control is good, although some work needs to be done to measure and, if need be, to correct the vertical temperature gradient. Electrical and temperature readouts are convenient and provide a quick permanent record of experimental conditions. The variable plate spacing and the easy access of the ESP allow rapid modification of the wire-duct geometry, which is a valuable experiment feature.

Some observations were made during the first few months of operation of other features of the pilot-scale ESP. The first is that automatic power supplies, which control operating voltage by detecting current or spark rate changes, are not needed for the ESP. (Manual supplies control current level adequately, and sparking is avoided in normal operation.) A second is that an automatic program to control the plate rappers would be desirable. (In several-hour test runs, the plates should be rapped on a regular schedule to realistically reflect the amount of dust reentrained during rapping.) A third is that some type of corona wire and corona frame rapping should be included, because significant amounts of dust accumulate on the wires and frame.

Future measurements will doubtless improve understanding of the capabilities and limitations of the pilot-scale ESP, but even now it is clear that it is a versatile research tool.

8.0 REFERENCES

1. Nichols, G. B. and J. P. Gooch. "An Electrostatic Precipitator Performance Model," EPA-650/2-74-132 (NTIS PB 238923), July 1972.
2. Gooch, J. P., J. McDonald, and S. Oglesby, Jr. "A Mathematical Model of Electrostatic Precipitation," EPA-650/2-75-037 (NTIS PB 246188), April 1975.
3. Work performed under EPA Contracts 68-01-4141 and 68-02-2612.
4. McDonald, J. R., W. B. Smith, H. W. Spencer, III, and L. E. Spar "Mathematical Model for Calculating Electrical Conditions in W Electrostatic Precipitation Devices," Journal of Applied Phys 2231, 1977.

APPENDIX A
ESP FLOW CONTOUR PLOTS

This Appendix contains flow contour plots for the ESP for three nominal channel widths and a number of flow conditions. Numbers in the plotting area are the measured values of flow velocity in meters per minute. For convenience, traverse point locations are in inches and the distance from the centerline in feet.* The unlabelled contour lines have the values of the mean of the measured velocities and the mean ± integer multiples of the standard deviation. All measurements were at ambient temperature. Locations of the sections referred to in this Appendix are in Figure 1.1. The fact that the width of Section A is fixed and that the width of Section E depends only slightly on plate spacing should be kept in mind.

*Readers more familiar with the metric system should convert these units to that system: in. x 2.5 = cm; and ft x 0.3 = m.

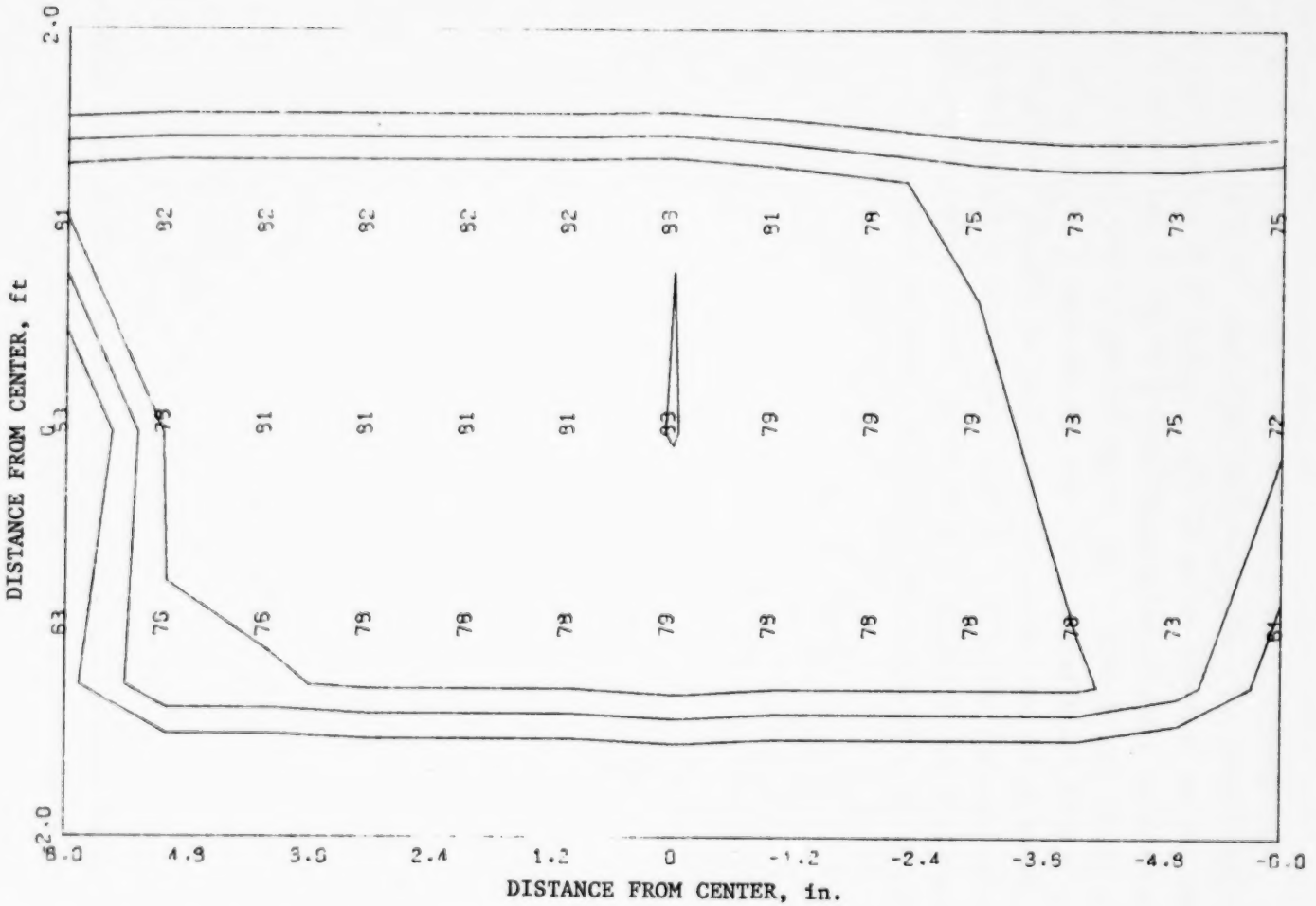

Figure A1.A. Flow distribution in nominal 5 in. channel. Velocities in m/min for a volume flow of 42 m^3/min. Section A.

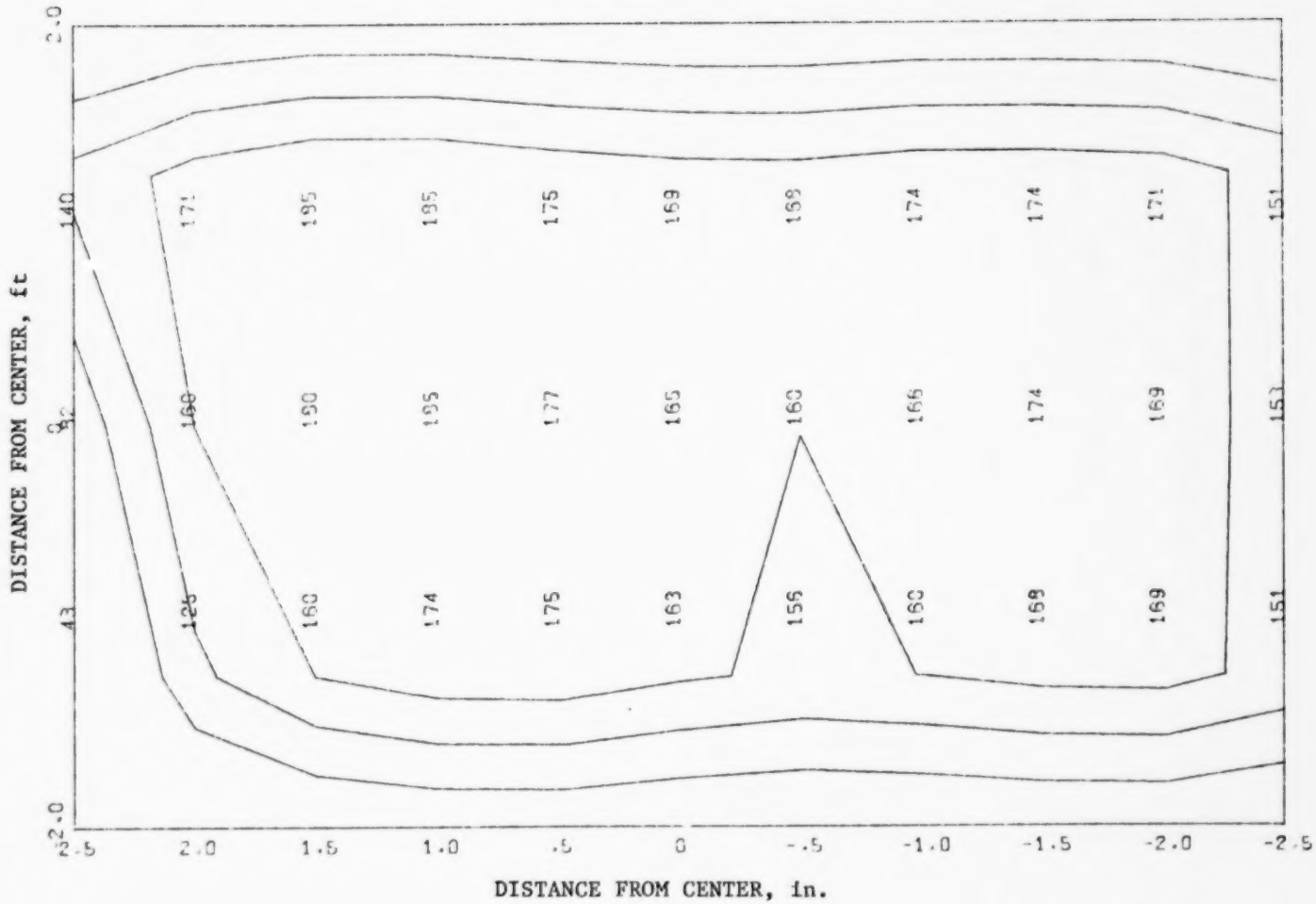

Figure A1.B. Same conditions as Figure A1.A. Section B.

Reproduced from best available copy.

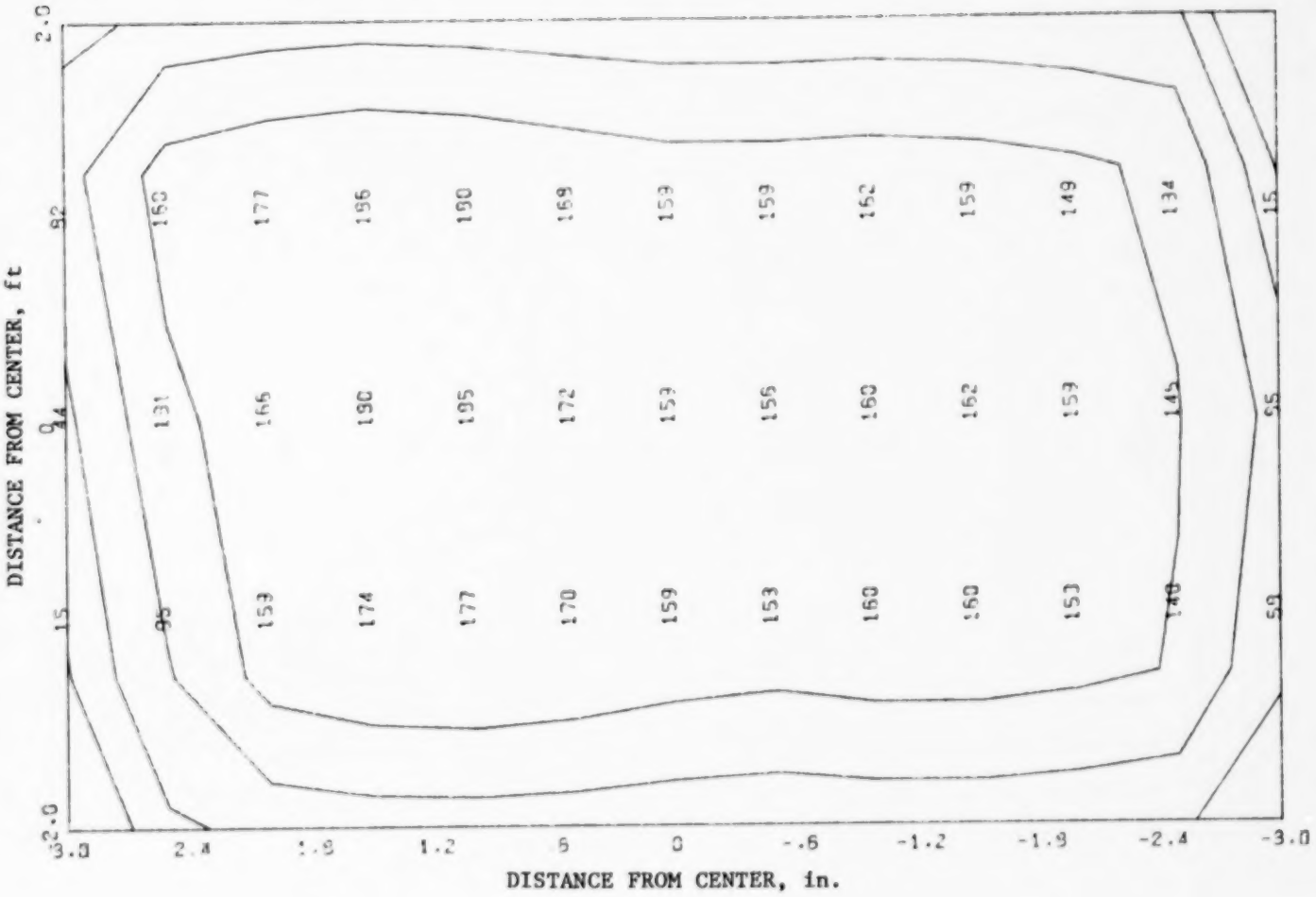

Figure A1.C. Same conditions as Figure A1.A. Section C.

Figure A1.D. Same conditions as Figure A1.A. Section D.

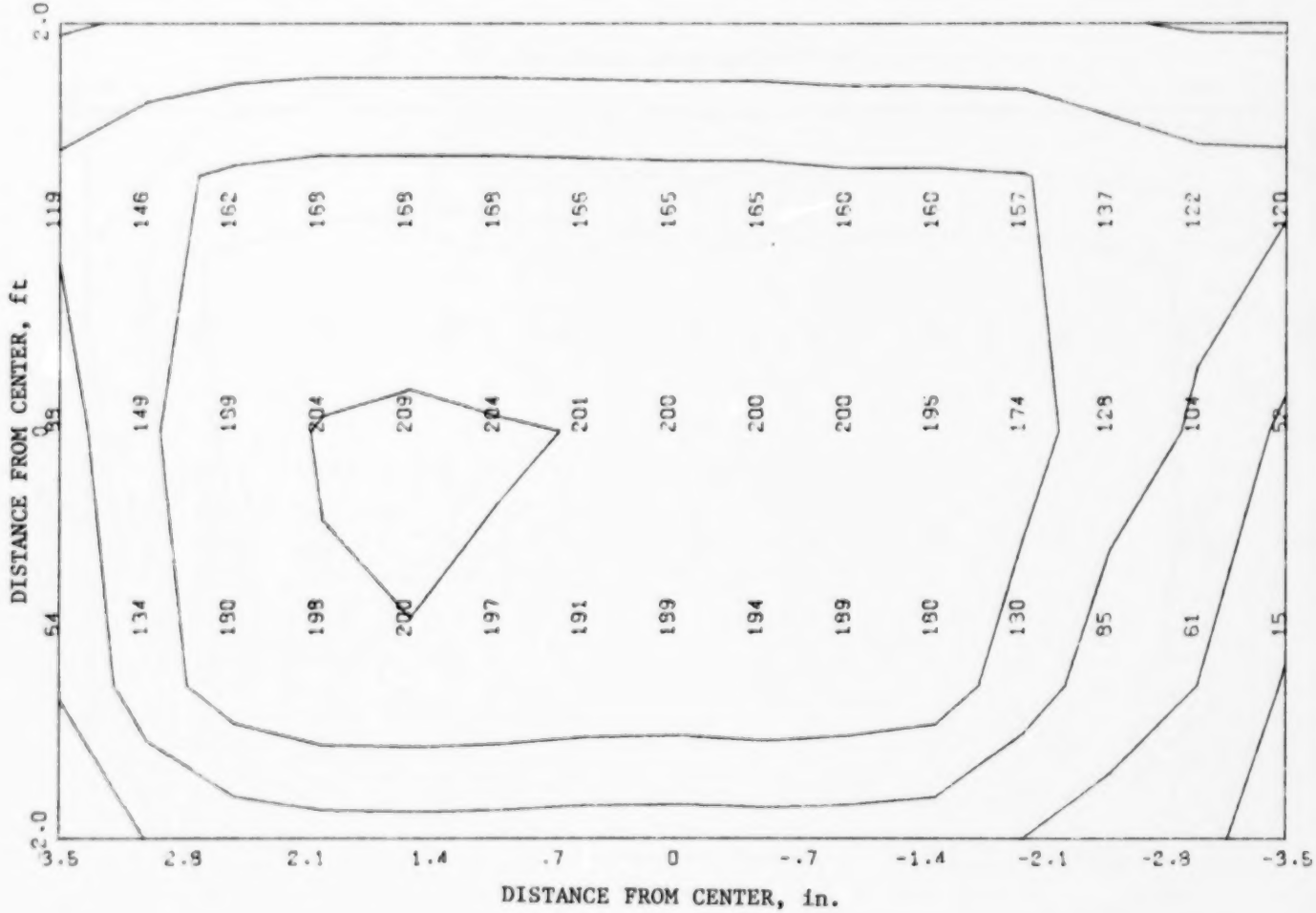

Figure A1.E. Same conditions as Figure A1.A. Section E.

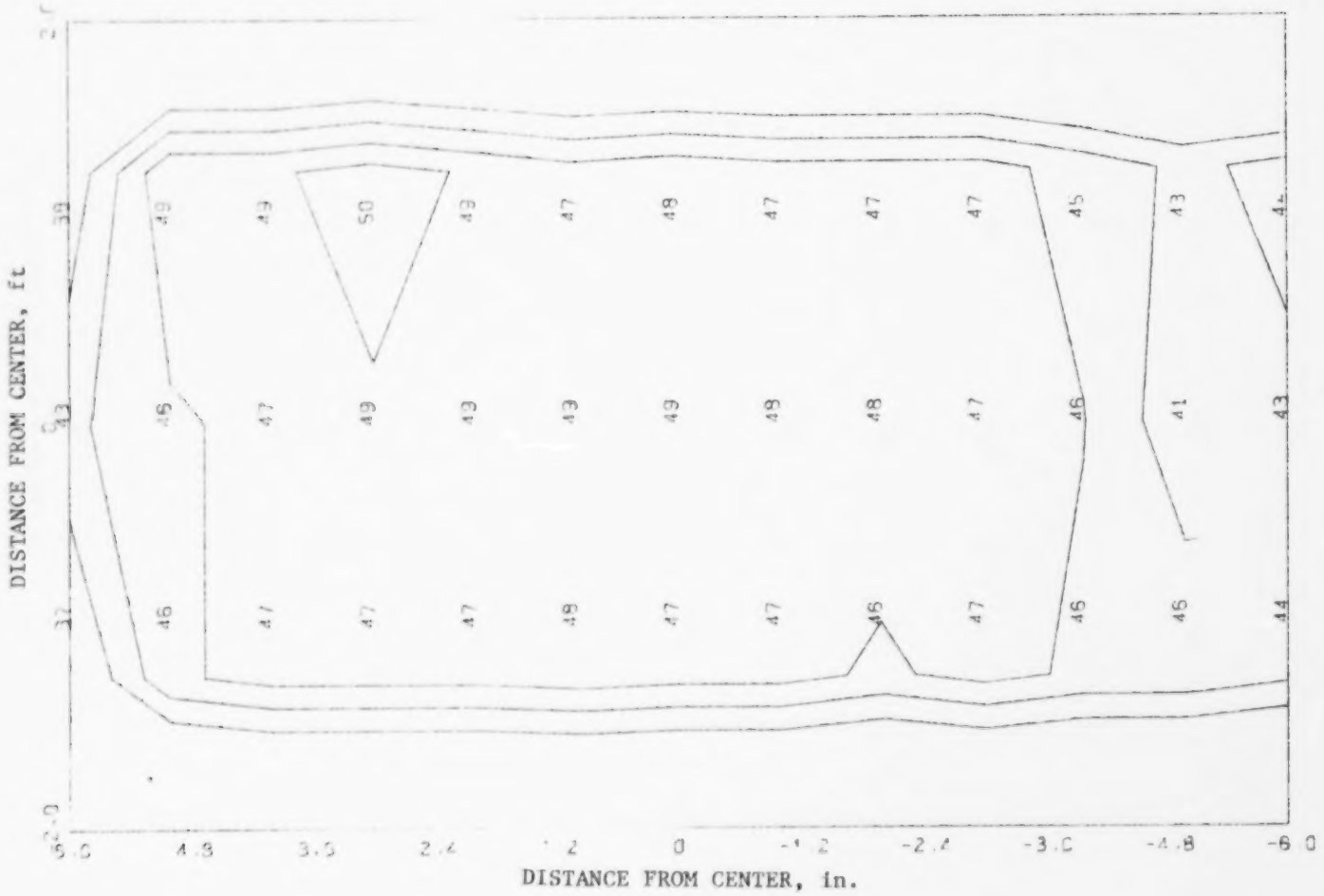

Figure A2.A. Flow distribution in nominal 5-in. channel. Velocities in m/min for a volume flow 23.5 m^3/min. Section A.

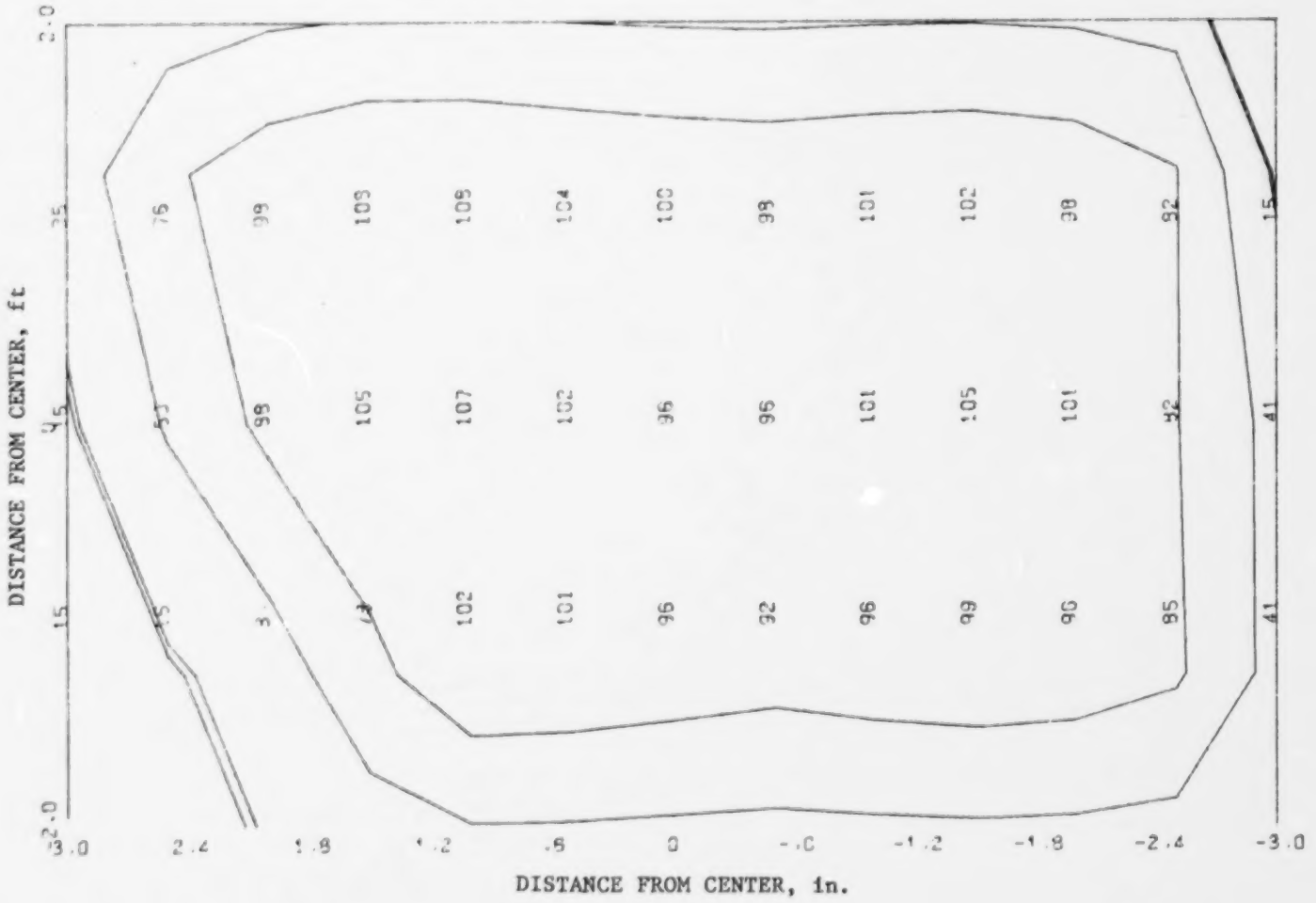

Figure A2.B. Same conditions as Figure A2.A. Section B.

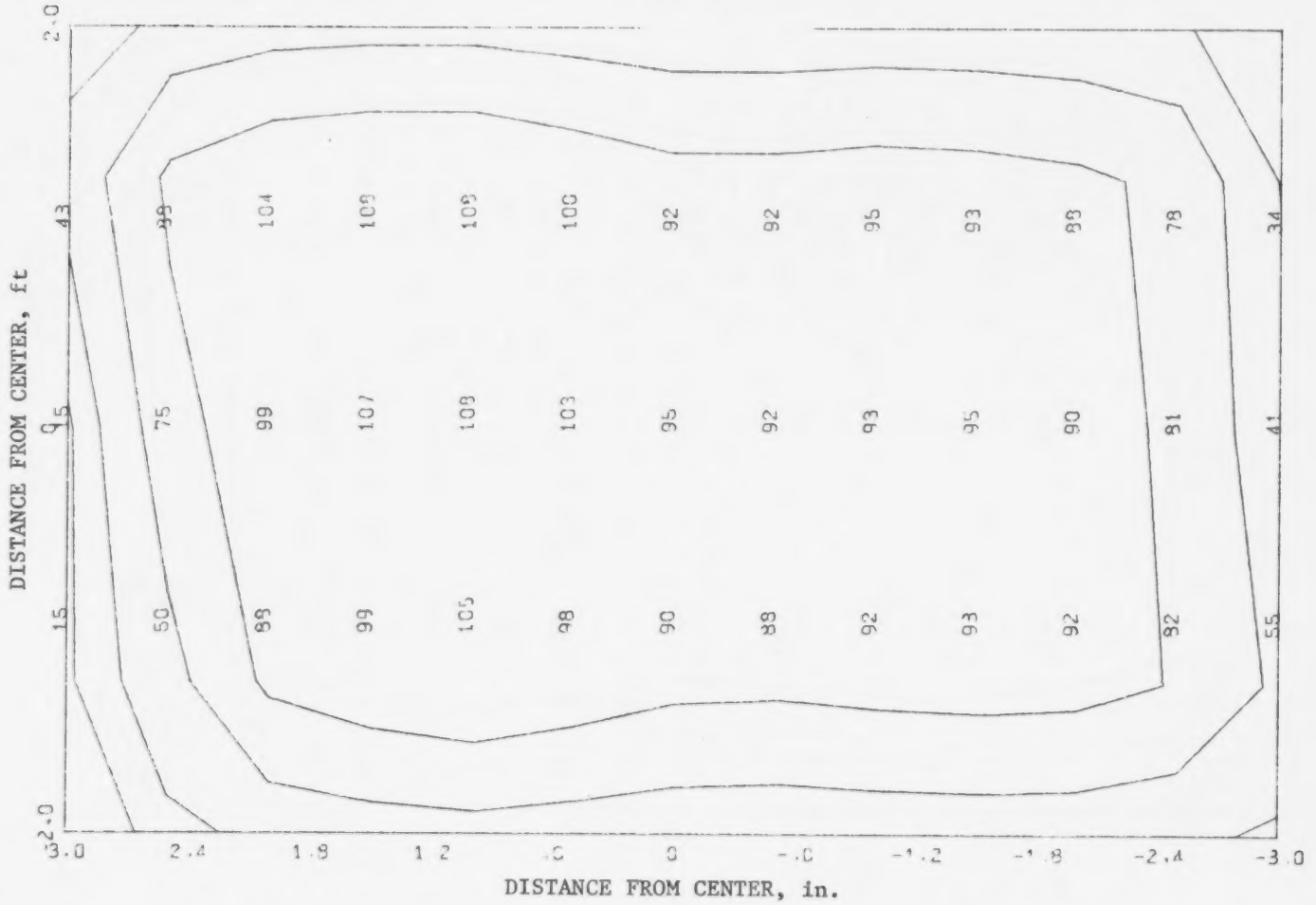

Figure A2.C. Same conditions as Figure A2.A. Section C.

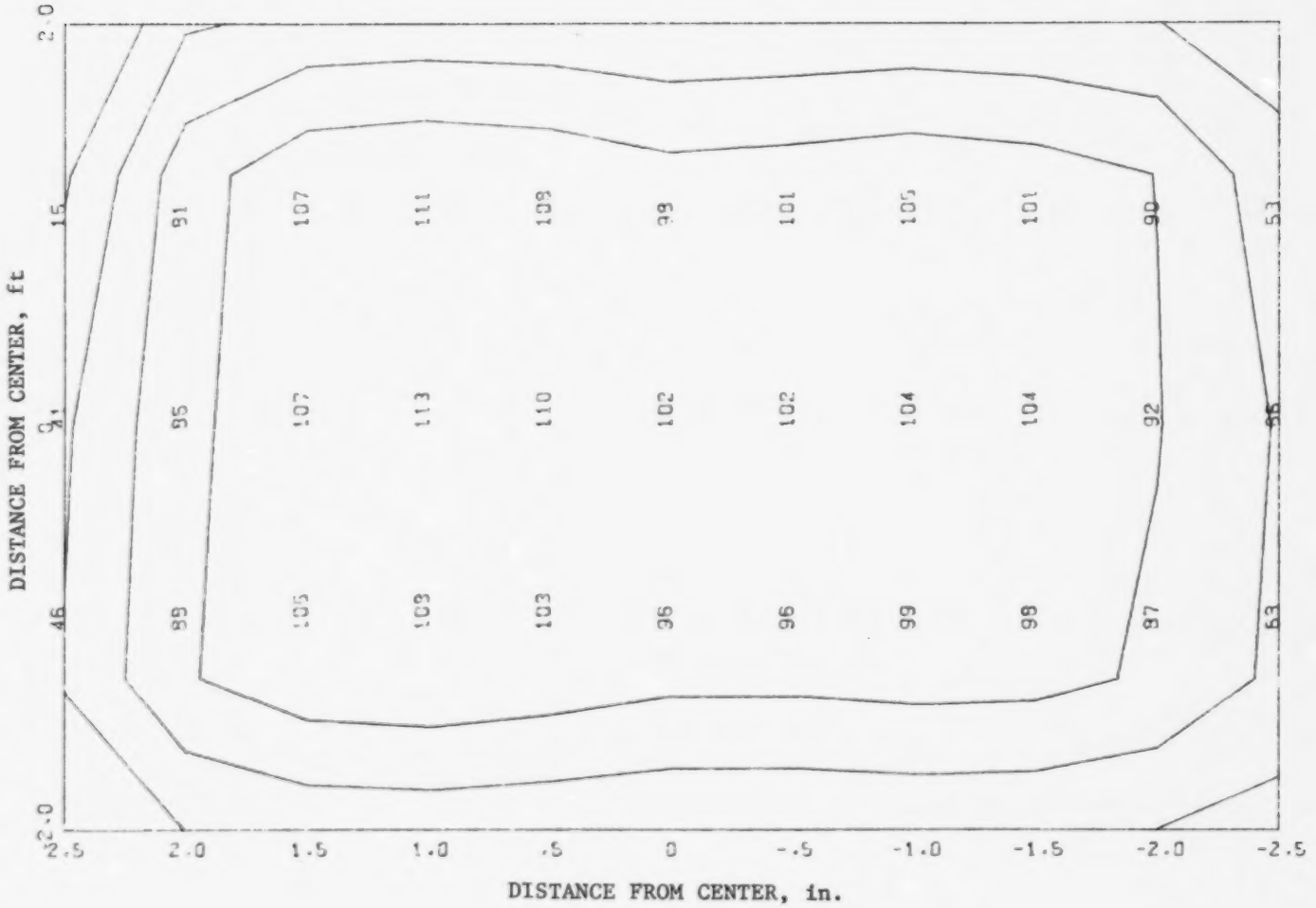

Figure A2.D. Same conditions as Figure A2.A. Section D.

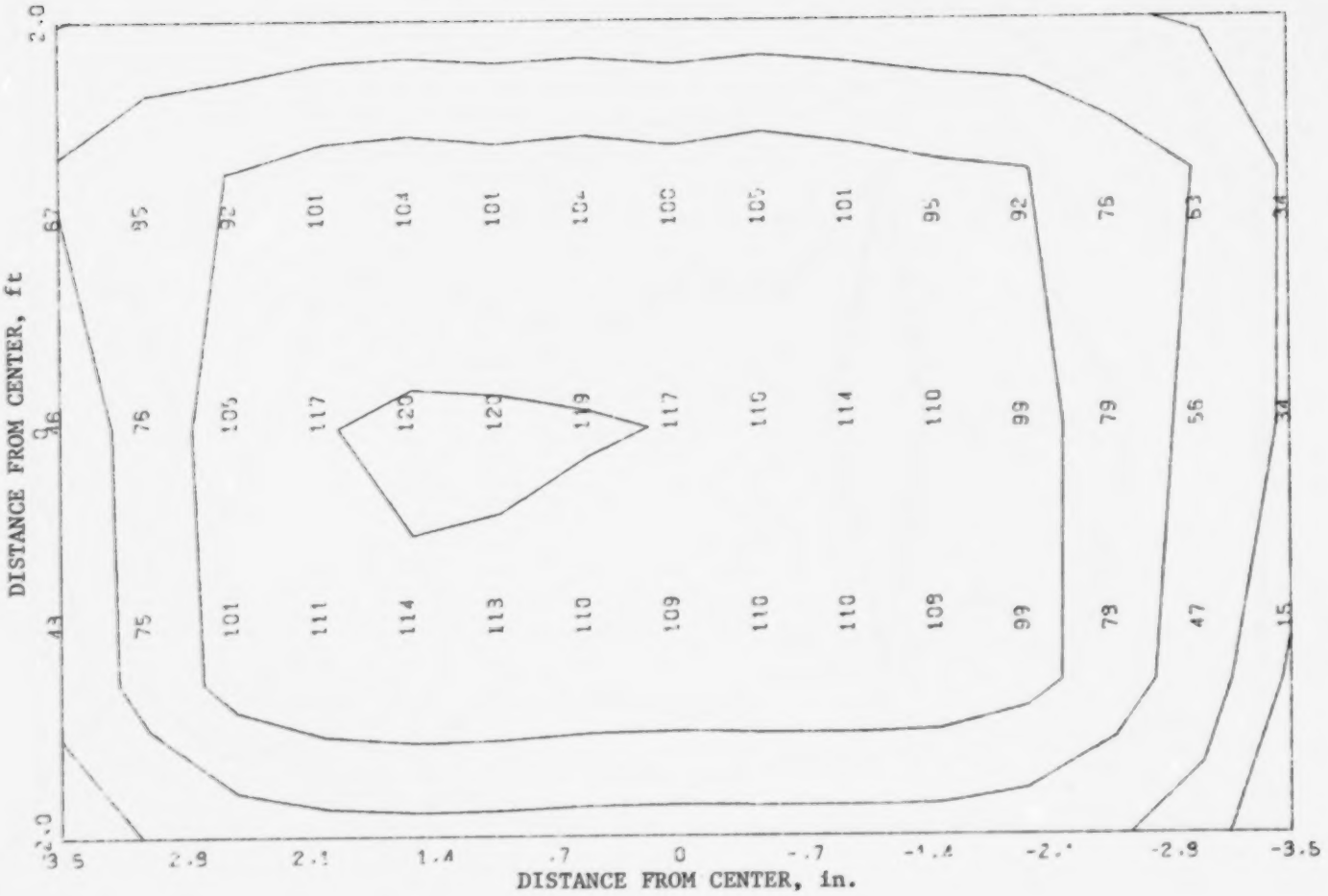

Figure A2.E. Same conditions as Figure A2.A. Section E.

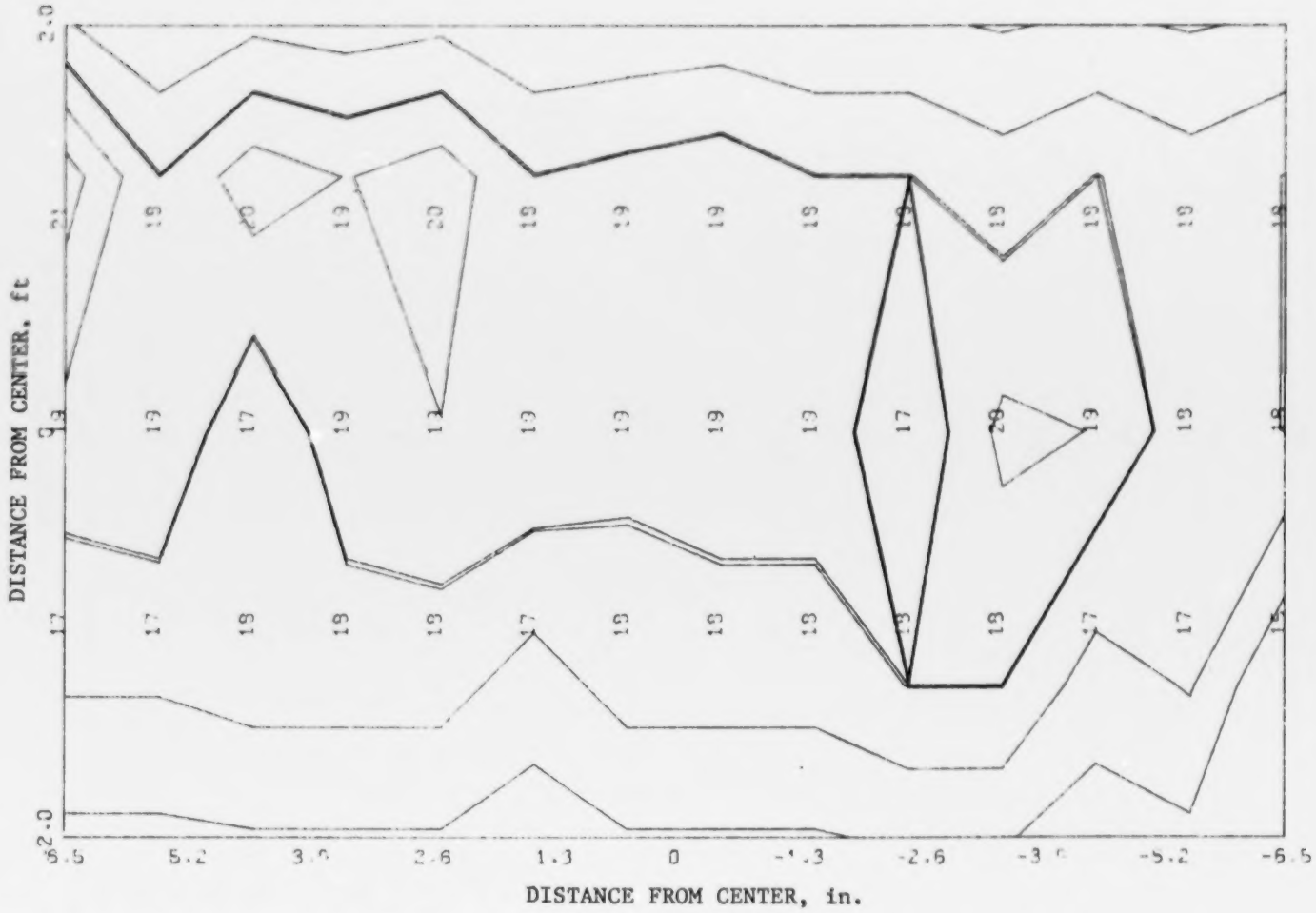

Figure A3.A. Flow distribution in nominal 5-in. channel. Velocities in m/min for a volume flow of 7.0 m^3/min. Section A.

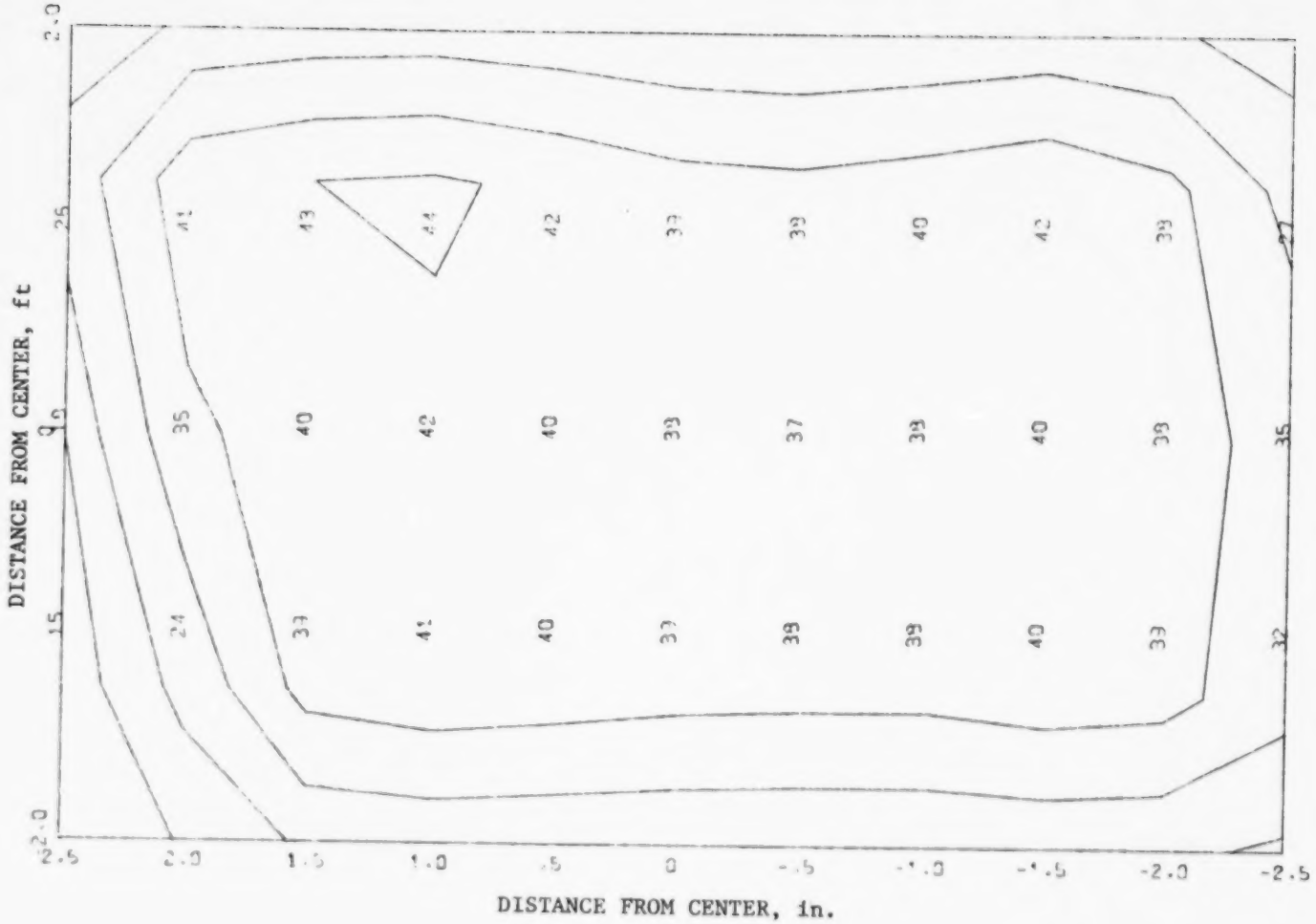

Figure A3.B. Same conditions as Figure A3.A. Section B.

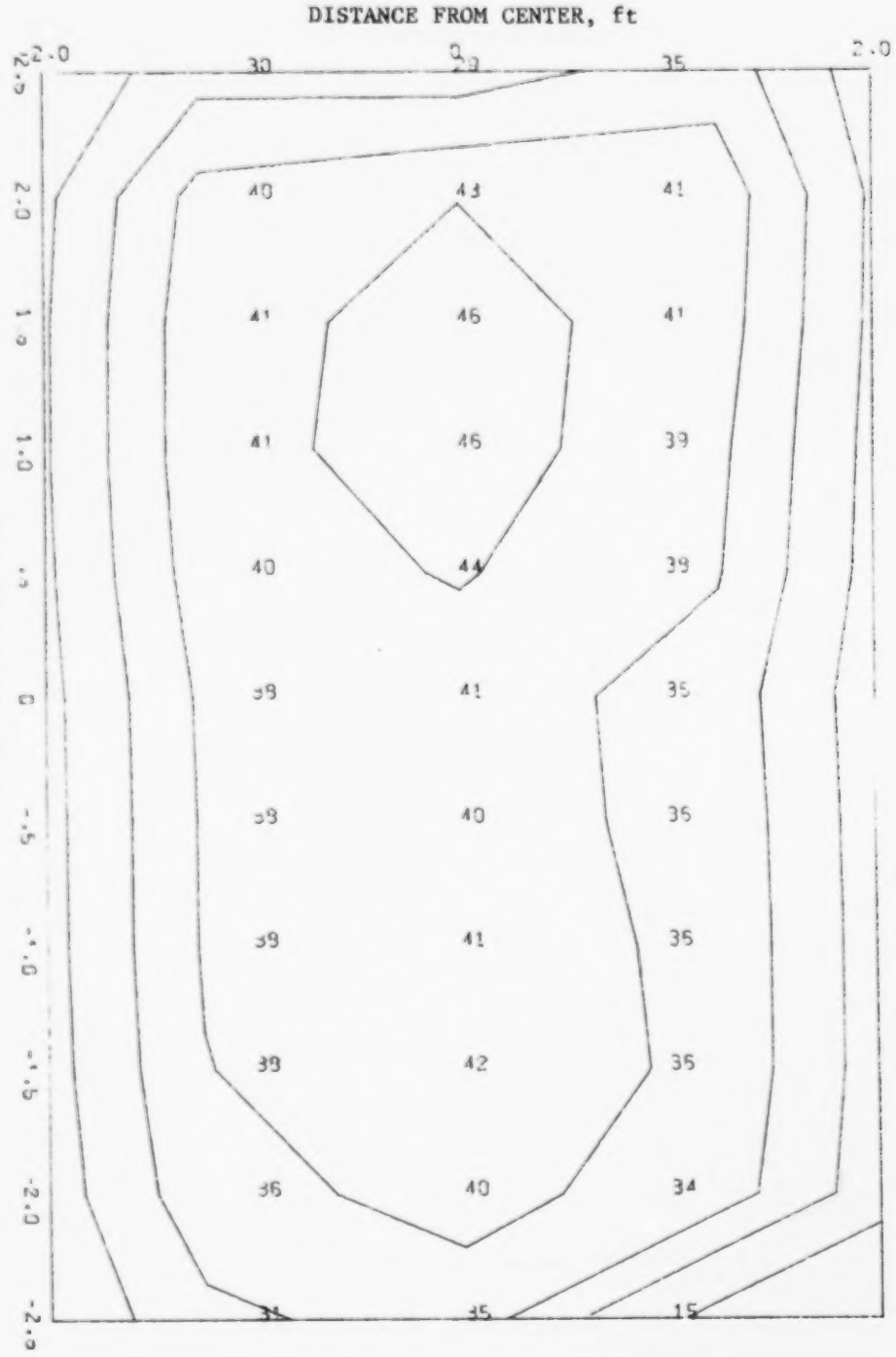

Figure A3.C. Same conditions as Figure A3.A. Section C.

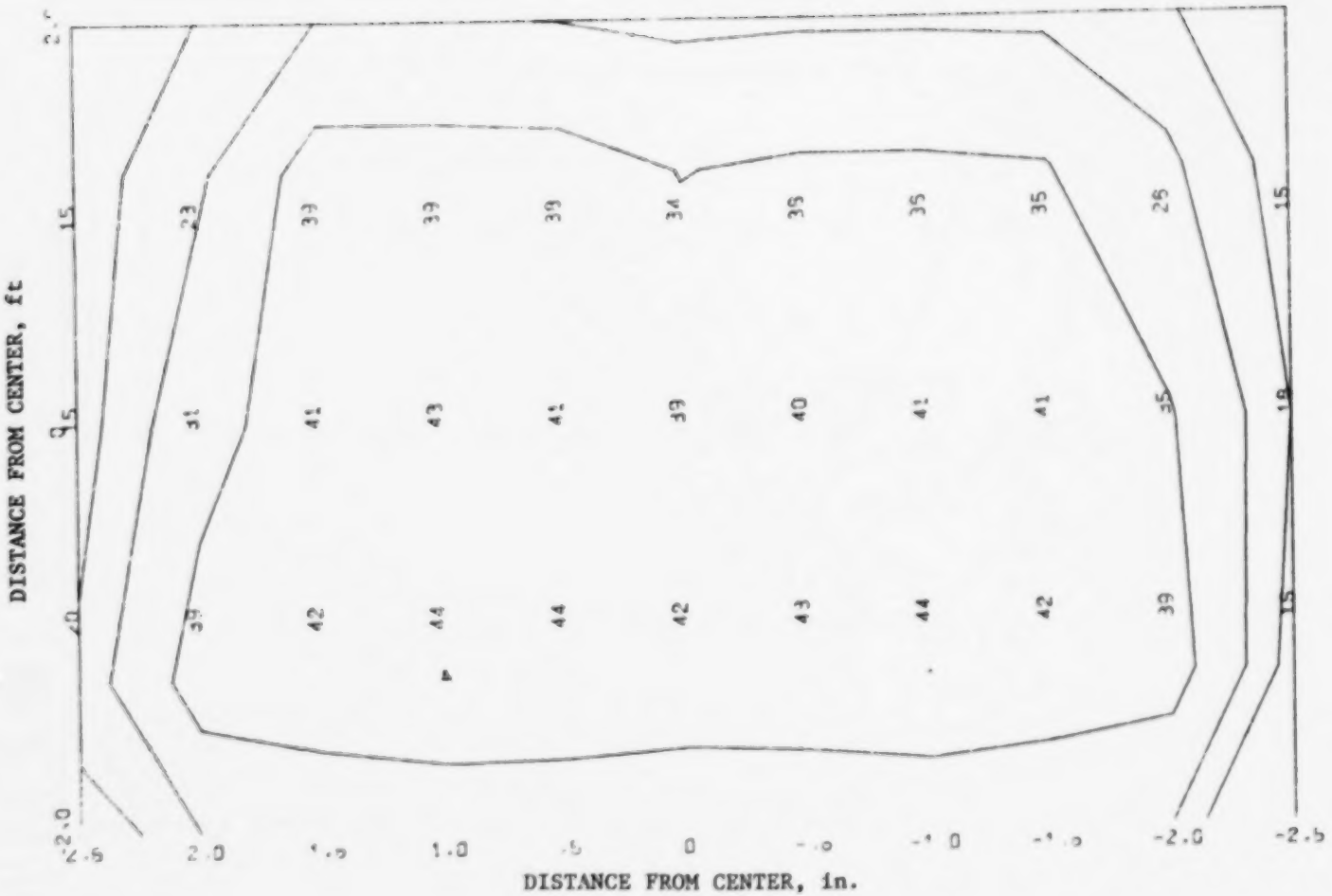

Figure A3.D. Same conditions as Figure A3.A. Section D.

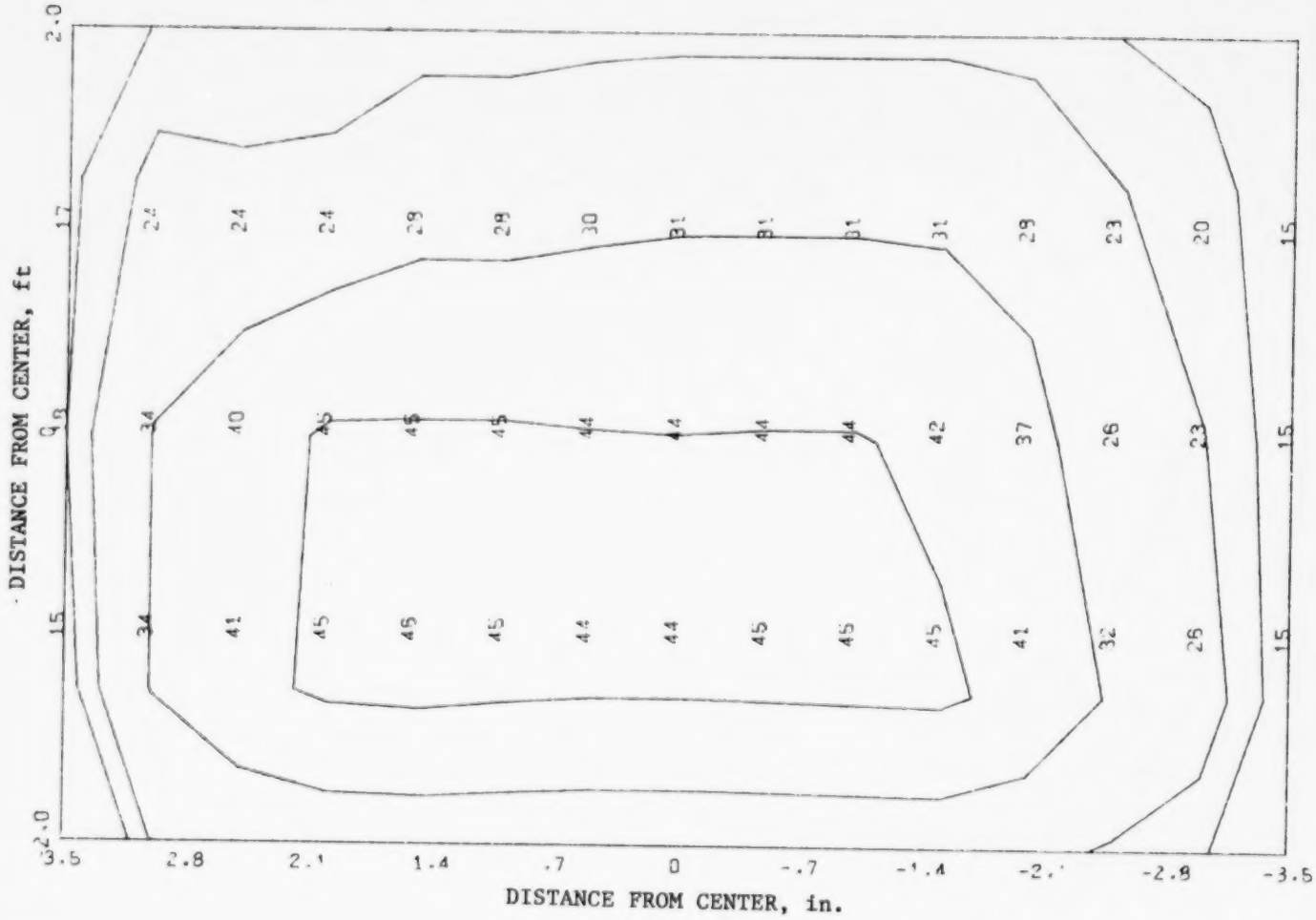

Figure A3.E. Same conditions as Figure A3.A. Section E.

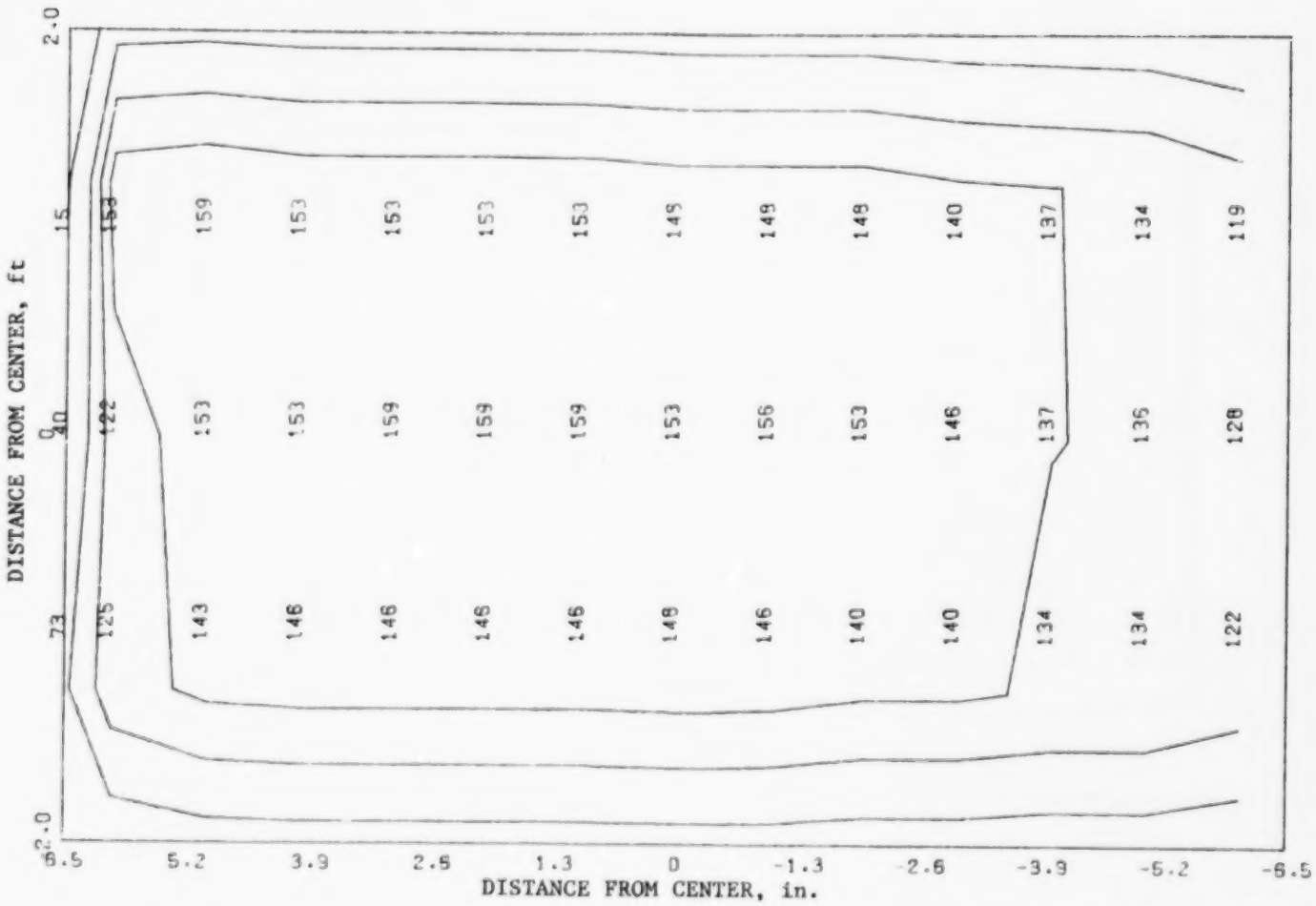

Figure A4.A. Flow distribution in nominal 10-in. channel. Velocities in m/min for a volume flow of 77 m^3/min. Section A.

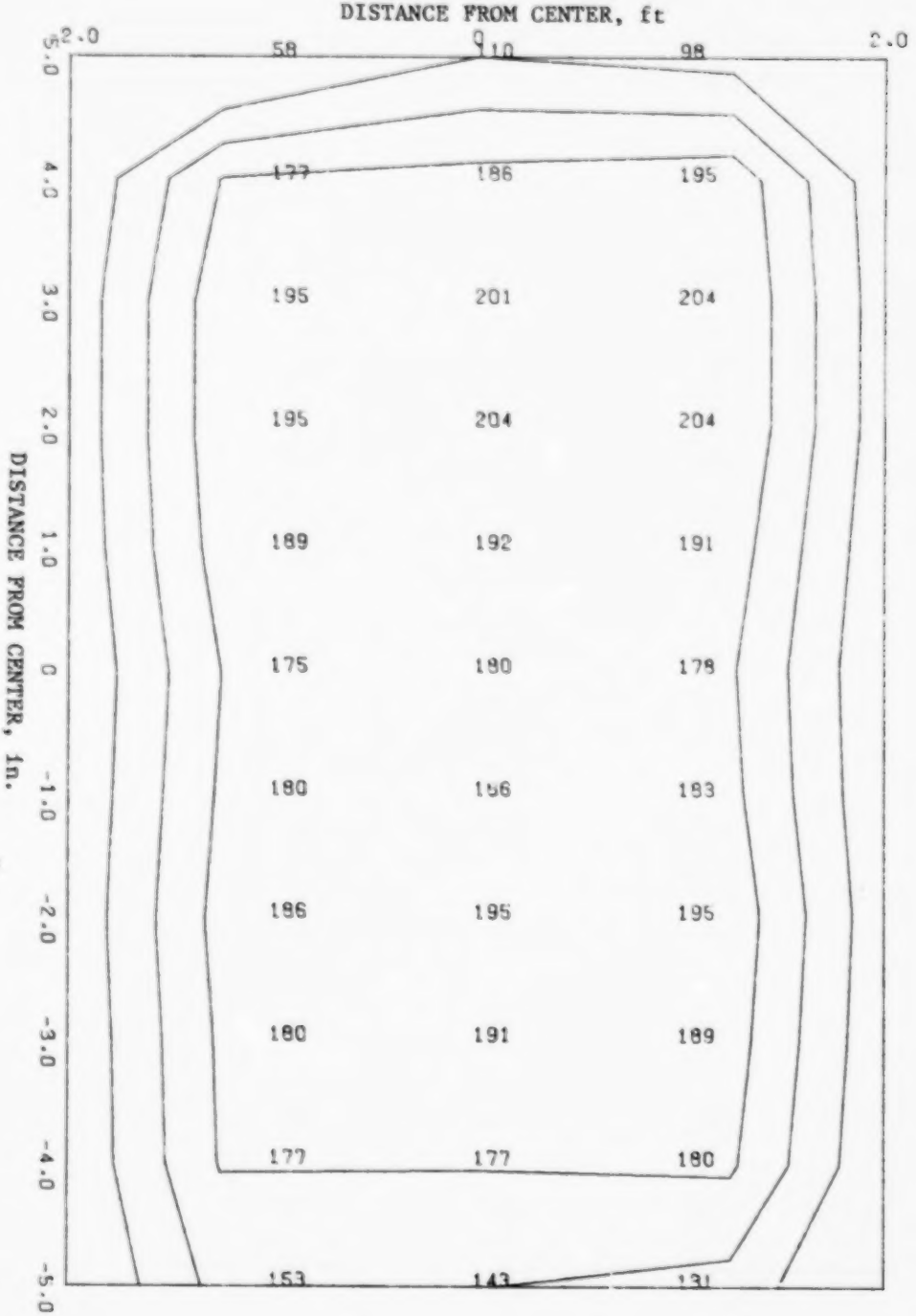

Figure A4.B. Same conditions as Figure A4.A. Section B.

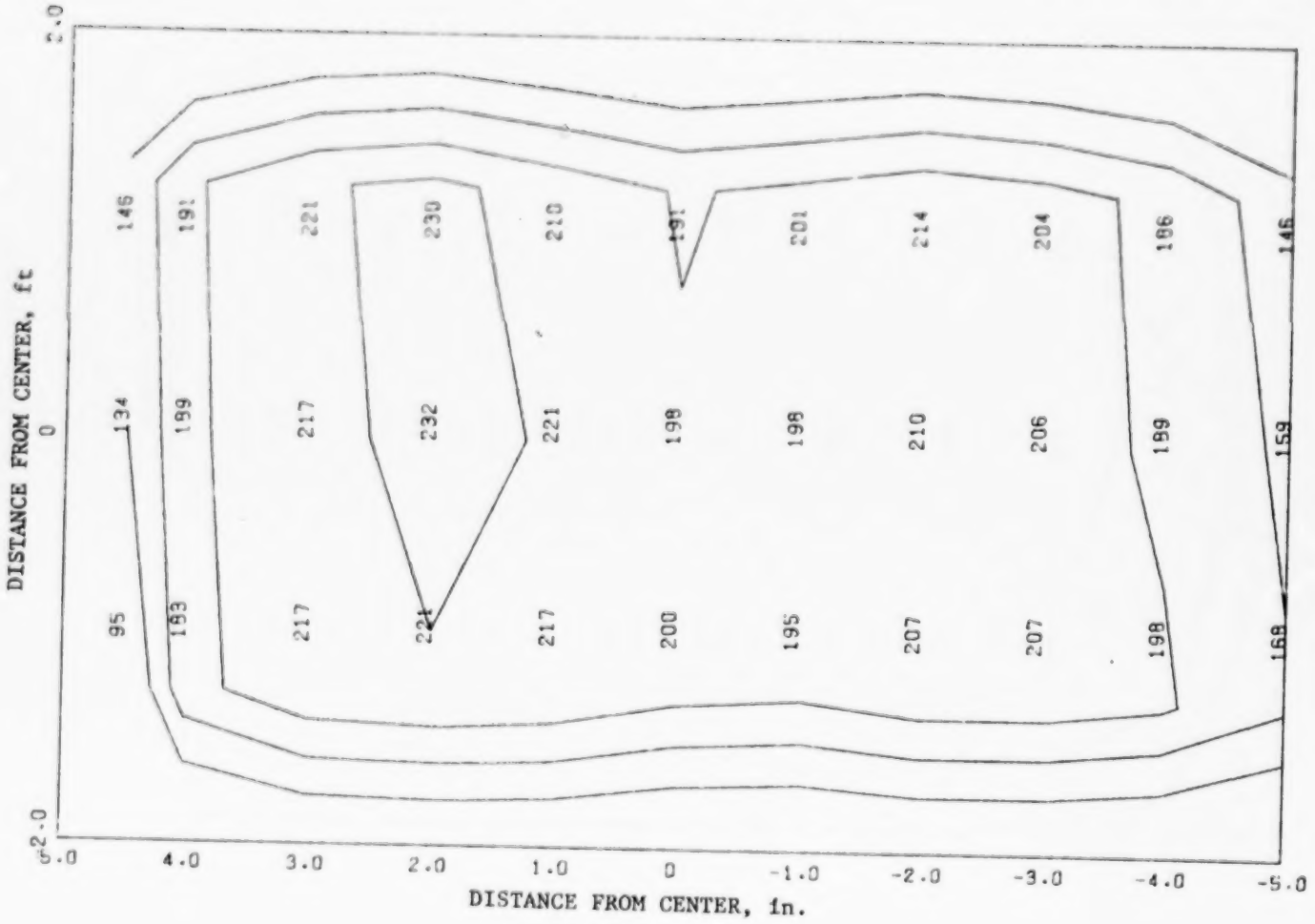

Figure A4.C. Same conditions as Figure A4.A. Section C.

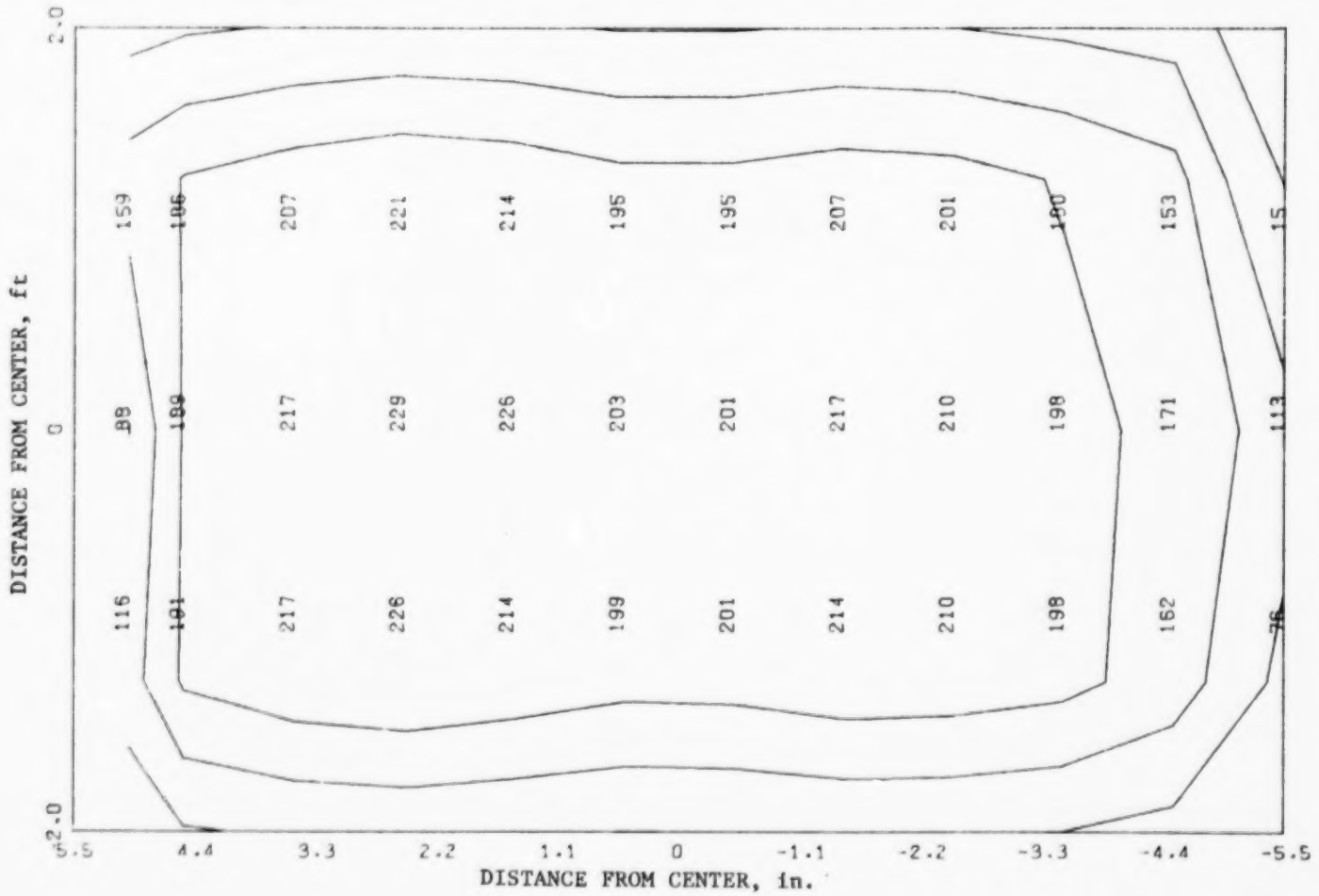

Figure A4.D. Same conditions as Figure A4.A. Section D.

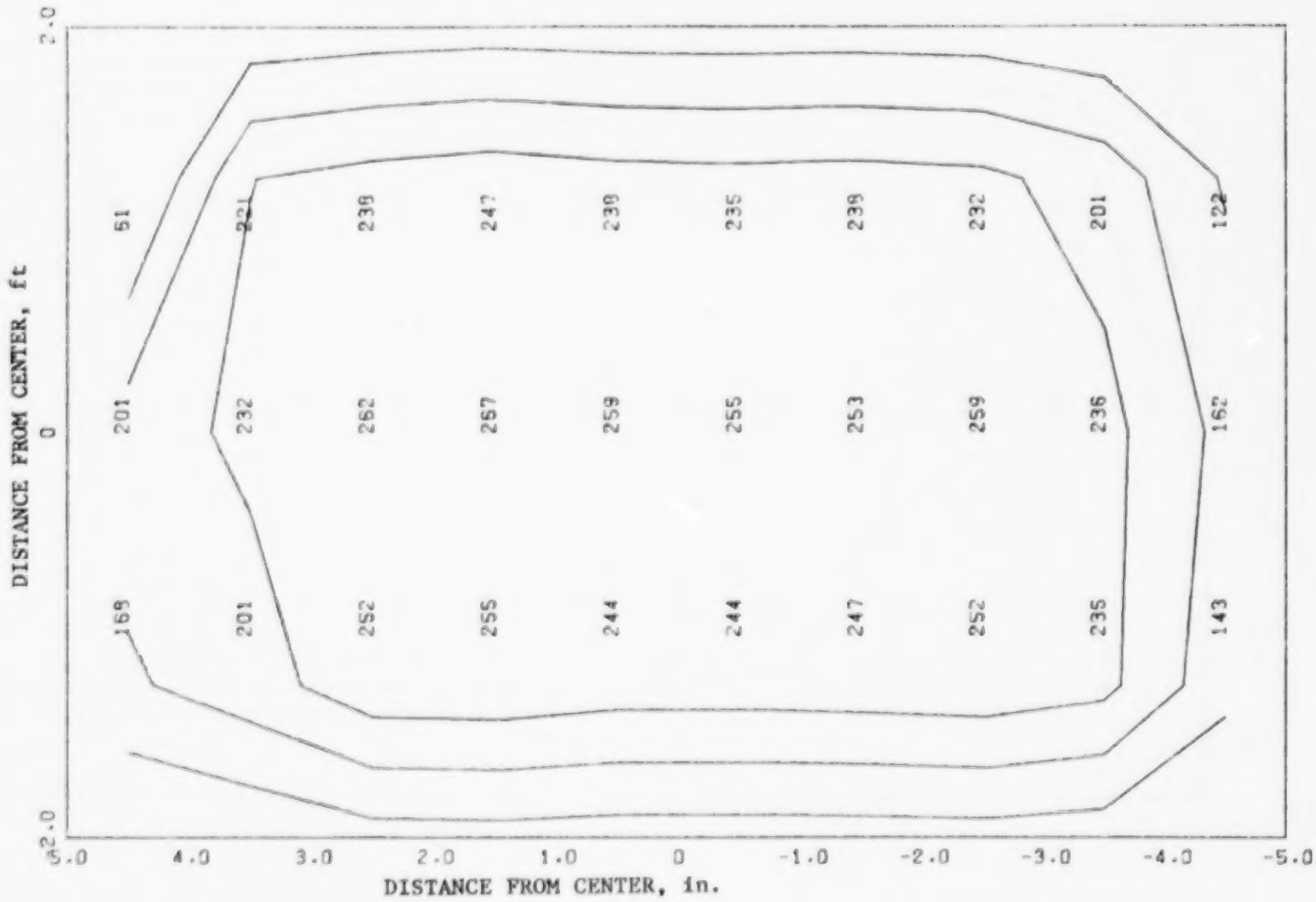

Figure A4.E. Same conditions as Figure A4.A. Section E.

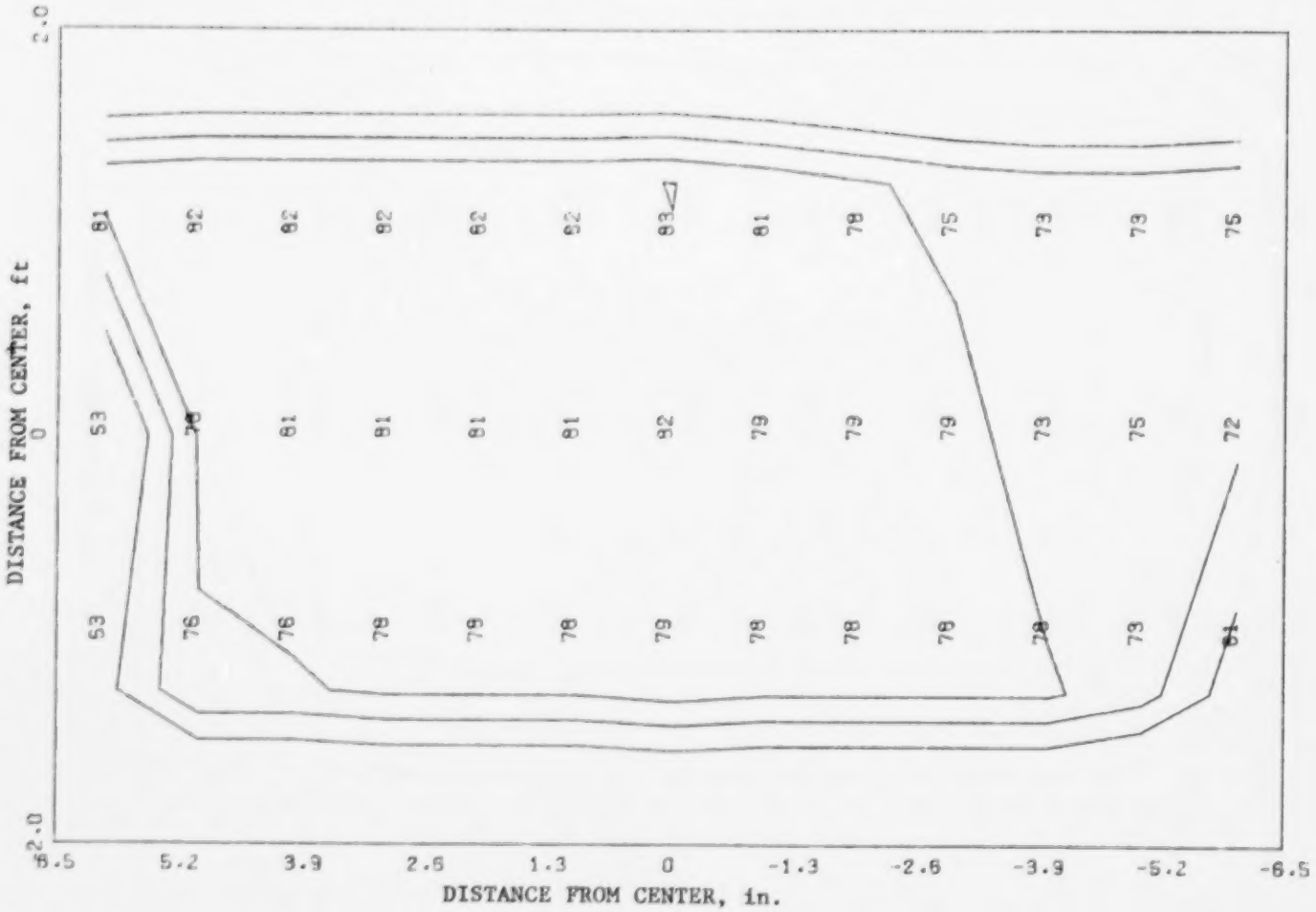

Figure A5.A. Flow distribution in nominal 10-in. channel. Velocities in m/min for a volume flow of 42.5 m^3/min. Section A.

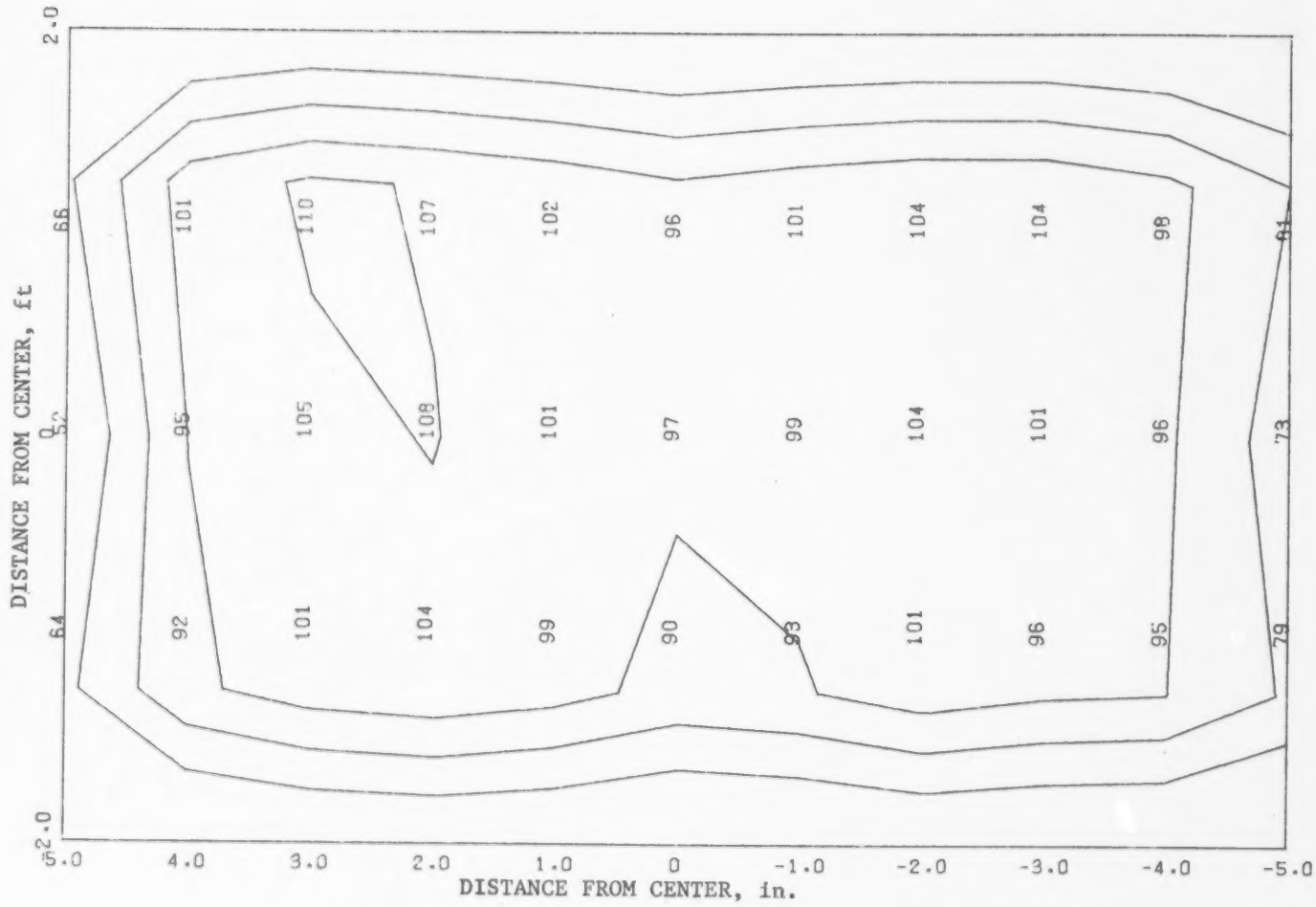

Figure A5.B. Same conditions as Figure A5.A. Section B.

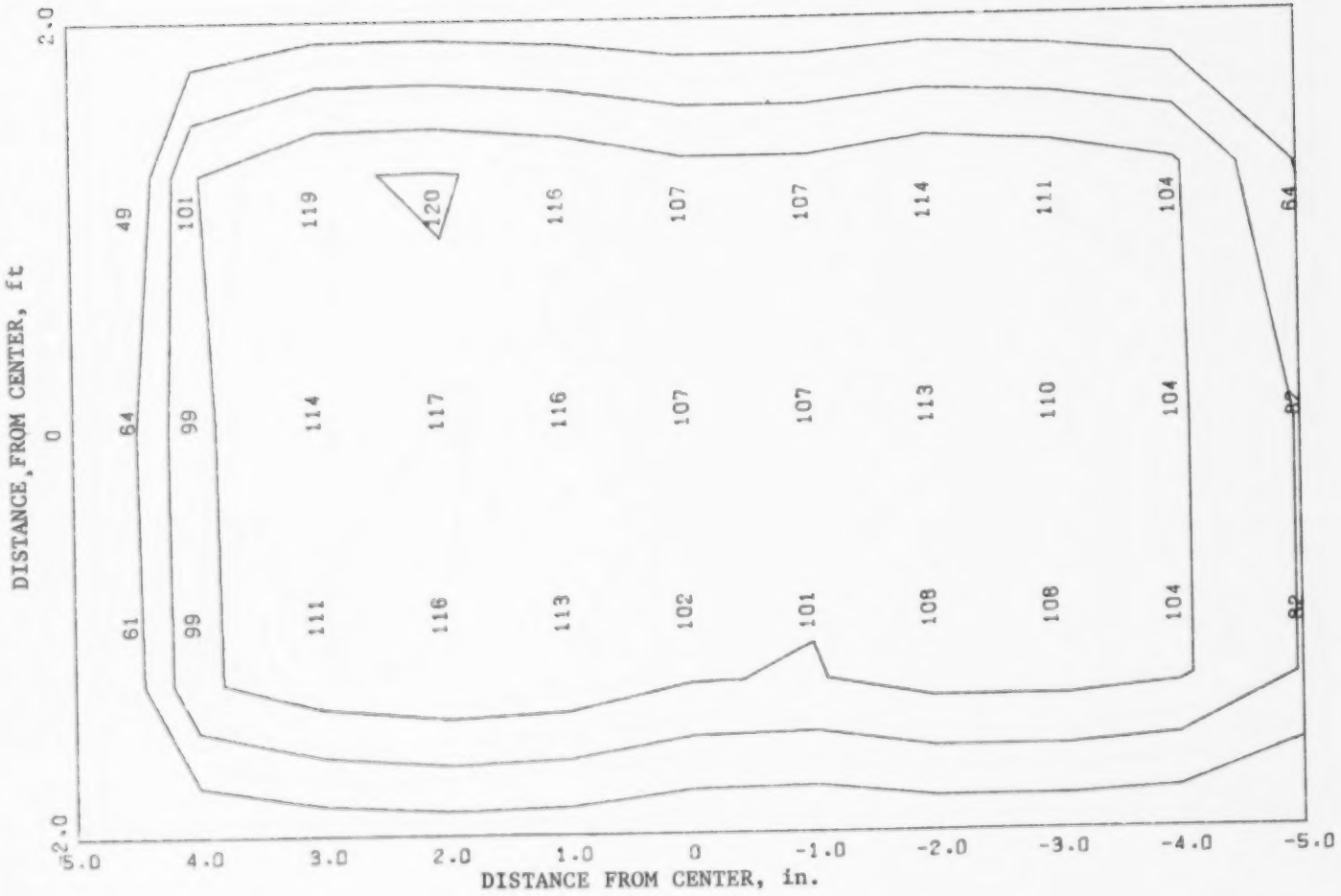

Figure A5.C. Same conditions as Figure A5.A. Section C.

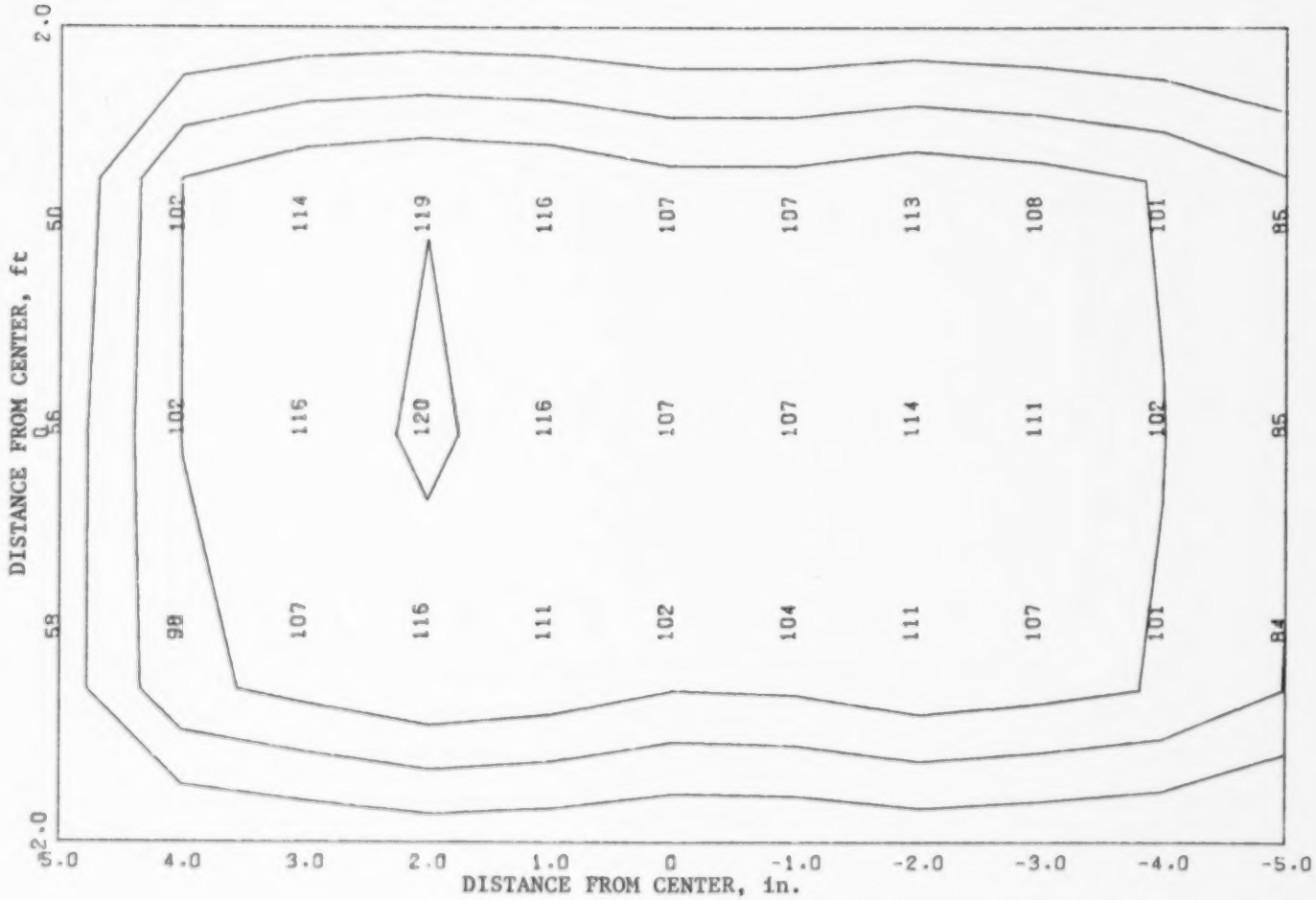

Figure A5.D. Same conditions as Figure A5.A. Section D.

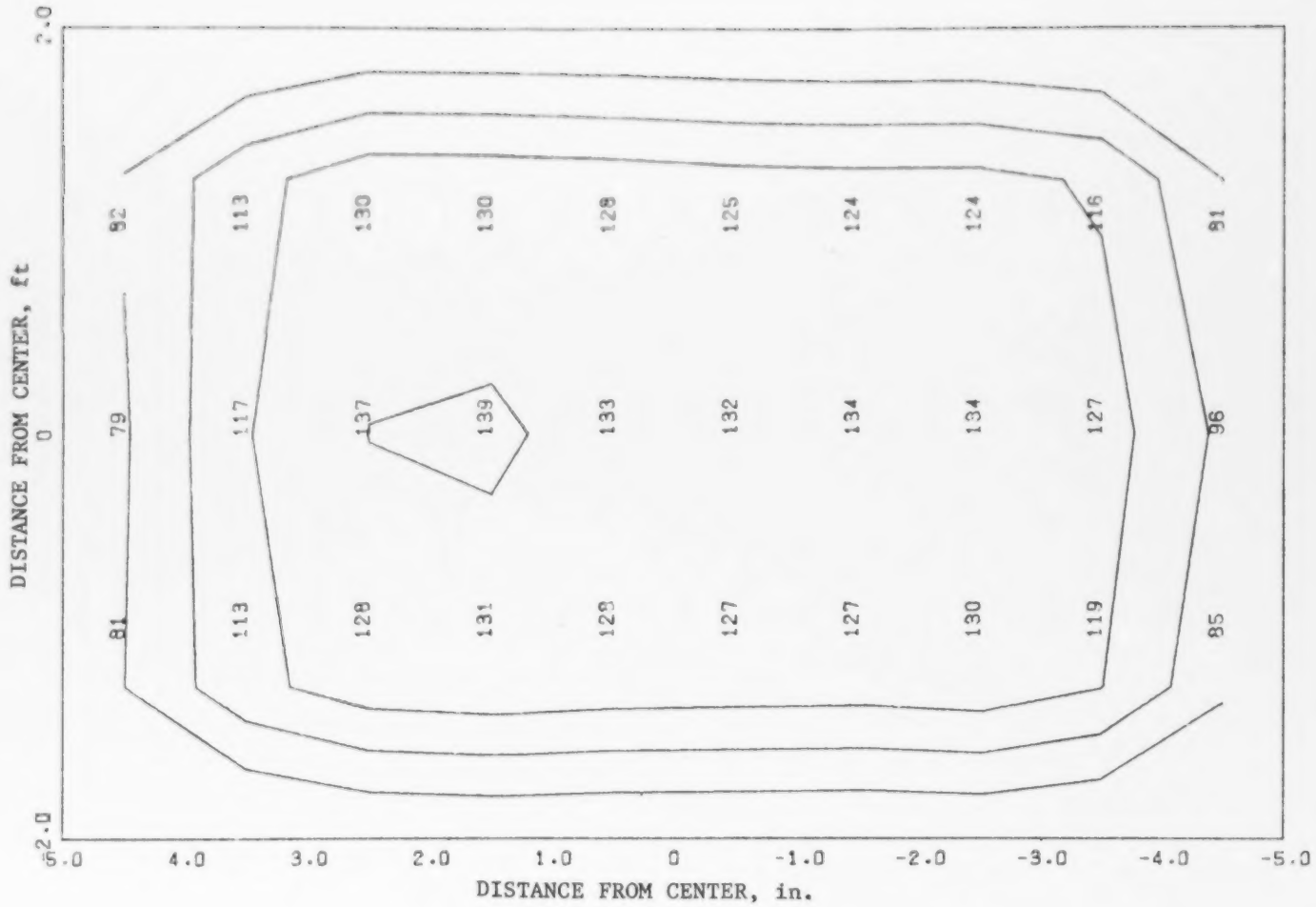

Figure A5.E. Same conditions as Figure A5.A. Section E.

Figure A6.A. Flow distribution in nominal 10-in. channel. Velocities in m/min for a volume flow of 28 m^3/min. Section A.

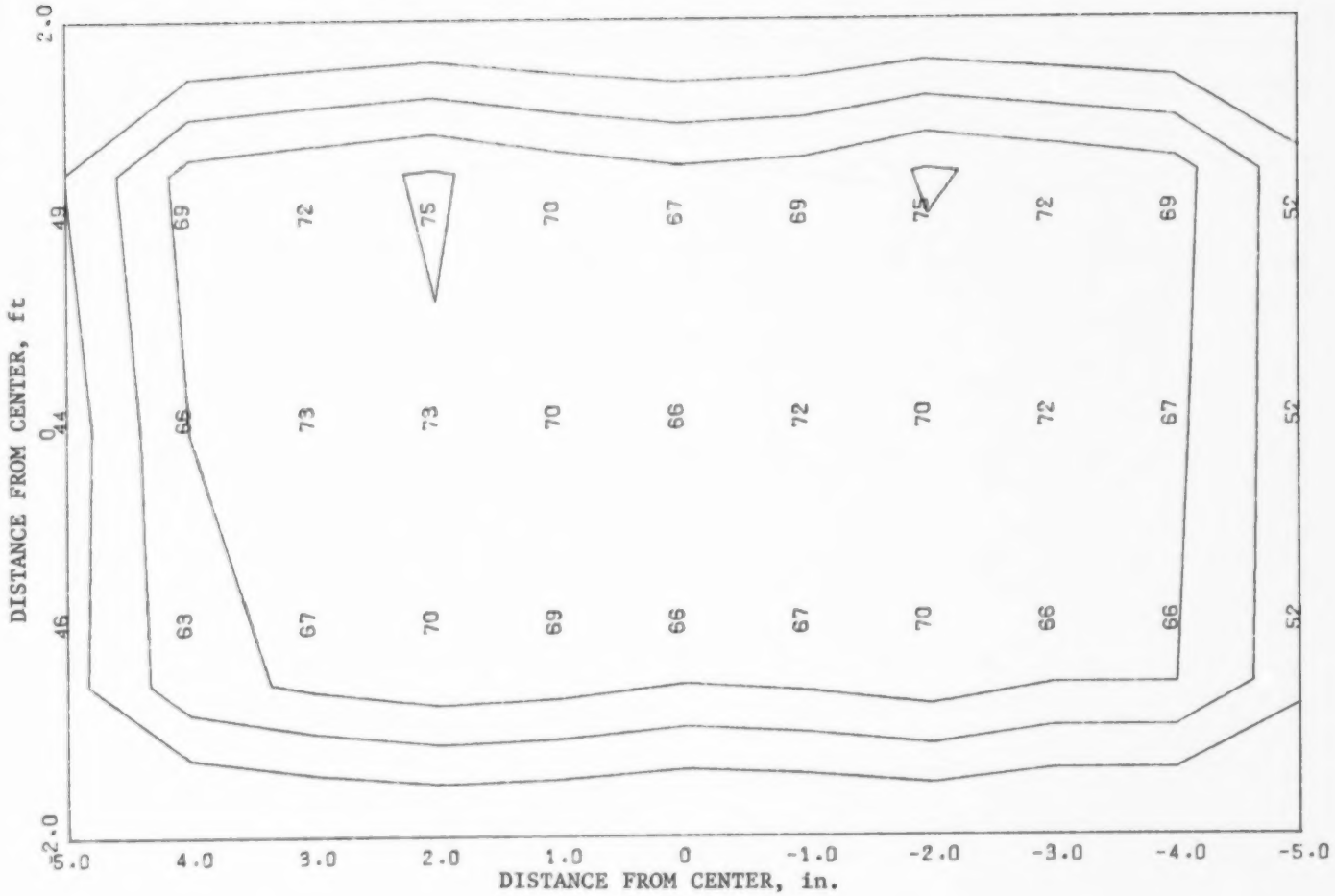

Figure A6.B. Same conditions as Figure A6.A. Section B.

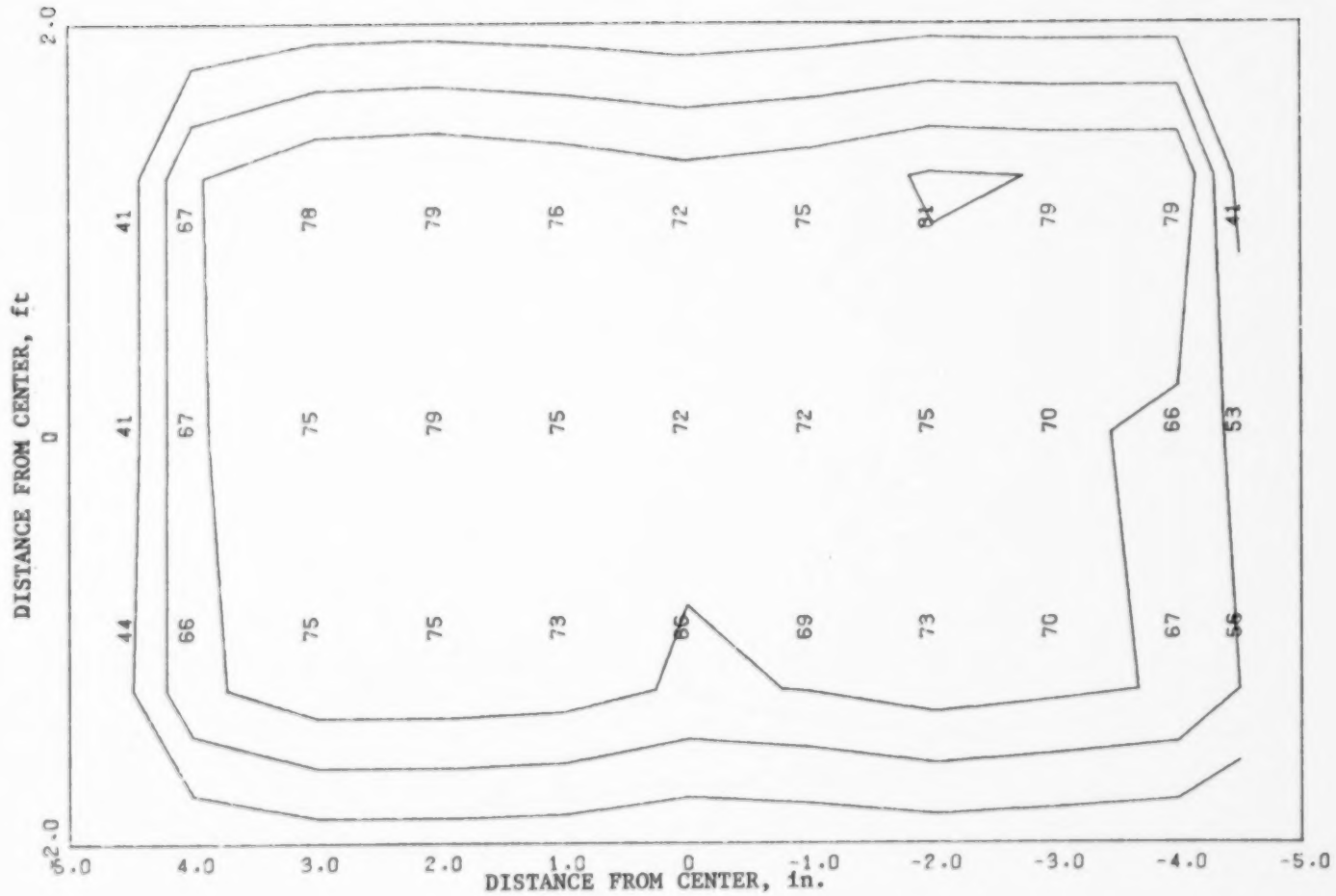

Figure A6.C. Same conditions as Figure A6.A. Section C.

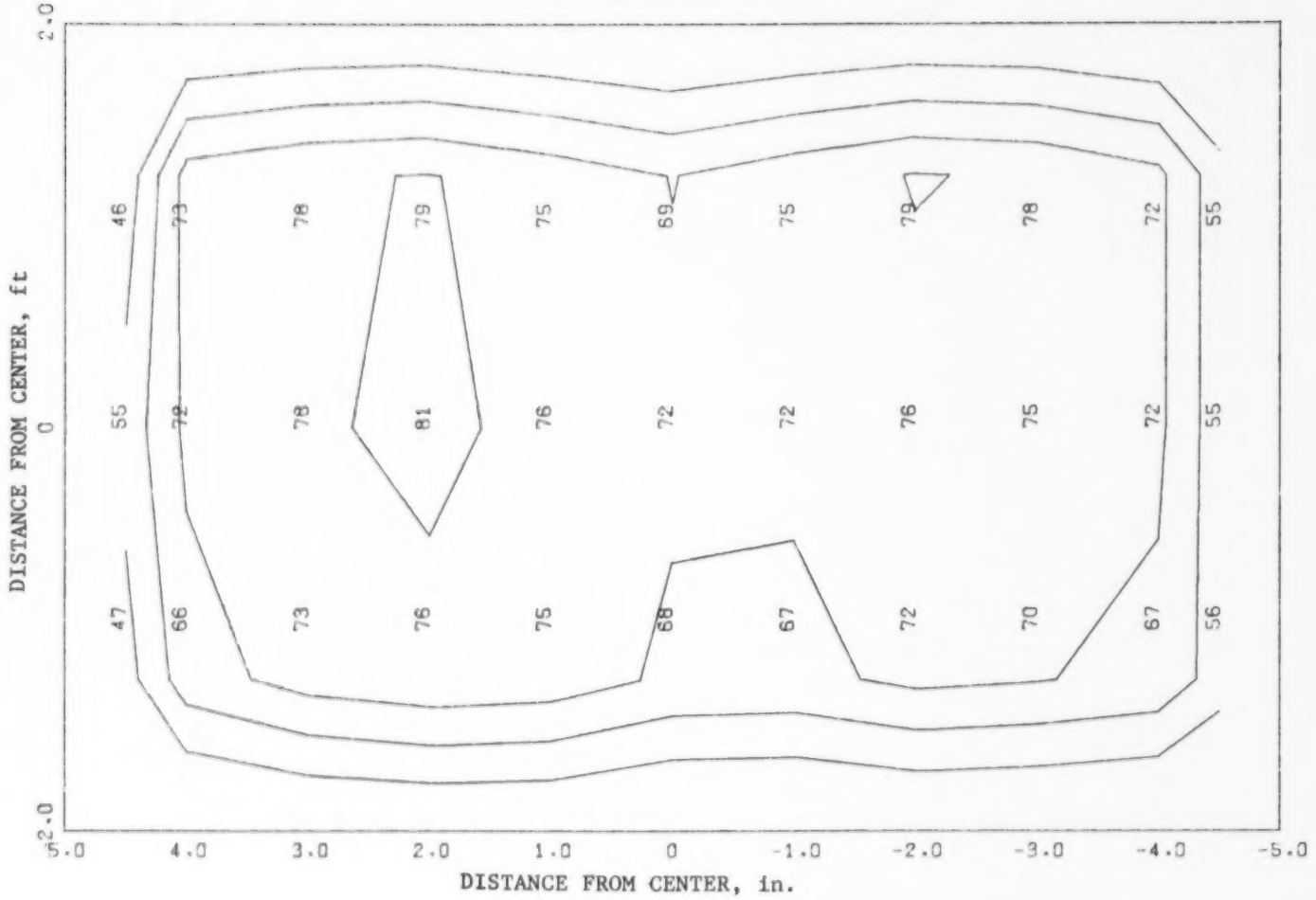

Figure A6.D. Same conditions as Figure A6.A. Section D.

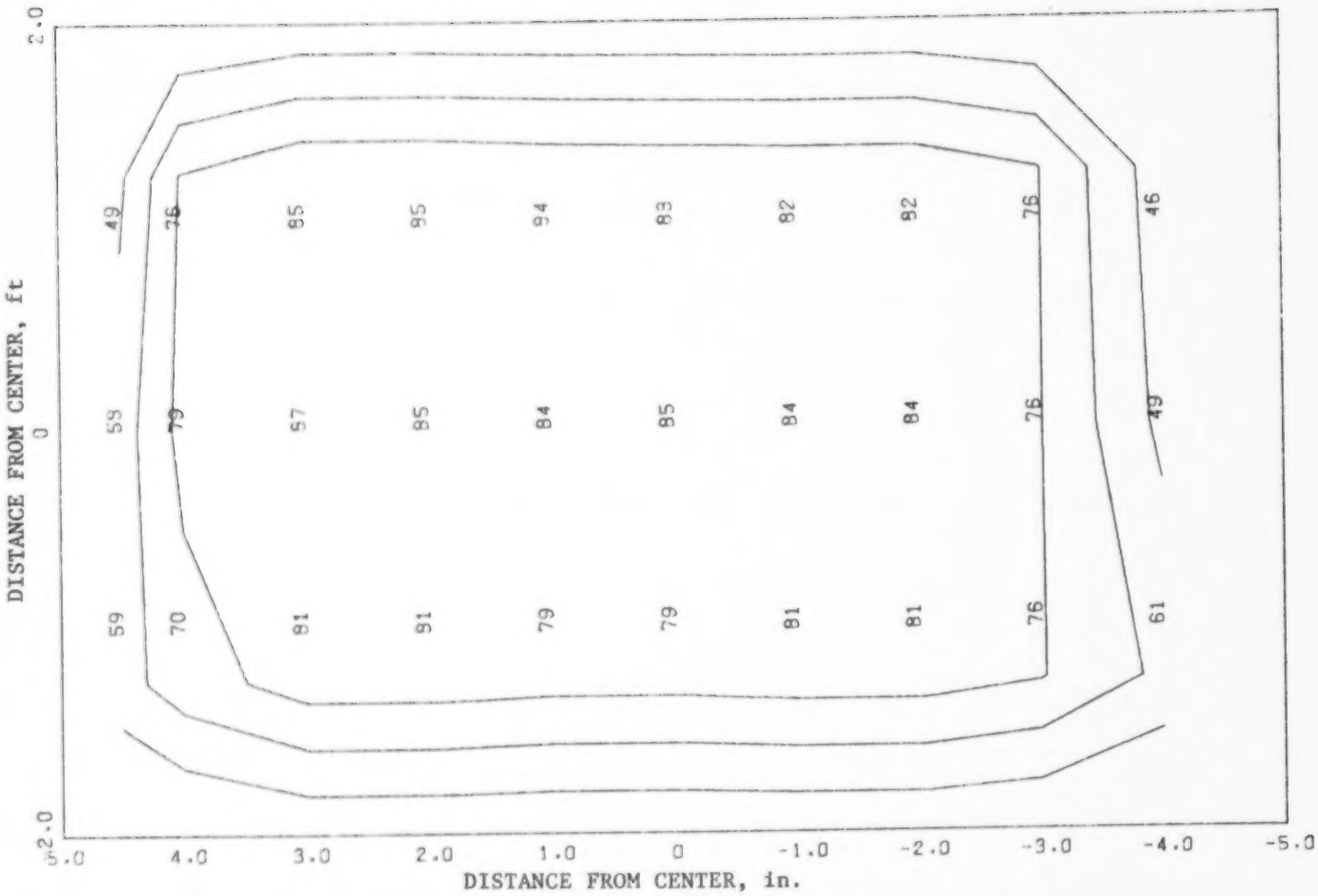

Figure A6.E. Same conditions as Figure A6.A. Section E.

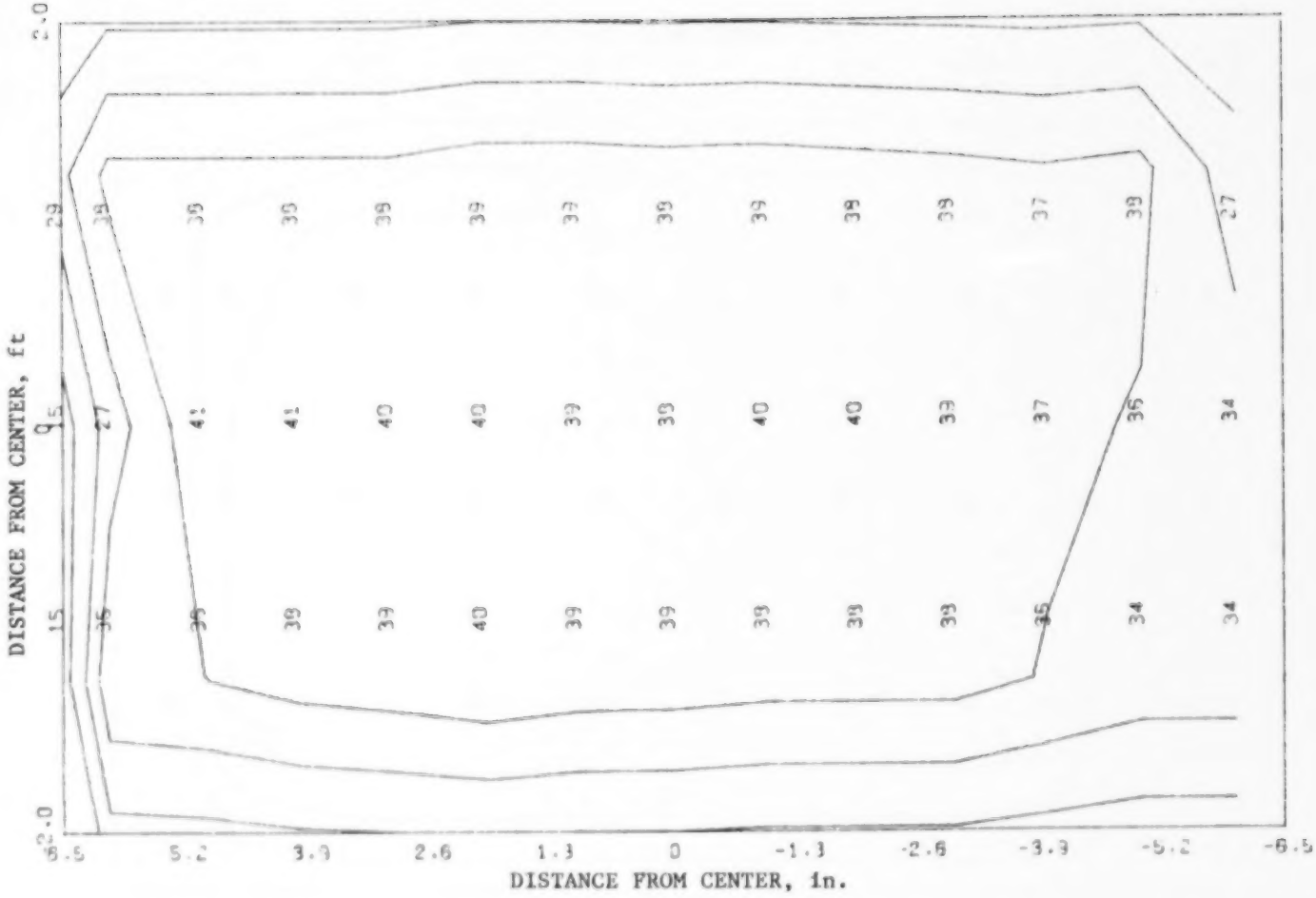

Figure A7.A. Flow distribution in nominal 15-in. channel. Velocities in m/min for a volume flow of 89 m^3/min. Section A.

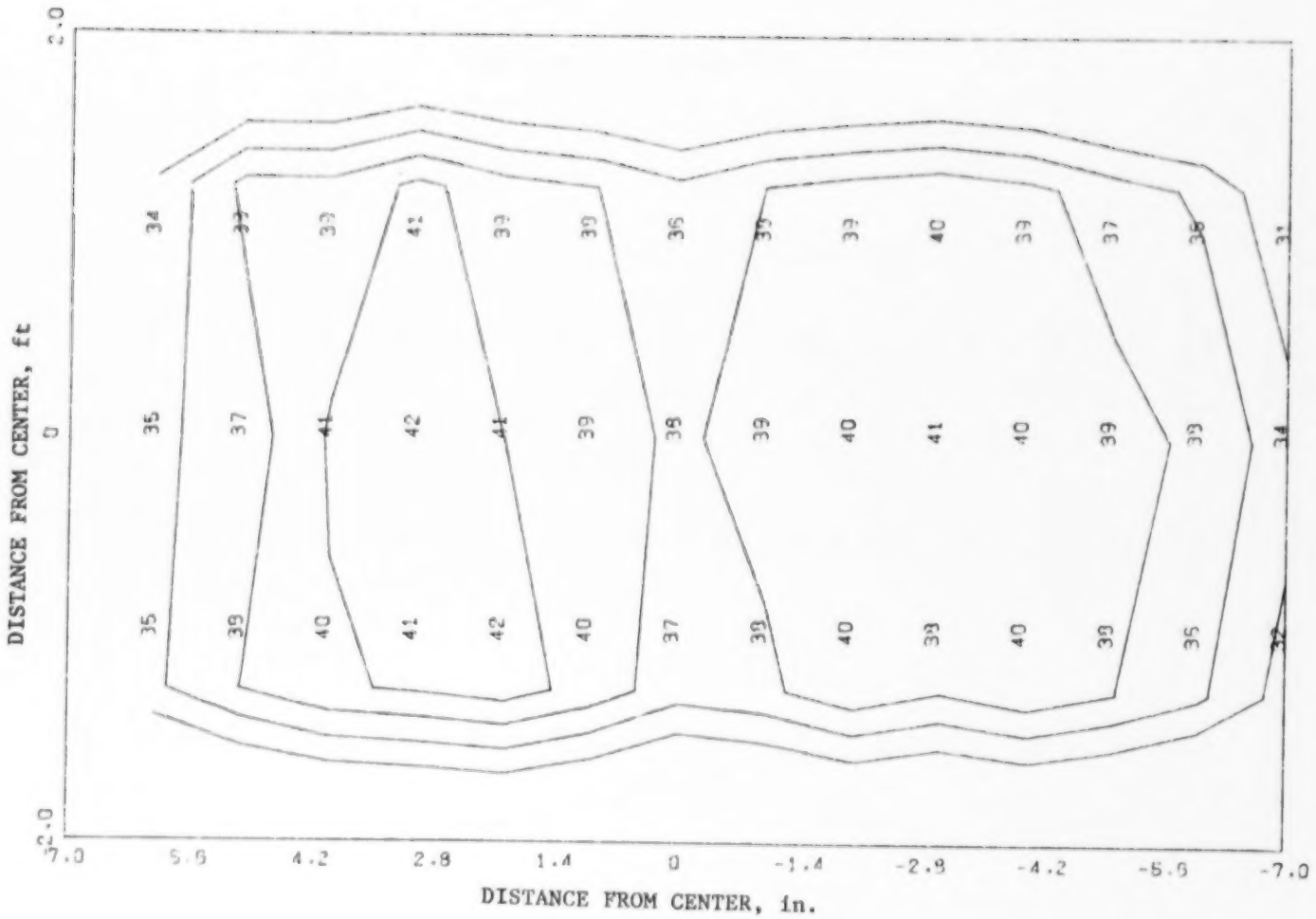

Figure A7.B. Same conditions as Figure A7.A. Section B.

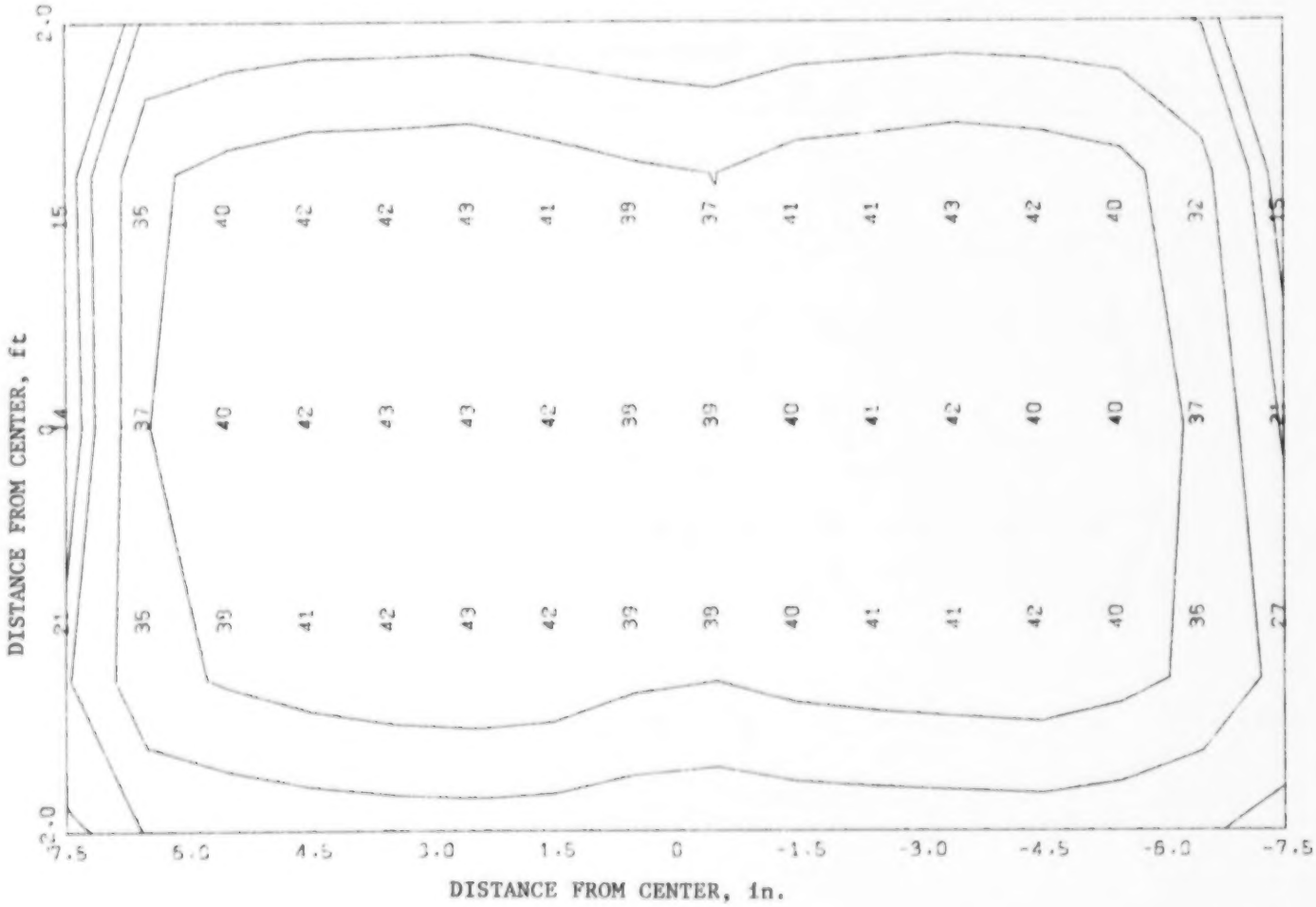

Figure A7.C. Same conditions as Figure A7.A. Section C.

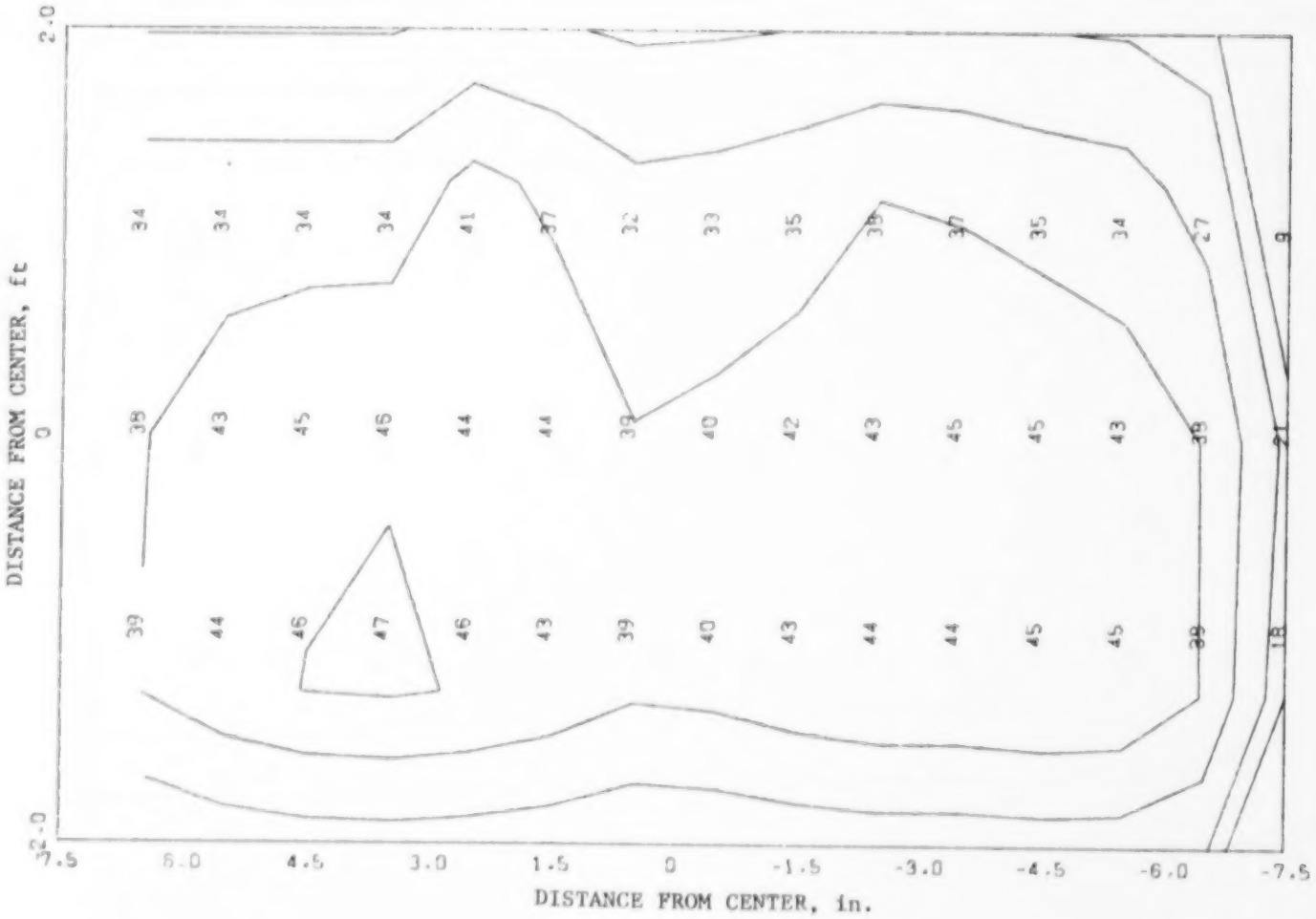

Figure A7.D. Same conditions as Figure A7.A. Section D.

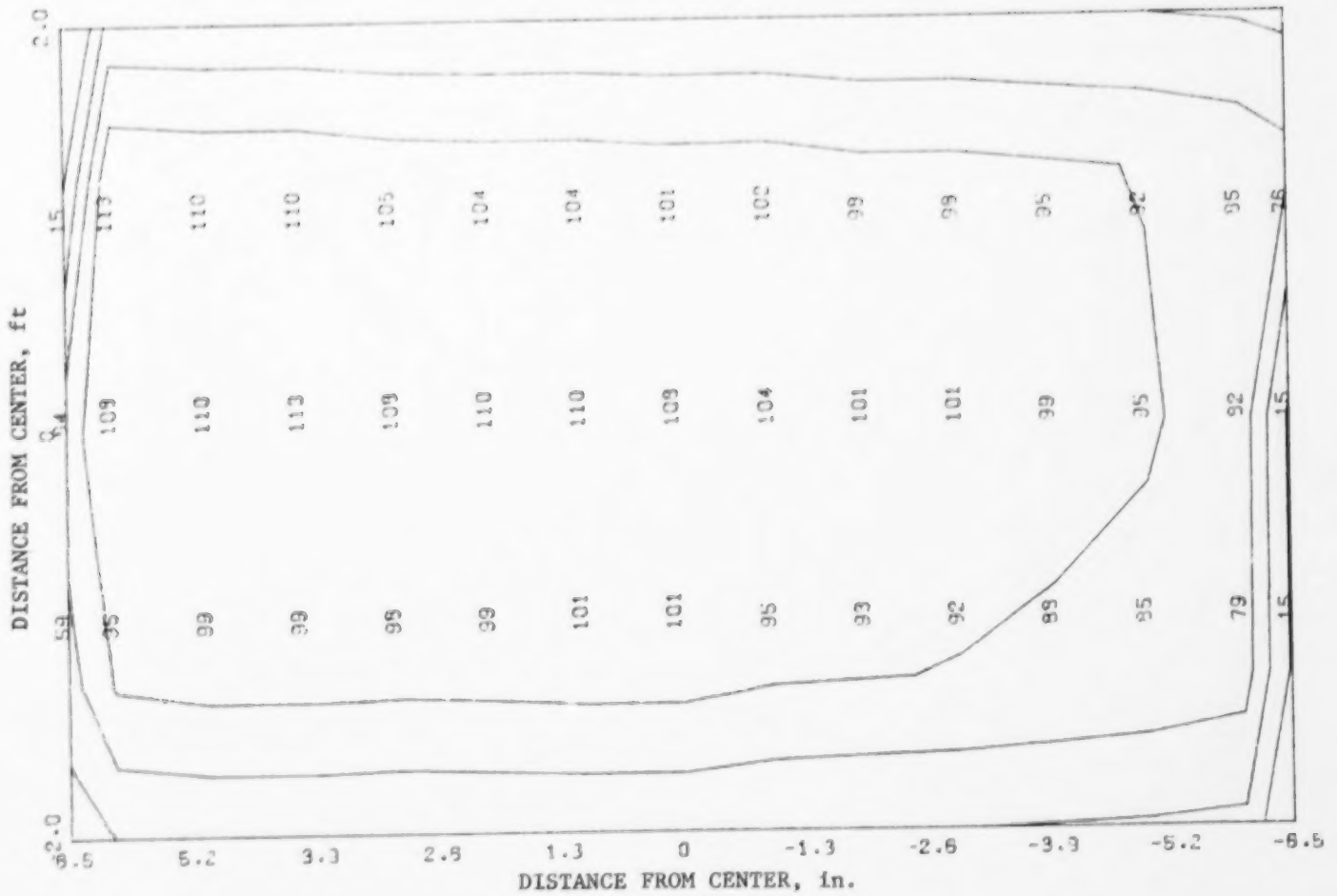

Figure A8.A. Flow distribution in nominal 15-in. channel. Velocities in m/min for a volume flow of 49 m^3/min. Section A.

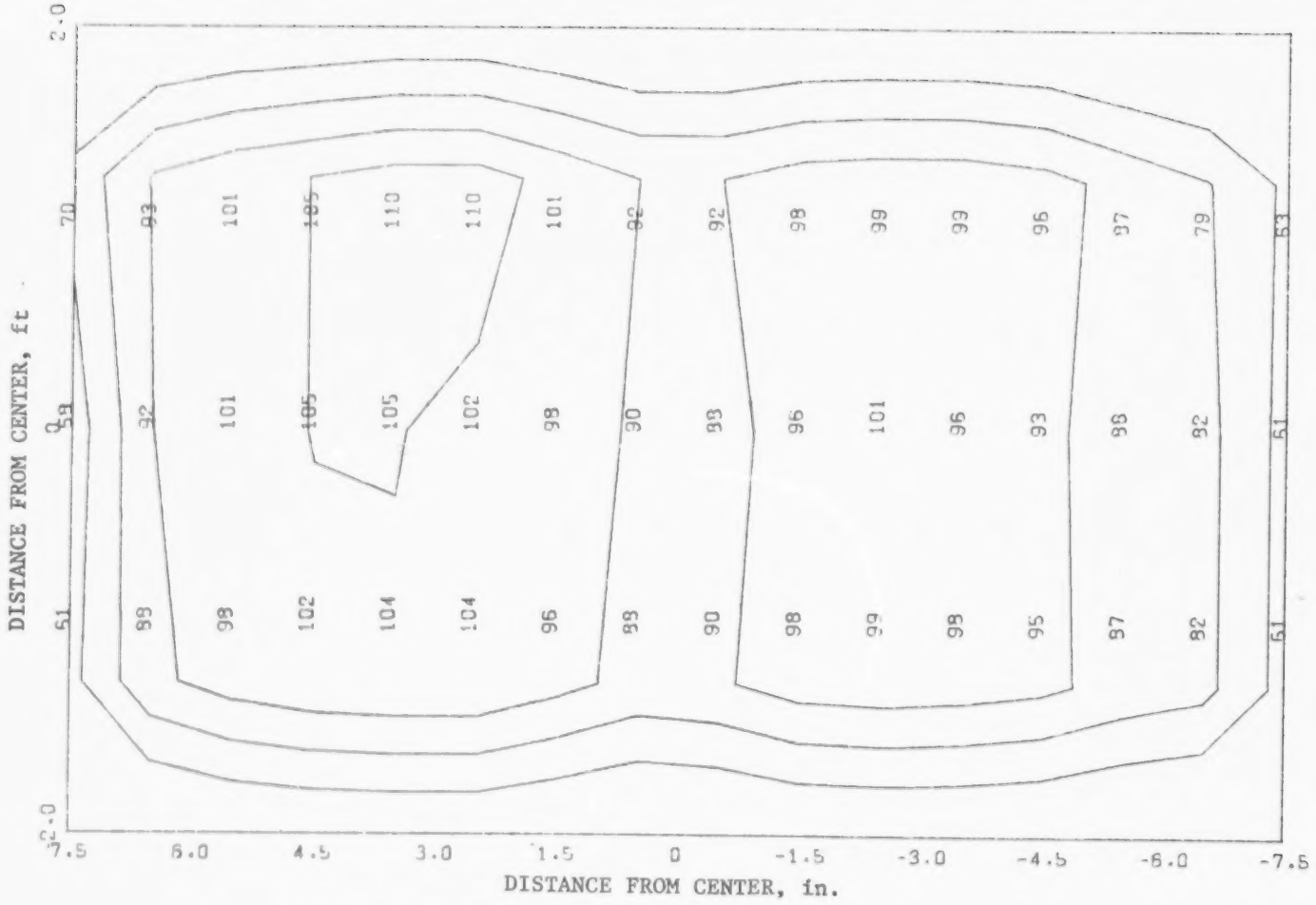

Figure A8.B. Same conditions as Figure A8.A. Section B.

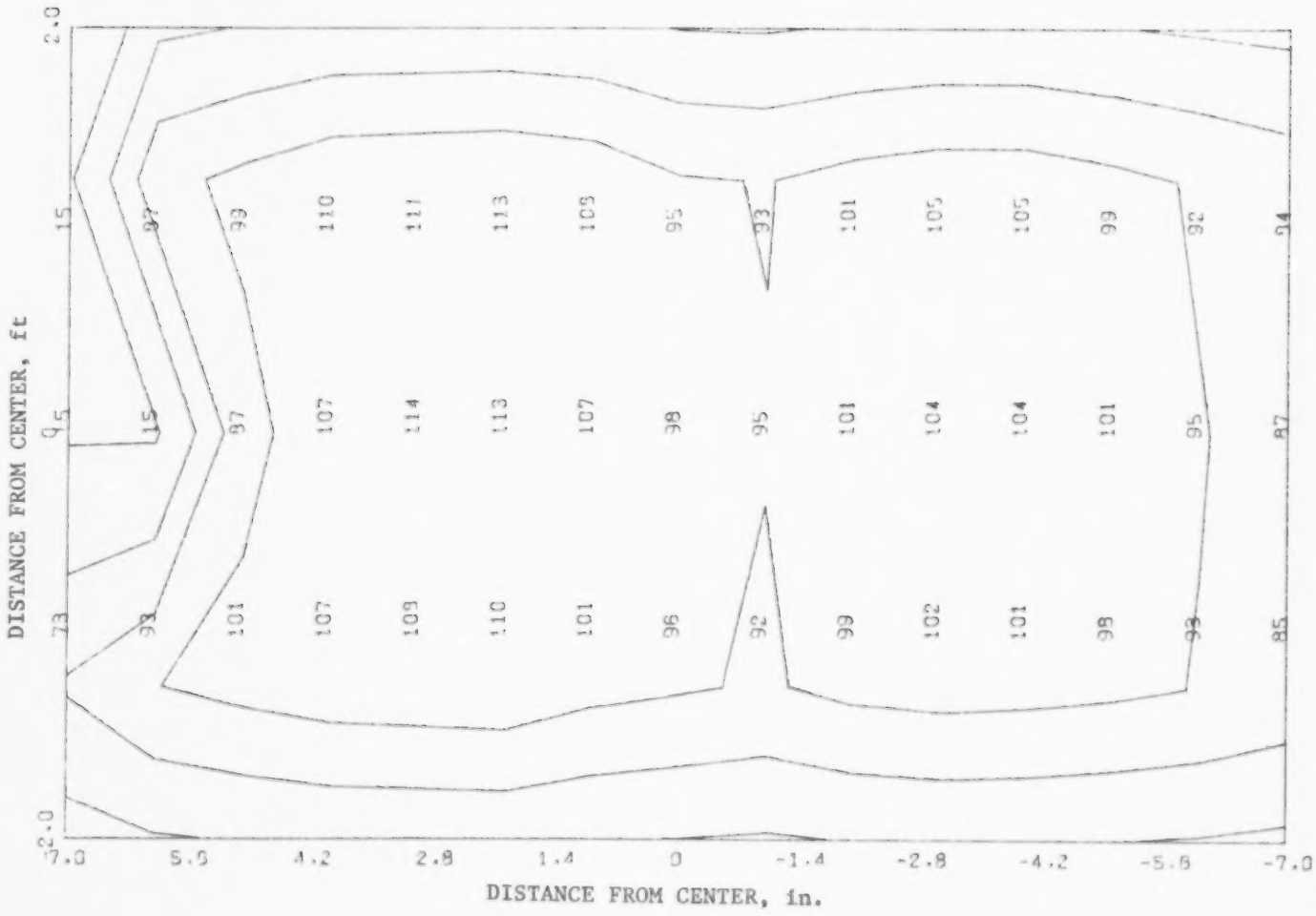

Figure A8.C. Same conditions as Figure A8.A. Section C.

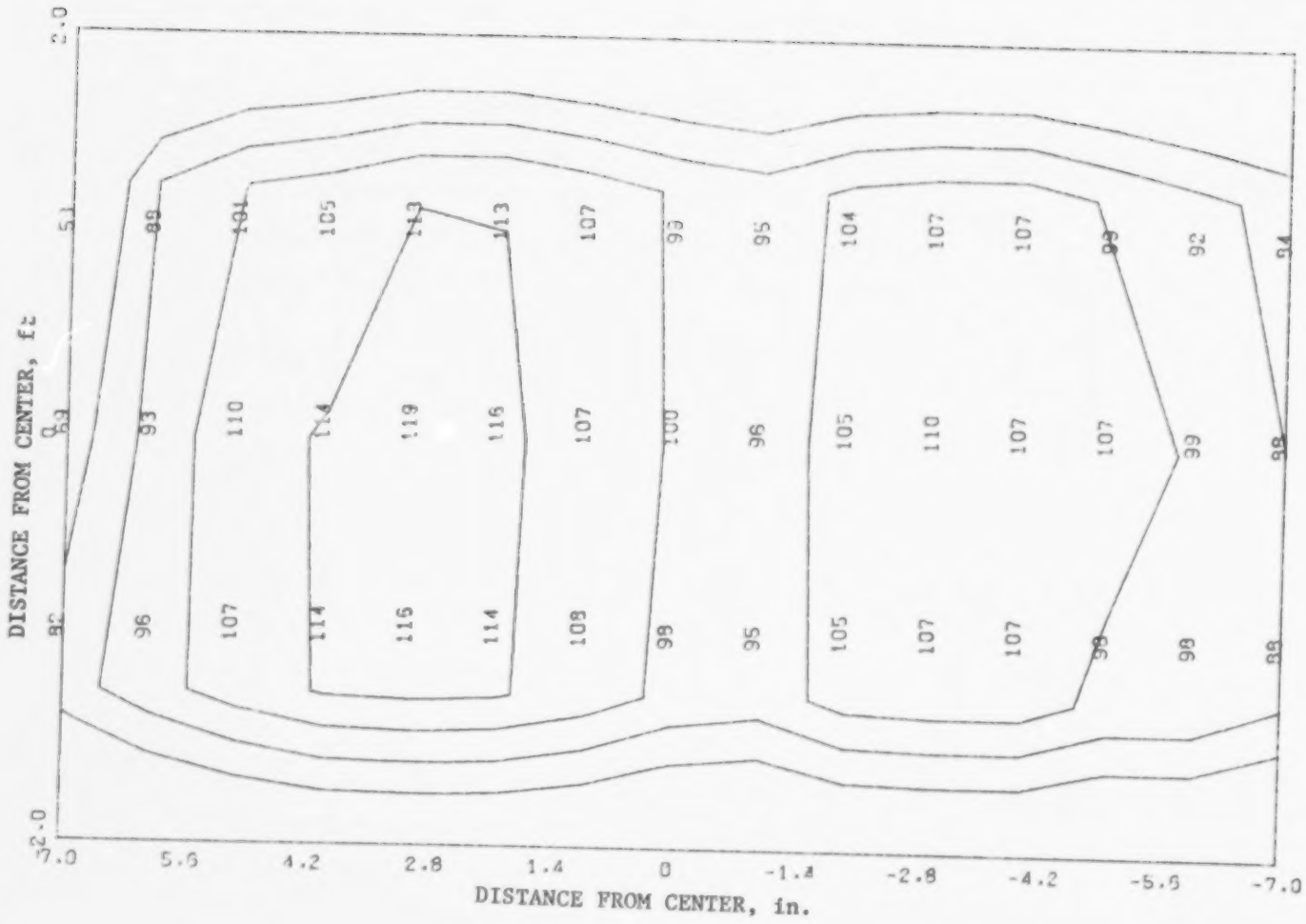

Figure A8.D. Same conditions as Figure A8.A. Section D.

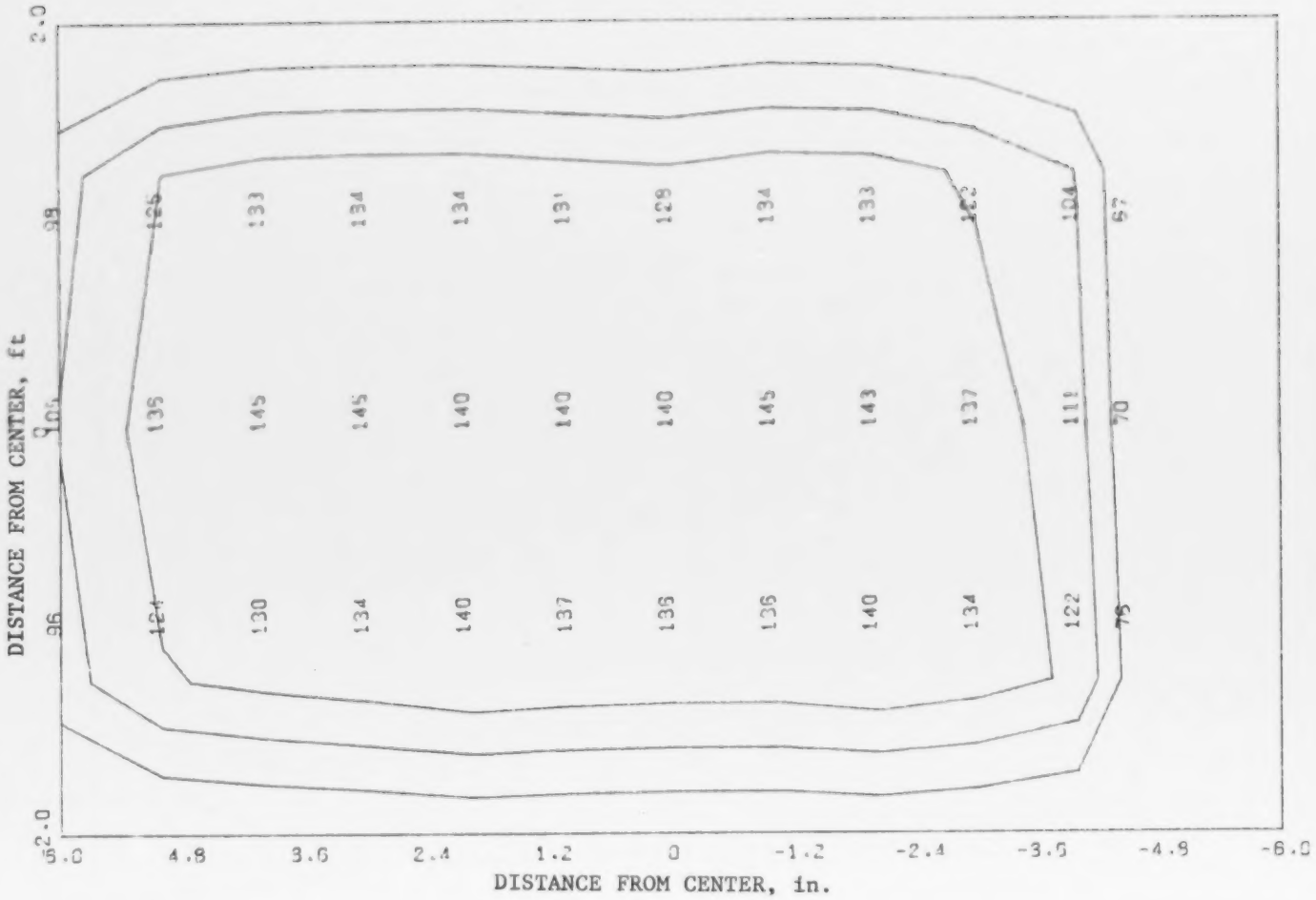

Figure A8.E. Same conditions as Figure A8.A. Section E.